UNIVERSITÀ DEGLI STUDI DI CAMERINO

School of Advanced Studies

Nanoparticle-Based Imaging and Therapy of Chronic Pain in the Dorsal Root Ganglia (PIANO), a H2020 MSCA ITN Project

Doctoral Course In

Chemical and Pharmaceutical Sciences and Biotechnology

Cycle XXXVII

Novel Polymeric Delivery Systems for Targeting Chronic Pain and Inflammation

PhD Student

Saniya Salathia

Supervisors

Prof. Piera Di Martino

Prof. Roberta Censi

Table of Contents

Chapter 1

Introduction

1. Chronic pain and inflammation

The consequences of sustaining a spinal cord injury (SCI) can be overwhelming and can impact many areas of one's life. An injury to the spinal cord can have catastrophic consequences on physical movement, bladder function and other voluntary and involuntary functions [1–3] . Furthermore, SCI often results in debilitating pain that becomes chronic, and can either be neuropathic or nociceptive [4,5]. Neuropathic pain arises from damage or dysfunction of the nervous system, affecting both the peripheral and central pathwaysNeuropathic pain typically develops months or years after SCI and is often localized below the level of injury, though above-level pain can also occur.It is also aided with two sensory conditions – allodynia and hyperalgesia [6,7]. Allodynia can be described as the pain sensation to a stimulus that does not generally induce pain, whereas hyperalgesia is the abnormally heightened sensitivity to pain [8]. This increased discomfort caused by chronic pain can prevail for approximately 20% of a person's lifespan [9]. The development and maintenance of this chronic pain has been attributed to the hyper-excitability of the dorsal root ganglion (DRG) neurons [10,11]. In turn, this sensitization of the DRG neurons can be manipulated with regulation of inflammatory cytokines, neuronal plasticity and ion channels transmissions [12–14]. Along with the nervous system, the immune system plays an equally important role in regulating chronic pain and inflammation. Many cells of the immune system – toll-like receptors (TLRs), glia cells, microglia, macrophages, amongst others, orchestrate a cascade of cytokine and enzymatic responses in opposition to adverse environmental conditions [14]. Neutrophils are the first immune cells to respond to injury, followed by macrophages, which play a key role in inflammation and healing (Figure 1). Macrophages exhibit remarkable plasticity, adapting their function in response to local environmental cues such as cytokines and tissue signals. In simple terms, macrophages can be categorized into inflammatory macrophages (M1-m) and anti-inflammatory macrophages (M2-m). At the site of injury, M1-m trigger an inflammatory response by releasing inflammatory cytokines. M2 macrophages contribute to tissue repair and resolution of inflammation by releasing anti-inflammatory cytokines and growth factors. The immune system regulates the resolution of inflammation through mechanisms such as regulatory T cells (Tregs) and anti-inflammatory cytokines.However, if inflammatory signals persist due to

unresolved tissue damage or dysregulated immune responses, inflammation can become chronic, contributing to conditions like neuropathic pain.

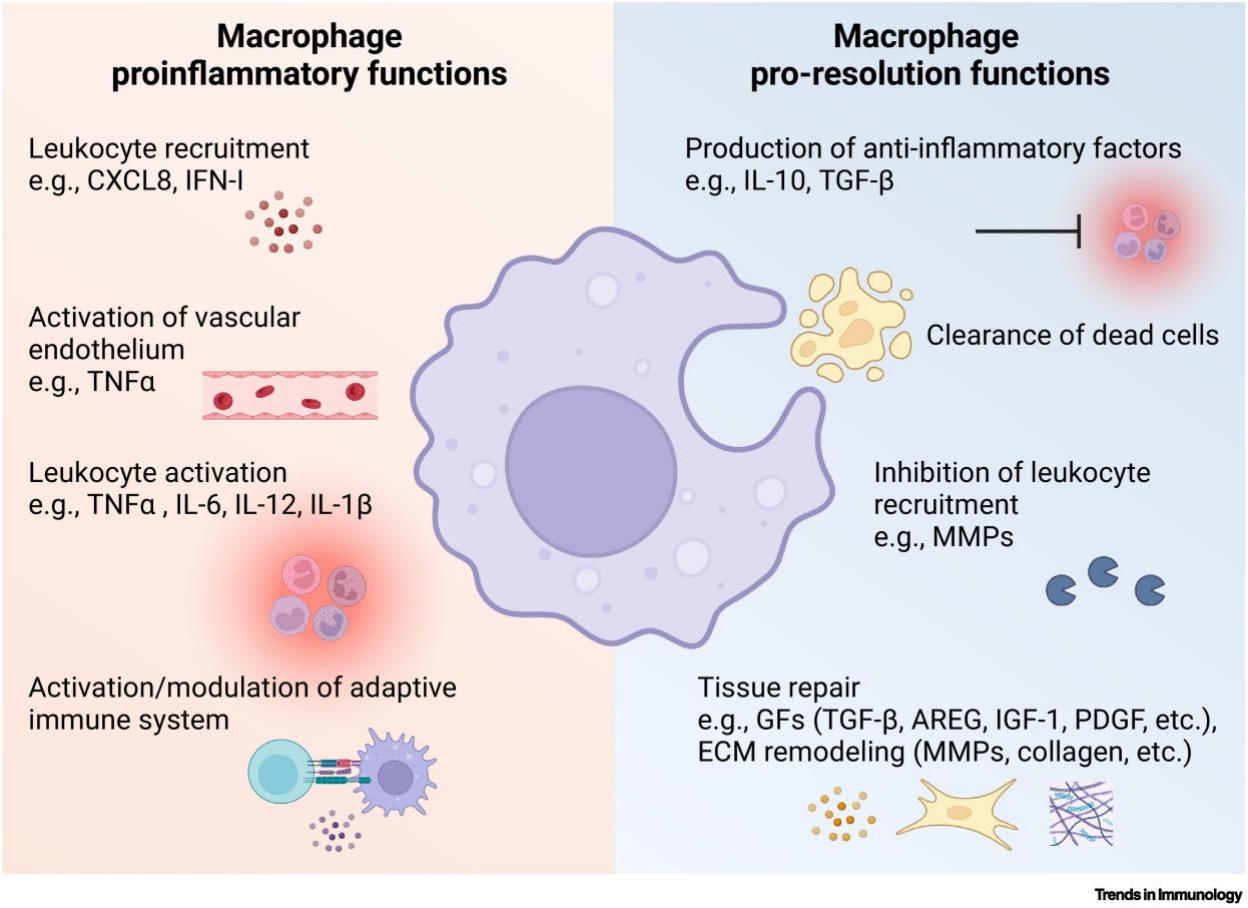

Figure 1: Proinflammatory and pro-resolution functions of macrophages. Following exposure to an inflammatory trigger (e.g., infection), macrophages can respond by: (i) promoting leukocyte recruitment to the site of infection through the secretion of chemokines and other cytokines; (ii) activating the vascular endothelium through tumor necrosis factor alpha (TNFα) secretion, which can aid leukocyte entry; (iii) activating leukocytes, including natural killer (NK) cells, T cells, and B cells, through the secretion of cytokines such as TNFα, IL-6, IL-12, and IL-1β; and (iv) participating in the activation of the adaptive immune system through antigen presentation and cytokine production. Macrophages help to resolve inflammation by: (i) producing anti-inflammatory factors such as IL-10 and transforming growth factor beta (TGF-β); (ii) clearing dead cells; (iii) inhibiting leukocyte recruitment through mechanisms such as matrix metalloproteinase (MMP) secretion; and (iv) promoting tissue repair through the production of growth factors and remodeling of the extracellular matrix (ECM). Abbreviations: AREG,

amphiregulin; GF, growth factor; IFN-I, type I interferon; IGF-1, insulin-like growth factor 1; PDGF, platelet-derived growth factor. Reprinted with permission [15].

2. Nanoparticles and drug delivery

Modulating M1 macrophages, either by repolarization or inhibition of excessive inflammatory signaling, is a promising therapeutic strategy for chronic pain and inflammation. Many studies aim at depleting or repolarizing macrophage phenotypes to resolve inflammation. Drugs like thyroxine [16], nitrate esters [17], tannic acid [18] and β-caryophyllene [19] have been suggested to inhibit M1-m phenotype and promote M2 proliferation. Selecting the right drug also depends on the ailment being targeted. Chronic inflammation can sometimes be a symptom of joint diseases [20,21], cancer [22,23], skin lesions [24,25], gastritis [26,27], and inflammatory bowel disease [28–30].

It is one thing to choose the appropriate therapeutic drug but another to choose the optimal drug delivery system (DDS). While a drug's intrinsic properties influence its efficacy, employing an optimized drug delivery system (DDS) can significantly enhance therapeutic outcomes by improving stability, targeting, and controlled release [31]. Employing a DDS can prolong drug half-life and enable sustained release for extended therapeutic effects [32], reduce dosing frequency by enhancing bioavailability, stability and targeted cellular uptake [33,34], provide a shielding effect from the reticuloendothelial system (RES) and the immune system [35], and specifically target the drug [36], decreasing collateral cell damage [37,38].

Polymeric nanoparticles are a promising drug delivery platform. Polymers used for biomedical purposes are biocompatible and have been widely used as DDSs for delivering hydrophobic and hydrophilic drugs. Poly(lactic-co-glycolic acid) (PLGA) is a known biodegradable polymer that can be used for the encapsulation of anti-tumour hydrophobic agents like paclitaxel [39,40] and curcumin [41]. In many cases, polymeric DDSs can reduce drug cytotoxicity by improving drug stability, targeted delivery, and controlled release. [42,43].The targeting ability of DDSs is achieved by their physical or chemical surface modification. Targeting moieties like ligands of the target cells or other functionalities are introduced to the surface of nanoparticles. Site-specific ligands can help nanoparticles to pass through biological barriers and improve drug specificity [44].

3. Polymeric Nanoparticles for Hydrophobic Drug Delivery

Despite their high potency, a large number of hydrophobic therapeutic compounds pose challenges in administration due to their poor solubility, potential cytotoxicity, and difficulties in achieving efficient loading into drug delivery systems [45,46]. Many approaches have been developed to increase the efficacy of these hydrophobic drugs by incorporating them in biodegradable pharmaceutical drug carriers [47]. Polymeric DDS are based on a variety of polymers, formulations, and have different physical and chemical characteristics. Hyaluronic acid (HA), poly(lactic-co-glycolic) acid (PLGA), polyethylene glycol (PEG), poly(2-(dimethylamino)ethyl methacrylate) (PDMAEMA), polyacrylates and their co-polymers are some of the widely popular polymers used for loading hydrophobic and hydrophilic drugs [48–51].

Controlled drug release is an inherent advantage of using polymers as drug carriers [52]. Polymers are flexible and tuneable in nature. Polymers can be made into nanoparticles that provide the added benefit of smaller size that improves cell internalization, high surface area to volume ratio for high loading capacity, and active targeting by surface modification. Drug encapsulation in polymeric nanoparticles helps shielding the bioactive cargos from rapid clearance by RES and increasing retention time [52]. Moreover, this shielding effect can also provide stability to compounds prone to rapid physiological degradation. Chemical and physical modification on the surface of the nanoparticles with biological ligands provides specific targeting. Many methods for functionalization of polymeric nanoparticles with targeting ligands are employed, like adsorption and covalent binding [53]. These surface moieties can be aptamers, peptides, antibodies, antagomirs, and other small molecules [54].

4. Polyplexes and non-viral gene delivery

Advancements in our understanding of nucleic acid (NA) functions have created new opportunities for the therapeutic use of NAs, such as plasmid DNA (pDNA) and microRNA (miRNA) [54]. However, there are challenges to delivering naked NAs – low *in vivo* stability, rapid clearance and poor permeability owing to their anionic change in physiological environment [55]. Moreover, nucleic acids have a high molecular weight that

also impedes their uptake into cells. The use of polymers as DDSs for nucleic acids can help overcome these difficulties.

Approximately 70% of clinical gene therapy trials involve viral vectors [56], making them the most common vectors for delivering NAs. This is because the poor permeability of NAs is effectively countered by the high transfection efficiency of viruses like adenovirus, lentivirus and retrovirus [57]. However, there are certain side effects of high viral infectivity, like a propensity to trigger immunogenic responses and promote insertion mutations [58]. This is a major clinical safety concern which also accompanies the inability of viruses to load bulky NAs, and low gene capacity. On the other hand, non-viral vectors, like cationic polymers, have displayed high gene loading capacity with a much lower cytotoxicity than their viral counterparts. Cationic polymers can form complexes with anionic NAs to form polyplexes (Figure 2). Polyplexes are compounds that increase the transfection efficiency of NAs and provide a shielding effect from rapid degradation by RES. One important consideration in the formulation of polyplexes is the N/P ratio. This ratio refers to the positively charged amine groups (N) of the polymer and the negatively charged phosphorus (P) of the NA. Manipulation of N/P ratio in the formulation stage can help exploit the surface charge of the polyplexes. Positively charged compounds have been observed to have increased cell internalization. Modification of the N/P ratio can be used to achieve stabilisation and condensation of the polyplex for the optimal positive charge.

Small non-coding RNA molecules with 19-25 nucleotide length have a prominent role in gene expression. Some miRNAs are also identified in the regulation of inflammatory environment and delivering synaptic signals of pain. A therapeutic avenue that can be taken in targeting miRNAs is the adoption of antagomir technology [59]. Antagomirs are chemically modified oligonucleotides that interfere with their endogenous counterparts [60]. These have already been used as silencing agents of miRNAs in many diseases like cancer. The combined use of nanopolyplexes with synthetic antagomirs can result in a targeting and effective therapeutic delivery system.

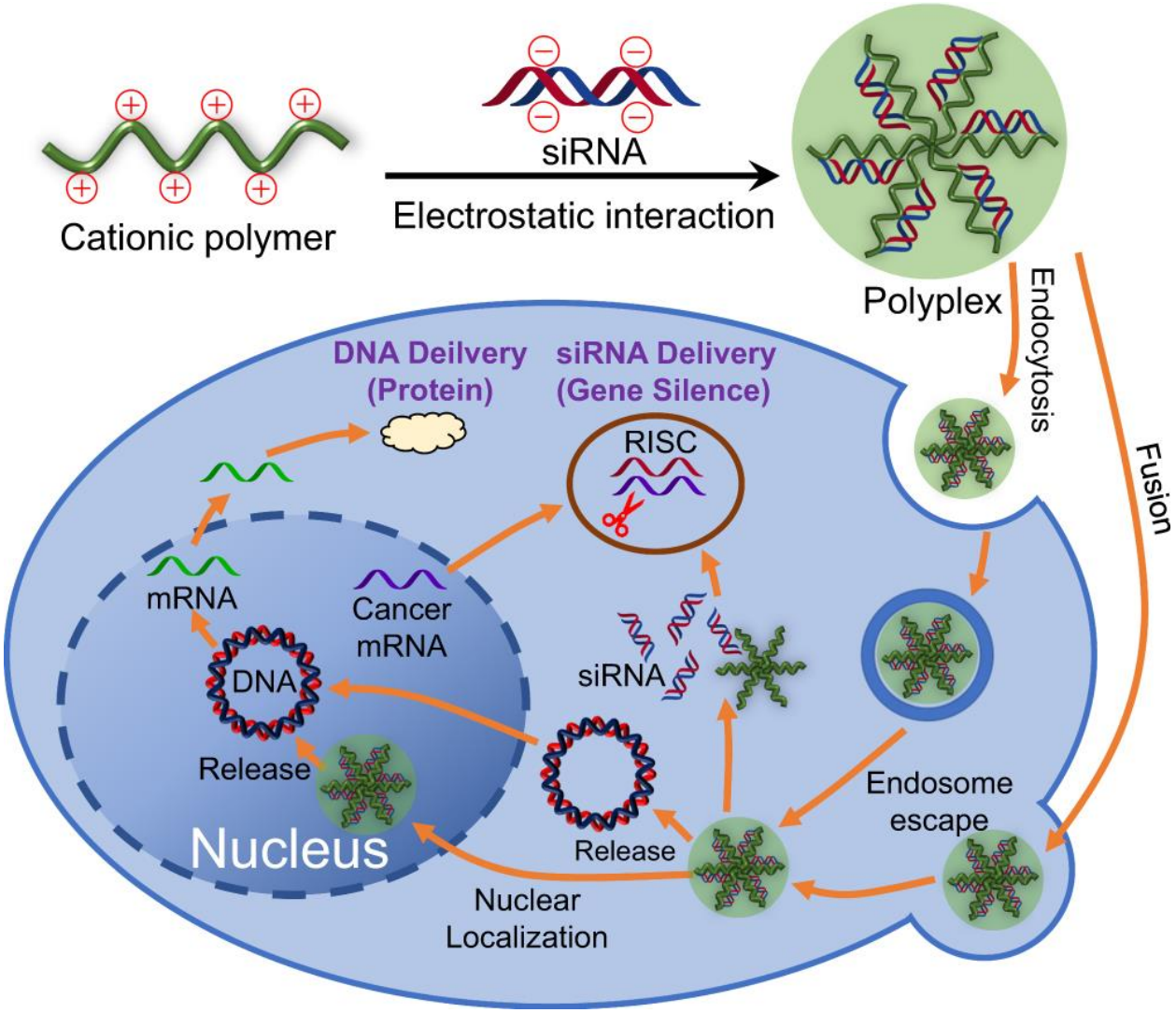

Figure 2: Gene delivery mechanism of polyplexes. Reprinted with permission [61].

5. Aim and outline of the thesis

The aim of the project in this thesis is to present multiple solutions to resolve inflammation and neuropathic pain by the targeted use of polymeric DDSs encapsulating potent hydrophobic drugs and nucleic acids. The versatility of polymers is displayed by employing them for synthesising nanoparticles, temperature sensitive hydrogels and even bases for nucleic acid conjugation. High encapsulation and sustained release of hydrophobic drug was achieved and tested in inflammatory macrophages. The advances in genetic technology were used to synthesise polyplexes of cationic polymers and anionic antagomirs to suppress inflammatory gene expression in rat models of compression spinal cord injury.

This thesis is sectioned into 6 chapters, where **Chapter 1** provides an introductory insight into polymeric nanosystems, non-viral delivery of NAs, and targeted drug delivery.

Chapter 2 gives the overview of currently employed therapeutic strategies for nociception based on hyaluronic acid (HA). The chapter focuses on the different methods of delivery of HA in the form of nanoparticles, hydrogels, nanovesicles, and others, all targeting the CD44 receptor on the surface of M1-m.

In **Chapter 3**, we employ some of the strategies mentioned above by formulating a polymer-based drug delivery system coated with hyaluronic acid (HA) and loaded with carvacrol, an organic, hydrophobic, anti-inflammatory compound. This system was shown to be effective in modulating cytokine production and polarizing macrophage phenotypes by targeting M1 macrophages and reducing inflammation.

Chapter 4 shows the effect of gene silencing with antagomirs (antagomir-21/155) in non-viral DDS (polyplexes) on neurons, glial cells and inflammatory macrophages. A pilot *in vivo* study of a compression spinal cord injury (SCI) rat model is created and administered with a thermosensitive hydrogel loaded with gold-complexed polyplexes (antagomir-155) aimed at a targeted controlled release and neuroregeneration. The nucleic acid polyplexes are synthesised and characterised for surface charge, size and stability for maximum efficacy. Polyplexes with antagomir-21 were cultured with inflammatory macrophages and analyses for macrophage polarization to anti-inflammatory phenotype.

Polymer-based nanosystems are employed in **Chapter 5** to encapsulate capsaicin – an anti-inflammatory and anti-nociceptive drug that targets voltage-dependent sodium channels. The drug-loaded nanosystem is proposed to be trapped in a biocompatible hydrogel patch aimed for topical nociceptive therapy.

We conclude our findings with a critical review and conclusion about the exploration of varying kinds of drugs, materials and delivery methods that can effectively target pain and counter inflammation in **Chapter 6**.

6. References

(1) Masri, R.; Keller, A. Chronic Pain Following Spinal Cord Injury. *Adv Exp Med Biol* **2012**, *760*, 74–88. https://doi.org/10.1007/978-1-4614-4090-1_5.

(2) Van Hedel, H. J. A.; Dietz, V. Rehabilitation of Locomotion after Spinal Cord Injury. *Restor Neurol Neurosci* **2010**, *28* (1), 123–134. https://doi.org/10.3233/RNN-2010-0508.

(3) Persu, C.; Caun, V.; Dragomiriţeanu, I.; Geavlete, P. Urological Management of the Patient with Traumatic Spinal Cord Injury. *J Med Life* **2009**, *2* (3), 296.

(4) Yezierski, R. P. Pain Following Spinal Cord Injury: Pathophysiology and Central Mechanisms. *Prog Brain Res* **2000**, *129*, 429–449. https://doi.org/10.1016/S0079-6123(00)29033-X.

(5) Rekand, T.; Hagen, E. M.; Grønning, M. Chronic Pain Following Spinal Cord Injury. *Tidsskrift for Den norske legeforening* **2012**, *132* (8), 974–979. https://doi.org/10.4045/TIDSSKR.11.0794.

(6) Calmels, P.; Mick, G.; Perrouin-Verbe, B.; Ventura, M. Neuropathic Pain in Spinal Cord Injury: Identification, Classification, Evaluation. *Ann Phys Rehabil Med* **2009**, *52* (2), 83–102. https://doi.org/10.1016/J.REHAB.2008.12.012.

(7) Hadjipavlou, G.; Cortese, A. M.; Ramaswamy, B. Spinal Cord Injury and Chronic Pain. *BJA Educ* **2016**, *16* (8), 264–268. https://doi.org/10.1093/BJAED/MKV073.

(8) Jensen, T. S.; Finnerup, N. B. Allodynia and Hyperalgesia in Neuropathic Pain: Clinical Manifestations and Mechanisms. *Lancet Neurol* **2014**, *13* (9), 924–935. https://doi.org/10.1016/S1474-4422(14)70102-4.

(9) Geneen, L. J.; Moore, R. A.; Clarke, C.; Martin, D.; Colvin, L. A.; Smith, B. H. Physical Activity and Exercise for Chronic Pain in Adults: An Overview of Cochrane Reviews. *Cochrane Database Syst Rev* **2017**, *2017* (1). https://doi.org/10.1002/14651858.CD011279.PUB2.

(10) Berta, T.; Qadri, Y.; Tan, P. H.; Ji, R. R. Targeting Dorsal Root Ganglia and Primary Sensory Neurons for the Treatment of Chronic Pain. *Expert Opin Ther Targets* **2017**, *21* (7), 695–703. https://doi.org/10.1080/14728222.2017.1328057.

(11) Zhang, L.; Xie, R.; Yang, J.; Zhao, Y.; Qi, C.; Bian, G.; Wang, M.; Shan, J.; Wang, C.; Wang, D.; Luo, C.; Wang, Y.; Wu, S. Chronic Pain Induces Nociceptive Neurogenesis in Dorsal Root Ganglia from Sox2-Positive Satellite Cells. *Glia* **2019**, *67* (6), 1062–1075. https://doi.org/10.1002/GLIA.23588.

(12) Walker, S. M.; Beggs, S.; Baccei, M. L. Persistent Changes in Peripheral and Spinal Nociceptive Processing after Early Tissue Injury. *Exp Neurol* **2016**, *275 Pt 2* (0 2), 253–260. https://doi.org/10.1016/J.EXPNEUROL.2015.06.020.

(13) Ramer, M. S.; Thompson, S. W. N.; McMahon, S. B. Causes and Consequences of Sympathetic Basket Formation in Dorsal Root Ganglia. *Pain* **1999**, *Suppl 6* (SUPPL.1). https://doi.org/10.1016/S0304-3959(99)00144-X.

(14) Miller, R. J.; Jung, H.; Bhangoo, S. K.; White, F. A. Cytokine and Chemokine Regulation of Sensory Neuron Function. *Handb Exp Pharmacol* **2009**, *194* (194), 417–449. https://doi.org/10.1007/978-3-540-79090-7_12.

(15) Rodríguez-Morales, P.; Franklin, R. A. Macrophage Phenotypes and Functions: Resolving Inflammation and Restoring Homeostasis. *Trends in Immunology*. Elsevier Ltd December 2023, pp 986–998. https://doi.org/10.1016/j.it.2023.10.004.

(16) Zhu, S.; Wang, Y.; Liu, H.; Wei, W.; Tu, Y.; Chen, C.; Song, J.; Xu, Z.; Li, J.; Wang, C.; Sun, S. Thyroxine Affects Lipopolysaccharide-Induced Macrophage Differentiation and Myocardial Cell Apoptosis via the NF-KB P65 Pathway Both In Vitro and In Vivo. *Mediators Inflamm* **2019**, *2019*, 2098972–2098982. https://doi.org/10.1155/2019/2098972.

(17) Wei, C. Y.; Wang, Y. M.; Han, L.; Chen, F. F.; Li, Y. H.; Tang, M. X.; Zhang, W.; Wang, Z. H.; Zhong, M. Nitrate Esters Alleviated Coronary Atherosclerosis Through Inhibition of NF-B-Regulated Macrophage Polarization Shift in Epicardial Adipose Tissue. *J Cardiovasc Pharmacol* **2020**, *75* (5), 475–482. https://doi.org/10.1097/FJC.0000000000000818.

(18) Sivanantham, A.; Pattarayan, D.; Rajasekar, N.; Kannan, A.; Loganathan, L.; Bethunaickan, R.; Mahapatra, S. K.; Palanichamy, R.; Muthusamy, K.; Rajasekaran, S. Tannic Acid Prevents Macrophage-Induced pro-Fibrotic Response in Lung Epithelial Cells via Suppressing TLR4-Mediated Macrophage Polarization. *Inflammation Research* **2019**, *68* (12), 1011–1024. https://doi.org/10.1007/S00011-019-01282-4/FIGURES/9.

(19) Tian, X.; Liu, H.; Xiang, F.; Xu, L.; Dong, Z. β-Caryophyllene Protects against Ischemic Stroke by Promoting Polarization of Microglia toward M2 Phenotype via the TLR4 Pathway. *Life Sci* **2019**, *237*, 116915. https://doi.org/10.1016/J.LFS.2019.116915.

(20) Zerrillo, L.; Que, I.; Vepris, O.; Morgado, L. N.; Chan, A.; Bierau, K.; Li, Y.; Galli, F.; Bos, E.; Censi, R.; Di Martino, P.; van Osch, G. J. V. M.; Cruz, L. J. PH-Responsive Poly(Lactide-Co-Glycolide) Nanoparticles Containing near-Infrared Dye for Visualization and

Hyaluronic Acid for Treatment of Osteoarthritis. *Journal of Controlled Release* **2019**, *309*, 265–276. https://doi.org/10.1016/j.jconrel.2019.07.031.

(21) Storozhylova, N.; Crecente-Campo, J.; Cabaleiro, D.; Lugo, L.; Dussouy, C.; Simões, S.; Monteiro, M.; Grandjean, C.; Alonso, M. J. An In Situ Hyaluronic Acid-Fibrin Hydrogel Containing Drug-Loaded Nanocapsules for Intra-Articular Treatment of Inflammatory Joint Diseases. *Regen Eng Transl Med* **2020**, *6* (2), 201–216. https://doi.org/10.1007/s40883-020-00154-2.

(22) Murata, M. Inflammation and Cancer. *Environ Health Prev Med* **2018**, *23* (1), 1–8. https://doi.org/10.1186/S12199-018-0740-1/FIGURES/3.

(23) Hussain, S. P.; Harris, C. C. Inflammation and Cancer: An Ancient Link with Novel Potentials. *Int J Cancer* **2007**, *121* (11), 2373–2380. https://doi.org/10.1002/IJC.23173.

(24) Novak-Bilić, G.; Vučić, M.; Japundžić, I.; Meštrović-štefekov, J.; Stanić-Duktaj, S.; Lugović-Mihić, L. Irritant and Allergic Contact Dermatitis – Skin Lesion Characteristics. *Acta Clin Croat* **2018**, *57*. (4.), 713–719. https://doi.org/10.20471/ACC.2018.57.04.13.

(25) Tauchi, M.; Hida, A.; Negishi, T.; Katsuoka, F.; Noda, S.; Mimura, J.; Hosoya, T.; Yanaka, A.; Aburatani, H.; Fujii-Kuriyama, Y.; Motohashi, H.; Yamamoto, M. Constitutive Expression of Aryl Hydrocarbon Receptor in Keratinocytes Causes Inflammatory Skin Lesions. *Mol Cell Biol* **2005**, *25* (21), 9360–9368. https://doi.org/10.1128/MCB.25.21.9360-9368.2005.

(26) Sipponen, P.; Maaroos, H. I. Chronic Gastritis. *Scand J Gastroenterol* **2015**, *50* (6), 657–667. https://doi.org/10.3109/00365521.2015.1019918.

(27) Rugge, M.; Sugano, K.; Sacchi, D.; Sbaraglia, M.; Malfertheiner, P. Gastritis: An Update in 2020. *Current Treatment Options in Gastroenterology 2020 18:3* **2020**, *18* (3), 488–503. https://doi.org/10.1007/S11938-020-00298-8.

(28) Sands, B. E. Biomarkers of Inflammation in Inflammatory Bowel Disease. *Gastroenterology* **2015**, *149* (5), 1275-1285.e2. https://doi.org/10.1053/J.GASTRO.2015.07.003.

(29) Baumgart, D. C.; Carding, S. R. Inflammatory Bowel Disease: Cause and Immunobiology. *The Lancet* **2007**, *369* (9573), 1627–1640. https://doi.org/10.1016/S0140-6736(07)60750-8.

(30) Rubin, D. C.; Shaker, A.; Levin, M. S. Chronic Intestinal Inflammation: Inflammatory Bowel Disease and Colitis-Associated Colon Cancer. *Front Immunol* **2012**, *3*, 22422. https://doi.org/10.3389/FIMMU.2012.00107/BIBTEX.

(31) He, W.; Kapate, N.; Shields, C. W.; Mitragotri, S. Drug Delivery to Macrophages: A Review of Targeting Drugs and Drug Carriers to Macrophages for Inflammatory Diseases. *Adv Drug Deliv Rev* **2020**, *165–166*, 15–40. https://doi.org/10.1016/J.ADDR.2019.12.001.

(32) Poletto, F. S.; Jäger, E.; Cruz, L.; Pohlmann, A. R.; Guterres, S. S. The Effect of Polymeric Wall on the Permeability of Drug-Loaded Nanocapsules. *Materials Science and Engineering: C* **2008**, *28* (4), 472–478. https://doi.org/10.1016/J.MSEC.2007.04.015.

(33) Almouazen, E.; Bourgeois, S.; Boussaïd, A.; Valot, P.; Malleval, C.; Fessi, H.; Nataf, S.; Briançon, S. Development of a Nanoparticle-Based System for the Delivery of Retinoic Acid into Macrophages. *Int J Pharm* **2012**, *430* (1–2), 207–215. https://doi.org/10.1016/J.IJPHARM.2012.03.025.

(34) Rodriguez-Emmenegger, C.; Jäger, A.; Jäger, E.; Stepanek, P.; Alles, A. B.; Guterres, S. S.; Pohlmann, A. R.; Brynda, E. Polymeric Nanocapsules Ultra Stable in Complex Biological Media. *Colloids Surf B Biointerfaces* **2011**, *83* (2), 376–381. https://doi.org/10.1016/J.COLSURFB.2010.12.013.

(35) Frank, L. A.; Contri, R. V.; Beck, R. C. R.; Pohlmann, A. R.; Guterres, S. S. Improving Drug Biological Effects by Encapsulation into Polymeric Nanocapsules. *Wiley Interdiscip Rev Nanomed Nanobiotechnol* **2015**, *7* (5), 623–639. https://doi.org/10.1002/WNAN.1334.

(36) Bender, E. A.; Cavalcante, M. F.; Adorne, M. D.; Colomé, L. M.; Guterres, S. S.; Abdalla, D. S. P.; Pohlmann, A. R. New Strategy to Surface Functionalization of Polymeric Nanoparticles: One-Pot Synthesis of ScFv Anti-LDL(-)-Functionalized Nanocapsules. *Pharm Res* **2014**, *31* (11), 2975–2987. https://doi.org/10.1007/S11095-014-1392-5/METRICS.

(37) Bernardi, A.; Zilberstein, A. A. C. C. V.; Jäger, E.; Campos, M. M.; Morrone, F. B.; Calixto, J. B.; Pohlmann, A. R.; Guterres, S. S.; Battastini, A. M. O. Effects of Indomethacin-Loaded Nanocapsules in Experimental Models of Inflammation in Rats. *Br J Pharmacol* **2009**, *158* (4), 1104–1111. https://doi.org/10.1111/J.1476-5381.2009.00244.X.

(38) El-Gogary, R. I.; Rubio, N.; Wang, J. T. W.; Al-Jamal, W. T.; Bourgognon, M.; Kafa, H.; Naeem, M.; Klippstein, R.; Abbate, V.; Leroux, F.; Bals, S.; Van Tendeloo, G.; Kamel, A. O.; Awad, G. A. S.; Mortada, N. D.; Al-Jamal, K. T. Polyethylene Glycol Conjugated Polymeric

Nanocapsules for Targeted Delivery of Quercetin to Folate-Expressing Cancer Cells in Vitro and in Vivo. *ACS Nano* **2014**, *8* (2), 1384–1401. https://doi.org/10.1021/NN405155B/SUPPL_FILE/NN405155B_SI_003.MPG.

(39) Danhier, F.; Lecouturier, N.; Vroman, B.; Jérôme, C.; Marchand-Brynaert, J.; Feron, O.; Préat, V. Paclitaxel-Loaded PEGylated PLGA-Based Nanoparticles: In Vitro and in Vivo Evaluation. *Journal of Controlled Release* **2009**, *133* (1), 11–17. https://doi.org/10.1016/J.JCONREL.2008.09.086.

(40) Fonseca, C.; Simões, S.; Gaspar, R. Paclitaxel-Loaded PLGA Nanoparticles: Preparation, Physicochemical Characterization and in Vitro Anti-Tumoral Activity. *Journal of Controlled Release* **2002**, *83* (2), 273–286. https://doi.org/10.1016/S0168-3659(02)00212-2.

(41) Yallapu, M. M.; Gupta, B. K.; Jaggi, M.; Chauhan, S. C. Fabrication of Curcumin Encapsulated PLGA Nanoparticles for Improved Therapeutic Effects in Metastatic Cancer Cells. *J Colloid Interface Sci* **2010**, *351* (1), 19–29. https://doi.org/10.1016/J.JCIS.2010.05.022.

(42) Northfelt, D. W.; Martin, F. J.; Working, P.; Volberding, P. A.; Russell, J.; Newman, M.; Amantea, M. A.; Kaplan, L. D. Doxorubicin Encapsulated in Liposomes Containing Surface-Bound Polyethylene Glycol: Pharmacokinetics, Tumor Localization, and Safety in Patients with AIDS-Related Kaposi's Sarcoma. *The Journal of Clinical Pharmacology* **1996**, *36* (1), 55–63. https://doi.org/10.1002/J.1552-4604.1996.TB04152.X.

(43) Memon, A.; Darif, M.; Al-Saleh, K.; Suresh, A. Pegylated Liposomal Tumor Necrosis Factor-α Results in Reduced Toxicity and Synergistic Antitumor Activity after Systemic Administration in Combination with Liposomal Doxorubicin (Doxil®) in Soft Tissue Sarcoma-Bearing Rats. *Int J Cancer* **2002**, *97* (1), 115–120. https://doi.org/10.1002/IJC.1578.

(44) Gaspar, D. P.; Faria, V.; Quintas, J. P.; Almeida, A. J. Targeted Delivery of Lipid Nanoparticles by Means of Surface Chemical Modification. *Curr Org Chem* **2017**, *21* (23). https://doi.org/10.2174/1385272820666161031161101.

(45) Wang, G.; Wang, J.; Wu, W.; Tony To, S. S.; Zhao, H.; Wang, J. Advances in Lipid-Based Drug Delivery: Enhancing Efficiency for Hydrophobic Drugs. *Expert Opinion on Drug Delivery*. 2015. https://doi.org/10.1517/17425247.2015.1021681.

(46) Yang, G.; Liu, Y.; Wang, H.; Wilson, R.; Hui, Y.; Yu, L.; Wibowo, D.; Zhang, C.; Whittaker, A. K.; Middelberg, A. P. J.; Zhao, C. Bioinspired Core–Shell Nanoparticles for Hydrophobic Drug Delivery. *Angewandte Chemie* **2019**. https://doi.org/10.1002/ange.201908357.

(47) Sung, Y. K.; Kim, S. W. Recent Advances in Polymeric Drug Delivery Systems. *Biomaterials Research*. 2020. https://doi.org/10.1186/s40824-020-00190-7.

(48) Sajeesh, S.; Sharma, C. P. Novel PH Responsive Polymethacrylic Acid-Chitosan-Polyethylene Glycol Nanoparticles for Oral Peptide Delivery. *J Biomed Mater Res B Appl Biomater* **2006**. https://doi.org/10.1002/jbm.b.30372.

(49) Greenhalgh, K.; Turos, E. In Vivo Studies of Polyacrylate Nanoparticle Emulsions for Topical and Systemic Applications. *Nanomedicine* **2009**. https://doi.org/10.1016/j.nano.2008.07.004.

(50) Sarmento, B.; Ribeiro, A.; Veiga, F.; Sampaio, P.; Neufeld, R.; Ferreira, D. Alginate/Chitosan Nanoparticles Are Effective for Oral Insulin Delivery. *Pharm Res* **2007**. https://doi.org/10.1007/s11095-007-9367-4.

(51) Hawkins, M. J.; Soon-Shiong, P.; Desai, N. Protein Nanoparticles as Drug Carriers in Clinical Medicine. *Advanced Drug Delivery Reviews*. 2008. https://doi.org/10.1016/j.addr.2007.08.044.

(52) Steichen, S. D.; Caldorera-Moore, M.; Peppas, N. A. A Review of Current Nanoparticle and Targeting Moieties for the Delivery of Cancer Therapeutics. *European Journal of Pharmaceutical Sciences*. 2013. https://doi.org/10.1016/j.ejps.2012.12.006.

(53) Wang, G.; Wang, J.; Wu, W.; Tony To, S. S.; Zhao, H.; Wang, J. Advances in Lipid-Based Drug Delivery: Enhancing Efficiency for Hydrophobic Drugs. *Expert Opinion on Drug Delivery*. 2015. https://doi.org/10.1517/17425247.2015.1021681.

(54) Lächelt, U.; Wagner, E. Nucleic Acid Therapeutics Using Polyplexes: A Journey of 50 Years (and Beyond). *Chem Rev* **2015**, *115* (19), 11043–11078. https://doi.org/10.1021/CR5006793/ASSET/IMAGES/LARGE/CR-2014-006793_0023.JPEG.

(55) Jones, C. H.; Chen, C. K.; Ravikrishnan, A.; Rane, S.; Pfeifer, B. A. Overcoming Nonviral Gene Delivery Barriers: Perspective and Future. *Mol Pharm* **2013**, *10* (11), 4082–4098. https://doi.org/10.1021/MP400467X/ASSET/IMAGES/MEDIUM/MP-2013-00467X_0008.GIF.

(56) Wang, C.; Pan, C.; Yong, H.; Wang, F.; Bo, T.; Zhao, Y.; Ma, B.; He, W.; Li, M. Emerging Non-Viral Vectors for Gene Delivery. *Journal of Nanobiotechnology*. BioMed Central Ltd December 2023. https://doi.org/10.1186/s12951-023-02044-5.

(57) Sarvari, R.; Nouri, M.; Agbolaghi, S.; Roshangar, L.; Sadrhaghighi, A.; Seifalian, A. M.; Keyhanvar, P. A Summary on Non-Viral Systems for Gene Delivery Based on Natural and Synthetic Polymers. *International Journal of Polymeric Materials and Polymeric Biomaterials* **2022**, *71*, 246–265. https://doi.org/10.1080/00914037.2020.1825081.

(58) Thomas, C. E.; Ehrhardt, A.; Kay, M. A. Progress and Problems with the Use of Viral Vectors for Gene Therapy. *Nature Reviews Genetics*. May 2003, pp 346–358. https://doi.org/10.1038/nrg1066.

(59) Preethi, K. A.; Lakshmanan, G.; Sekar, D. Antagomir Technology in the Treatment of Different Types of Cancer. *Epigenomics*. 2021. https://doi.org/10.2217/epi-2020-0439.

(60) Mohr, A. M.; Mott, J. L. Overview of MicroRNA Biology. *Seminars in Liver Disease*. 2015. https://doi.org/10.1055/s-0034-1397344.

(61) Chen, C. K.; Huang, P. K.; Law, W. C.; Chu, C. H.; Chen, N. T.; Lo, L. W. Biodegradable Polymers for Gene-Delivery Applications. *International Journal of Nanomedicine*. Dove Medical Press Ltd. 2020, pp 2131–2150. https://doi.org/10.2147/IJN.S222419.

Chapter 2

Hyaluronic Acid-Based Nanosystems for CD44 Mediated Anti-Inflammatory and Antinociceptive Activity

Saniya Salathia[1], Maria Rosa Gigliobianco[1], Cristina Casadidio[1], Piera Di Martino[1,2] and Roberta Censi[1]

[1]Universita di Camerino, School of Pharmacy, 62032 Camerino, Italy;

[2]Università "G. d'Annunzio" di Chieti e Pescara, Department of Pharmacy, Italy

International Journal of Molecular Sciences **2023**, 24 (8), 7286

Abstract

The nervous and immune systems go hand in hand in causing inflammation and pain. However, the two are not mutually exclusive. While some diseases cause inflammation, there are others that are caused by it. Macrophages play an important role in modulating inflammation to trigger neuropathic pain. Hyaluronic acid (HA) is a naturally occurring glycosaminoglycan that has a well-known ability to bind with the cluster of differentiation 44 (CD44) receptor on classically activated M1 macrophages. Resolving inflammation by varying the molecular weight of HA is a debated concept. HA-based drug delivery nanosystems like nanohydrogels and nanoemulsions, targeting macrophages can be used to relieve pain and inflammation by loading antinociceptive drugs and enhancing the effect of anti-inflammatory drugs. This review will discuss the ongoing research on HA-based drug delivery nanosystems for antinociceptive and anti-inflammatory effects.

1. Introduction

In response to environmental factors and noxious stimuli, the body uses pain as a defence mechanism. Pain is a proactive benefitting immune response in the acute phase, but neuropathic pain becomes problematic in the chronic phase. The nociceptive sensory neurons (nociceptors) activate the neuropathic pain signal, but the immune system also plays a significant factor that defines the active bidirectional crosstalk between pain and inflammation [1]. Nociceptors can control innate and adaptive immune functions by releasing neuropeptides and neurotransmitters [2–5]. In response, neuronal plasticity and chronic pain can be controlled by mediators (lipids, cytokines, and growth factors) released by the immune cells [6–8]. Signals and messages by the nervous system are propagated in milliseconds. This is theorised to be partly why nociceptors are ideally positioned to be first responders to pathogens and tissue injury. Nociceptors release neuropeptides in adverse situations that activate the macrophages of the immune system to control neuropathic pain and inflammation. Increasing evidence from studies shows that macrophages can induce and resolve pain via macrophage-nociceptor interaction [9–11].

Inflammation is a complicated process. It was previously known to be a response to infection, however, in recent years, it has been found that inflammation can cause multiple diseases like atherosclerosis [12], depression [13], Alzheimer's [14] and obesity [15] among others [16,17]. The elevation of inflammatory markers (C-reactive protein) or release of pro-inflammatory cytokines is detected to confirm its presence [18]. Even a minimal increase in the expression of these markers is eligible for inflammation, which can abnormally come without an externally harmful stimulus. Unhealthy lifestyle can be a cause of abnormal inflammation [19–21].

However, inflammation in some cases can be because of easily defined causes like gastritis [22], arthritis [23], neurodegenerative diseases [24] and sepsis [25] where inflammation is called a necessary evil. No doubt, it is a part of the first line of defence, but it is also necessary to keep it in check before chronic derelict harm is caused to the host [26].

Derived from monocytes (M0), macrophages can either polarise to pro-inflammatory or classically activated (M1), or anti-inflammatory or alternatively activated (M2) [27]. M1

macrophages activate pro-inflammatory cytokines and chemokines which initiate and modulate the inflammatory immune response [28].

M1 macrophages have a flat, round cell shape, whereas M2 macrophages are longer and elongated. The macrophage phenotype varies depending on the environmental stimulus as McWhorter *et al* proved in a study, where they tested if the elongation of cells could manipulate the macrophage phenotype [27]. M0 exposed to elongated channels expressed arginase-1 (Arg-1), a marker for M2, and those exposed to wider channels expressed inducible nitric oxide synthase (iNOS), a marker for M1. Modulation of cytokines due to factors such as viruses [29], infections [30] and fibrosis [31] can also manipulate macrophage phenotype. Extensive studies are being performed to imitate body functions and cytokine expressions to get a better understanding of the complicated mechanism of action of macrophage polarisation.

Recent technology and brainstorming have led to several nanosystem designs that can directly target M1 for antinociceptive activities. Ligand-specific nanosystems can directly target individual macrophage receptor to manipulate cytokine release, modulate phenotype expression and protect the cargo from clearance by the reticuloendothelial system (RES) [32,33].

Cluster of differentiation 44 (CD44) is a glycoprotein receptor heavily expressed on the surface of macrophages and tumour cells. It is also a well-known receptor for hyaluronic acid (HA) [34,35], which is a large natural polysaccharide. Hence, the use of HA has been widely studied in cancer research. The chemical composition of HA is repeating units of D-glucuronic acid and N–acetyl-d-glucosamine [33]. A hydrogen bond is formed between the C6-hydroxy group of HA with N-terminus of CD44 to stabilize the binding [36].

CD44 receptor is present in all immune cells but its binding with HA is dependent on homeostatic conditions of the body [37]. HA is heavily present in the extracellular matrix (ECM) during homeostatic conditions due to its ability to retain water [38,39]. During these conditions, alveolar macrophages (displaying a distinct hybrid M1/M2 phenotype [40]) are the only immune cells to bind to HA [37]. However, under inflammatory conditions, reactive oxygen species and nitrogen species break down HA into smaller fragments [41] that undergo phagocytosis by macrophages via CD44-mediated uptake. Lee-Sayer *et al* theorised that the binding of HA with CD44 during inflammation assists in keeping the

macrophages at the site of inflammation and further aiding their function [37]. Therefore, there is minimal HA-CD44 binding during homeostatic conditions.

M1 macrophages have the highest surface presence of CD44 receptor out of all phenotypes [42]. Since chronically inflamed tissue shows a consistent presence of M1, studies have been performed to design drug delivery systems to target the CD44 receptors of these M1 to polarise their phenotype to M2 [43].

'Nanoparticles' is an umbrella term for nanohydrogels, self-assembling nanosystems, nanoemulsions and nanocomposites to name a few. Nanoparticles of HA can be altered in many ways, including structurally and chemically, for drug loading purposes, surface modifications, transdermal delivery or nanoparticle uptake at the target site. Particle size affects the mode of cellular uptake and the efficiency of passing through the body without getting cleared by the RES, lungs, liver or spleen. If the particle size is small (10-20 nm), it is less likely to be taken up by macrophages, which is a problem if you are targeting macrophages, like during therapy for pain and inflammation. The clearance rate for large particles (>1μm) is also high since they tend to aggregate. Therefore, it is suggested that the particle size for drug delivery should be between 20 nm and 1 μm [44–46].

In this review, we focus on the exploitation of HA-based drug delivery nanosystems for optimal CD44 targeting to suppress acute and chronic inflammation, and subsequently neuropathic pain.

2. HA and Inflammation: Influence of Molecular Weight

Different molecular weights (MW) of HA are present in all biological tissues and fluids [47] (Figure 1). Indigenously, high molecular weight (HMW) HA is found, which is then degraded into smaller fragments of low molecular weight (LMW) depending on the environmental factors [48,49]. This degradation of HA is essential for a number of bodily functions, for instance as a lubricant in the synovial fluid [48,50].

Manipulation of MW of HA in drug delivery systems can lead to analgesic, anti-inflammatory and immunostimulatory results [48–51]. Even though there is a lack of detailed research on the specificity of the antinociceptive effects of HA of different MW, it is widely accepted that HMW HA inhibits the activation of lipopolysaccharide (LPS) by directly binding to the toll-like receptor-4 (TLR-4) in inflammatory conditions [52].

To maintain proper functioning, there needs to be a balance between the quantity of HA being produced and degraded in the body [48]. The MW of HA is controlled through the body by shifting between its cellular uptake and degradation under homeostatic conditions. The enzymes hyaluronidases control the degradation of HA [53,54]. Majorly, two types of hyaluronidases (HYAL), HYAL1 and HYAL2, are involved in the active degradation of HA. While HYAL1 targets LMW HA, HYAL2 is known for breaking down HMW HA chains to 20 kDa [53].

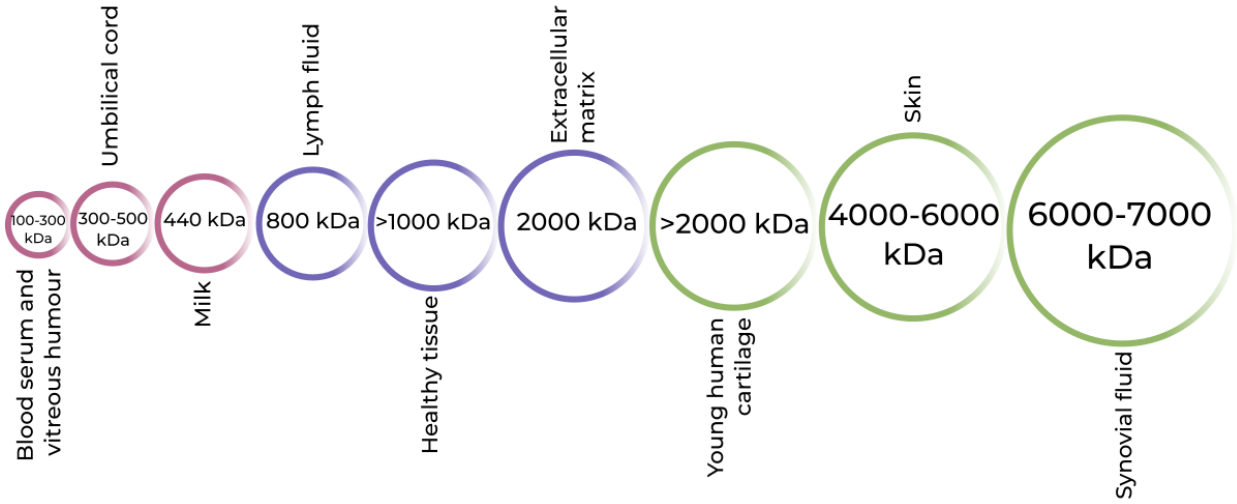

Figure 1. Molecular weights of hyaluronic acid in different parts of the human body.

There is a long-running debate in research regarding the pro/anti-inflammatory properties of HA of different molecular weights. Studies, including Isa *et al,* suggested that HMW HA is linked to having anti-inflammatory properties by inhibiting the production of interleukin-1β, one of the more prominent inflammatory cytokines, and LMW HA is a promoter of inflammation [55–60]. Baeva *et al* provided the explanation that the breakdown of longer chains of HMW HA by HYAL2 produces HA with fewer disaccharides of LMW HA that accumulate at inflamed sites to activate the nuclear factor kappa-light-chain-enhancer of activated B cells (NF-κB) pathway [58] (Figure 2). However, results from the HA hydrogel osteoarthritis (OA) therapy study by Agas *et al* showed that LMW HA (37900 Da) promotes anti-inflammatory properties. The LMW HA hydrogel significantly

lowered the expressions of pro-inflammatory cytokines, tumour necrosis factor-alpha (TNF-α) and interleukin (IL)-1 [59]. Chernos *et al* performed anti-inflammatory studies on human cell lines with butyrylated derivatives of LMW HA for optimal visco-supplements for OA therapy [56]. Chistyakov *et al* also noted that long-term exposure to LMW HA can suppress inflammation induced by the TNF-α pathway [61]. Inflammation is a complex mechanism that involves two major human systems, the nervous and the immune. Ongoing research constantly works on unravelling the mysteries that surround the molecular weights of HA and their effect on pain and inflammation but till now, there is no sure way to say which molecular weight causes and which resolves inflammation.

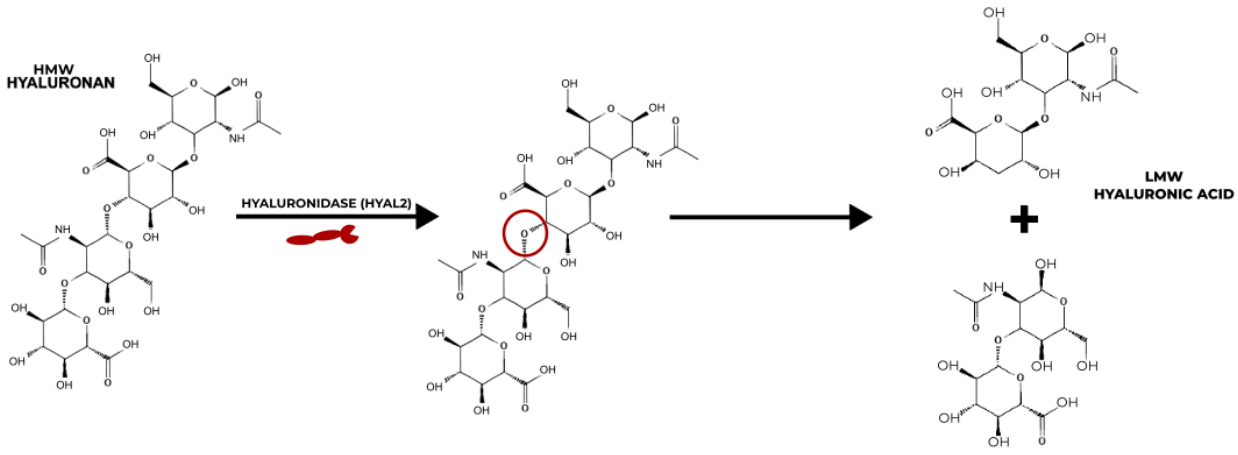

Figure 2: Mechanism of action of HYAL2 on the degradation of HMW HA to LMW HA.

3. HA-Based Nanosystems

HA-based nanosystems can be categorised in a number of ways like nanohydrogels, nanoparticles and self-assembling nanosystems, amongst others (Figure 3). A variety of delivery system designs have been considered for this review that display the vast potential of using HA to counter inflammation, which has been notoriously at the root of many chronic diseases.

3.1. Drug Delivery Systems

Drug delivery systems describe how the drugs are carried into and throughout the body. The following studies use HA to load drugs that are further tested *in vitro* and/or *in vivo*.

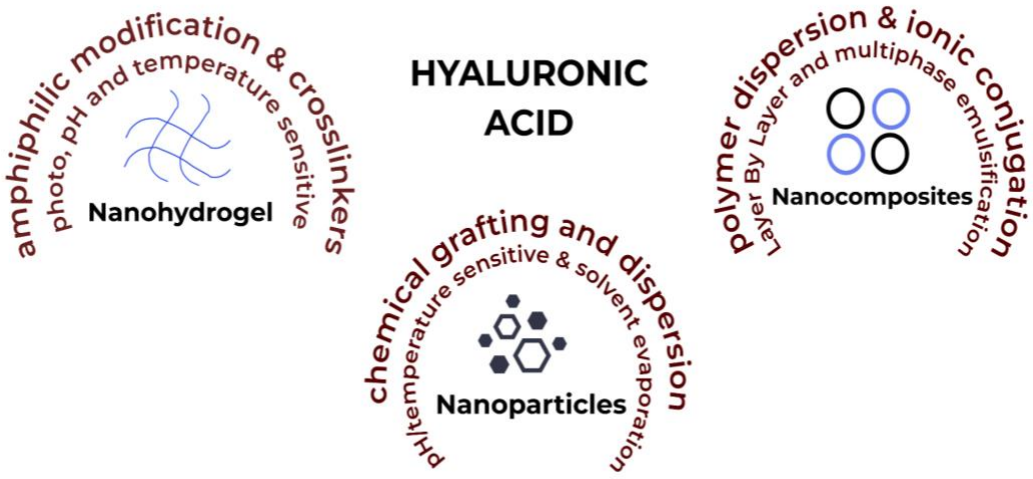

Figure 3. HA-based nanosystems with factors affecting their synthesis and production.

Nanohydrogels are three-dimensional (3D)-polymeric networks at a nanoscale dimension with a crosslinked structure that gives them potential flexibility and versatile behaviour [62,63]. They have the dual advantage of hydrogels for the high encapsulation efficiency of hydrophilic compounds, and of nanostructures for high cellular internalisation [64]. Environmental stimuli like temperature and pH can be used to develop site-specific nanoparticles which makes them an optimal choice for novel theranostic applications [65–67].

Quagliariello *et al* synthesized quercetin-loaded HA nanogel for anti-inflammatory effect in breast tumour cells [68]. The 200 kDa HA used provided protection to the drug from oxidative and enzymatic degradation in the tumour environment. Solvent-non solvent method was used for synthesis with glutaraldehyde as a crosslinker. Drug-loaded nanogel showed a size of 211 nm. Free HA was noted for insignificant cytotoxicity however the crosslinker in the nanogel posed a 10-20% cytotoxic effect. The expressions of anti-inflammatory cytokines (IL-8, IL-6 and IL-19) decreased by up to 55% with nanogel

when compared to the control. A 30-40% increase in anti-oxidative effect was observed when quercetin was co-loaded with everolimus. The group concluded that HA-nanohydrogels provided an excellent template for studying tumour microenvironments, opening perspectives for further studies.

Barbarisi *et al* tested the effect of co-loading quercetin and temozolomide in HA-nanogel as therapy for anti-inflammatory effect in glioblastoma tumour cells [69]. Solvent-non solvent method was used to make nanogel with 200 kDa HA and glutaraldehyde crosslinker. Drug-loaded nanogel had a size of 197 nm and a ζ-potential of -31.3 mV. Just like in their previous study [68], the group noted cytotoxic effects from the crosslinker in the nanogel in this research as well. HA-induced receptor-mediated endocytosis was noted with 30% nanogel internalization after 2 hours. HA on the surface was used for this nanosystem to avoid opsonization by the RES and provide longer drug retention.

While both above-mentioned studies [68,69] successfully synthesized anti-inflammation-promoting nanogels, it should be noted that glutaraldehyde used to stabilize these nanogels was responsible for increasing the cytotoxicity. Further studies need to be performed that can either suggest a lesser toxic crosslinker or a formulation method that does not require a crosslinker for stabilization.

Storozhylova *et al* were looking for an efficient drug delivery system that showed a longer retention rate for treating inflammatory joint diseases [70]. The group synthesised an *in situ* forming non-crosslinked HA-fibrin hydrogels containing HA-nanocapsules co-loaded with dexamethasone and galectin-3 inhibitor. The drug-loaded nanocapsules showed suppression of inflammation after intra-articular administration. However, the study noted that further investigation was required to treat chronic synovial inflammation.

It is beneficial to develop a drug delivery system that gives positive results in terms of efficiency, but it is even better to design a system that involves a hassle-free administration route. Even though injectable nanohydrogels are considered non-invasive techniques, nonetheless transdermal drug deliveries take this definition one step further. As previously mentioned, transdermal drug delivery (TDD) has classically more successfully been associated with the use of nanoparticles. TDD is a painless method of delivering therapeutics onto intact skin [71,72]. Nanosize [73], drug retention [74], and drug release rates [75] of polymeric nanohydrogels are a winning factor in their wide use as a targeted TDD method, and actually, nanohydrogel size is essential for successful skin

penetration. Nanohydrogels can be manipulated into loading drug-loaded nanocapsules that successfully penetrate the skin and intake water. This leads to the swelling of the nanocapsules and subsequent drug release [76–78].

Wei *et al* tested the anti-inflammatory effect of topically administered HA nanohydrogels with baicalin-nanocrystals (NC) [79]. An 800-100 kDa HA nanogel was used to assist the skin permeability of poorly soluble baicalin. Four w/v concentrations of HA were used to optimise the nanogel, 0.5%, 1%, 1.5% and 2%. The increase in HA concentration witnessed an increase in the viscosity and elasticity of the nanogel, however, it also saw a decrease in the drug release rate and skin permeation rate. The 1% w/v HA was chosen as the optimal concentration with a 20-fold increase in skin permeability as compared to the control. The size of 1% w/v HA nanogel was 193 nm.

The biodegradability of HA allows for homogenous drug distribution in the gel matrix [80,81]. Liu *et al* used electrospinning to make absorbable nanofibrous hydrogel for wound healing in chronic diabetic conditions [82] (Figure 4). A 1400 kDa thioether grafted HA, crosslinked with Fe^{3+} (FHHA-S/Fe) nanogel was synthesized for the purpose of wound healing by modulating the site of injury. Overall, the crosslinking increased the stability of the nanofibres by 2-fold. Complete absorption of the nanogel was observed at 72 hours. The thioether grafting increased IL-4 expression by 33% and 18% faster wound healing as compared to the non-ether nanogel. A 24% decrease in the expression of M1 macrophages was observed along with a 22% increase in the expression of M2 macrophages after treatment with HMW HA nanogel treatment.

Just like previously mentioned studies [68,69], this research [82] also used a crosslinker to stabilize their nanogel. However, Fe^{3+} showed no cytotoxic effect. In fact, it also provided antibacterial properties to the nanosystem.

Pleguezuelos-Villa *et al* synthesized mangiferin-loaded HA-based nanoemulsions for anti-inflammatory effect for skin lesions [83]. Two ranges of MW of HA were tested for the nanoemulsions, 40-50 kDa (LMW) and 1000-1200 kDa (HMW). The LMW HA nanoemulsion size was detected at 221 nm and for HMW it was at 393 nm. A gradually sustained release of the drug was found in all nanosystems after 24 hours but LMW HA nanoemulsion with surfactant was the highest with 10-15%. The different MW of HA did not affect the oedema inhibition for the anti-inflammatory activity of the nanoemulsion.

However, the use of surfactant decreased the oedema inhibition activity of the nanoemulsion. HMW HA only seemed to have affected the size of the nanoemulsion.

Manca *et al* used curcumin-loaded HA vesicles (hyalurosomes) for skin lesions [84]. This study evolved the field of vesicles by synthesizing hyalurosomes. The group enhanced the properties of conventional liquid vesicles by including a gel-core structure to provide more stability and a nanosized diameter to make them nanovesicles. The organic solvent-free polymer dispersion method was used for the synthesis. Two w/v concentrations of 200-400 kDa HA were tested, 0.1% and 0.5%. 0.1% showed a size of 166 nm and an encapsulation efficiency of 76% whereas 0.5% showed a size of 157 nm and a curcumin encapsulation efficiency of 79%. The enhanced nanovesicle structure increased the encapsulation by 10-13% as compared to conventional liposomal vesicles. On the contrary, 0.5% w/v hyalurosomes showed a higher viscosity than 0.1% and more stiffness by 14% with the addition of curcumin. Higher improvement in induced skin lesions in *in vivo* tests was seen in 0.5% w/v hyalurosomes. Re-epithelialized skin was also observed by day 6.

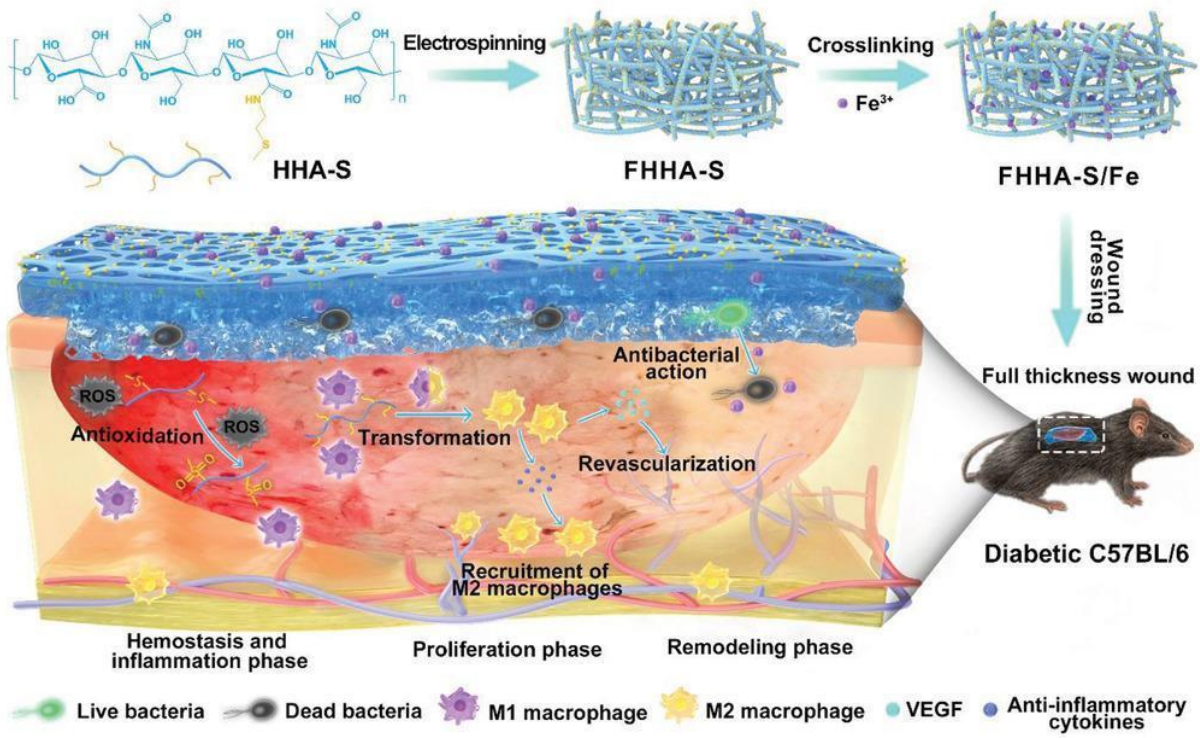

Figure 4. Schematic illustration of the absorbable thioether grafted hyaluronic acid nanofibrous hydrogel for synergistic modulation of the inflammation microenvironment

to accelerate chronic diabetic wound healing. Illustration of the preparation procedure of FHHA-S/Fe, dressing of FHHA-S/Fe on full-thickness wound model in diabetic C57BL/6 mouse, and the mechanism of FHHA-S/Fe for enhanced chronic wound healing effect. Copyright Wiley-VCH Verlag GmbH. Reprinted with permission from [82].

Yang *et al* synthesized HA nanostructured lipid carriers (NLCs) loaded with ropivacaine (RVC) and dexmedetomidine (DMDT) [85]. NLCs are evolved lipid nanoparticles that include both liquid and solid lipids that decrease the order of crystal arrangement of conventional lipid nanoparticles to provide a higher drug loading efficiency [86]. The group used the solvent diffusion method to create an HA-based (3 kDa) drug delivery system that increased the duration of analgesic effects of RVC and DMDT by 75%. The NLCs had a size of 108 nm, a ζ-potential of -30.7 mV due to the presence of HA and drug encapsulation efficiency of 89.5% for RVC and 88.1% for DMDT respectively. The HA NLCs also increased the cell viability of the drugs from 61.2% (free drug solution) to 80%. The group also performed *in vivo* skin permeation tests that showed that the encapsulation of the drugs in the NLCs increased their permeability by 67%. The NLCs also increased the antinociceptive effect of the drugs by 80 minutes. It was also found that co-loading RVC and DMDT had a higher analgesic effect than loading a single drug.

Yue *et al* also decided to formulate NLCs for TDD of their drug bupivacaine (BPV) for local anaesthesia [87]. The group used 300 kDa HA modified with linoleic acid and polyethylene glycol (PEG) for stealth properties. The NLCs were made with lipid melt-emulsification and solvent injection techniques that had a size of 154 nm, a ζ-potential of -40.1 mV and a BPV encapsulation efficiency of 88.9%. The NLCs showed cell viability of 70% as compared to 40% by free drug solution. *In vivo* tests showed an increased antinociceptive effect by the NLCs as compared to free drug solution by 50%.

Both the above-mentioned studies [85,87] used NLCs for their formulations, however, there were some notable differences between the two drug delivery systems. After 75 hours of administration, one of the NLCs [85] showed a 70% antinociceptive activity whereas it was only at 60% for the other NLC [87]. While it may not be a major difference, it is possible that the synergistic effect of co-loading two drugs favoured the former. The higher size of NLC by the latter can be attributed to their use of HMW HA.

Iannitti *et al* tested the efficacy of HA and chondroitin sulfate (CS) based medical device called Esoxx® for the treatment of the inflammation of the gastric mucosa, also known as gastritis [88]. The presence of HA and CS was seen to reduce inflammation and the discomfort that comes along with it in the tested patients. HA provides hydrophilicity to the submucosal connective tissue which provides it with a better chance of healing. The group, however, concluded that further studies are needed with a higher number of patients for definitive results.

3.2. Macrophage Targeting Nanosystems

It has been well established that macrophages have an important role to play in modulating inflammatory responses and pain [10,11,43]. The pro-inflammatory M1-macrophage phenotype is responsible for the first line of defence which is inflammation. Hence, for antinociceptive therapies, studies have developed nanosystems that target the CD44 receptor, heavily present on the surface of M1 macrophages. These therapies either work by lowering/inhibiting the effect of pro-inflammatory cytokines or polarising the macrophage phenotype from M1 to M2.

Zhang *et al* used layer by layer (LBL) NLC system for lidocaine (LA) loaded chitosan and HA drug delivery system [89] (Figure 5). LBL involves the alternative deposition of oppositely charged polyelectrolytes via electrostatic interaction for the assembly of multilayer films. This method decreases the drug release rate and enhances skin permeability. The group compared the characteristics of LBL-NLCs with simple NLCs. It is important to note that the size of the nanoparticles is a major deciding factor in whether the drug delivery system will reach the target site. The NLCs showed a size of 181 nm and a ζ-potential of +37.6 mV due to the outermost layer of chitosan. The *in vivo* tests for anaesthesia showed that NLCs had a 30% effect after 24 hours of administration whereas LBL-NLCs had an 80% effect. The combined biocompatibility of hyaluronic acid and chitosan provides a great template for the loading of drugs and target studies [90].

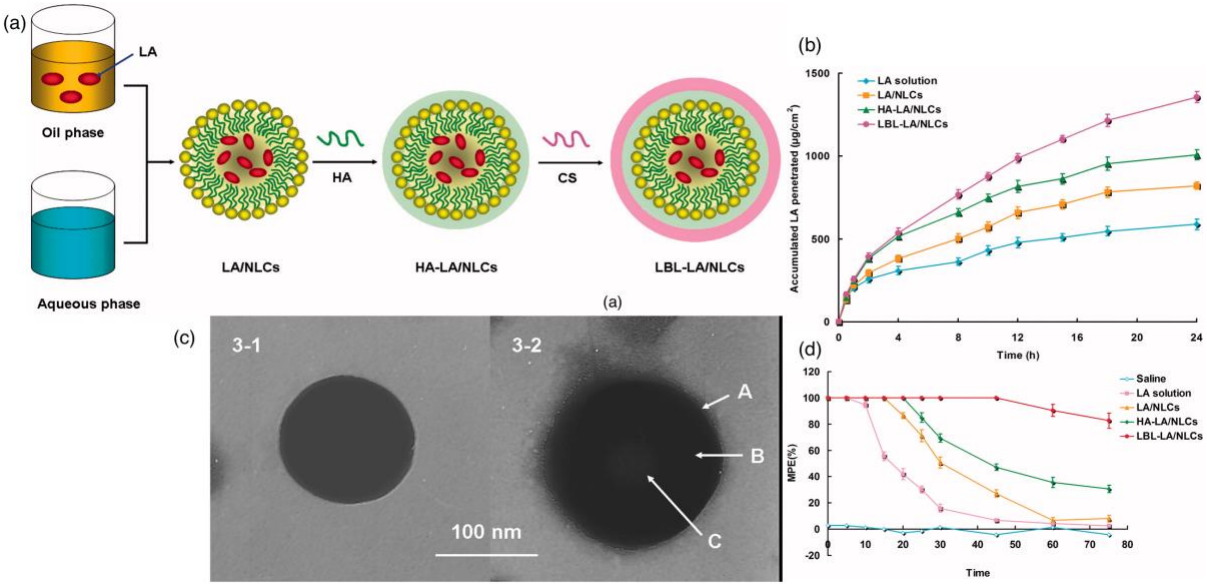

Figure 5. (a) Scheme of the fabrication of LBL-LA/NLCs. (b) In vitro permeation profiles of LA from different formulations. (c) TEM images of the structural morphology of the LBL-LA/NLCs and LA/NLCs. (d) In vivo TFL test for the evaluation of the local anesthetic effects of LA-containing formulations. Adapted with permission from [89].

Farajzadeh *et al* synthesized curcumin-loaded HA-polylactide (PLA) nanoparticles to test CD44-targeted antinociceptive activity and macrophage repolarization [43]. A HA of 20 kDa MW was used to prepare HA-PLA conjugates of 102 nm in size, ζ-potential of -24.5 mV and a curcumin encapsulation efficiency of 88%. Mouse peritoneal macrophages were used for *in vitro* studies that detected a burst release in the first 8 hours of administration and consistent subsequent release with 33% drug release after 144 hours (6 days). The initial burst release could be due to the presence of the drug closer to the surface of the nanoparticles. *In vivo* nanoparticle uptake is promoted by endocytosis, hence, it is necessary to stimulate the nanoparticles in similar conditions. Endocytosis is supported by an acidic environment, so the group also tested the drug release from the nanoparticles at a pH of 4.4. This test showed a 50% drug release after 120 hours of administration. Markers for M1 and M2 macrophages (iNOS and Arg-1, respectively) were quantified to check macrophage repolarization. Curcumin-loaded nanoparticles increased Arg-1 expression by 50% as compared to free drug administration. This concluded the successful repolarization of M1 macrophages to M2 macrophages. Expressions of pro-inflammatory cytokines, TNF-α, IL-1β and IL-6, were also reduced by 86%, 85% and 87% respectively, when compared to free drug administration.

Tran *et al* also experimented with shifting the macrophage polarity as a way of therapy for inflammation [91]. But instead of curcumin, they encapsulated plasmid deoxyribonucleic acid (pDNA) in their HA nanoparticles by modifying HA with a positively charged polymer poly(ethyleneimine) (PEI) (Figure 6). The pDNA expressed interleukin-4 (IL-4) and interleukin-10 (IL-10) genes that inhibit the production of TNF-α, which is a direct promoter of M1-expressed inflammatory cytokines. This reduction in the expression of TNF-α also leads to lower M1 polarisation and subsequent higher M2 polarisation [92]. However, direct administration of IL-4 and IL-10 is reported to have toxic effects. So, the group combined gene therapy with nanotechnology to synthesise a nanosystem that not only represses inflammatory cytokines but also polarises macrophages towards alternative activation.

Kosovrasti *et al* targeted another M1-specific cytokine for reducing inflammation, TNF-α [93]. The group encapsulated TNF-α specific small interfering RNA (siTNF-α) in HA nanoparticles. The formulation of the nanoparticles involved the blending of HA-PEI, HA-hexyl fatty acid and HA-PEG. The 78-90 nm diameter HA nanoparticles encapsulating siTNF-α reduced the level of production of LPS-induced TNF-α in macrophages and hence reduced inflammation. The group concluded that this study could be beneficial in researching therapy for acute inflammatory diseases.

It is important to note that the nanosystems developed in two previously mentioned studies [43,91] were not tested *in vivo,* and both groups concluded that further studies were needed to certain the effect of their respective HA-based nanosystems in complex *in vivo* homeostatic conditions. However, HA nanoparticles encapsulating siTNF-α by the group [93] were tested *in vivo* and expected anti-inflammatory results were found. But they also noted that the results from one study should not be considered conclusive evidence.

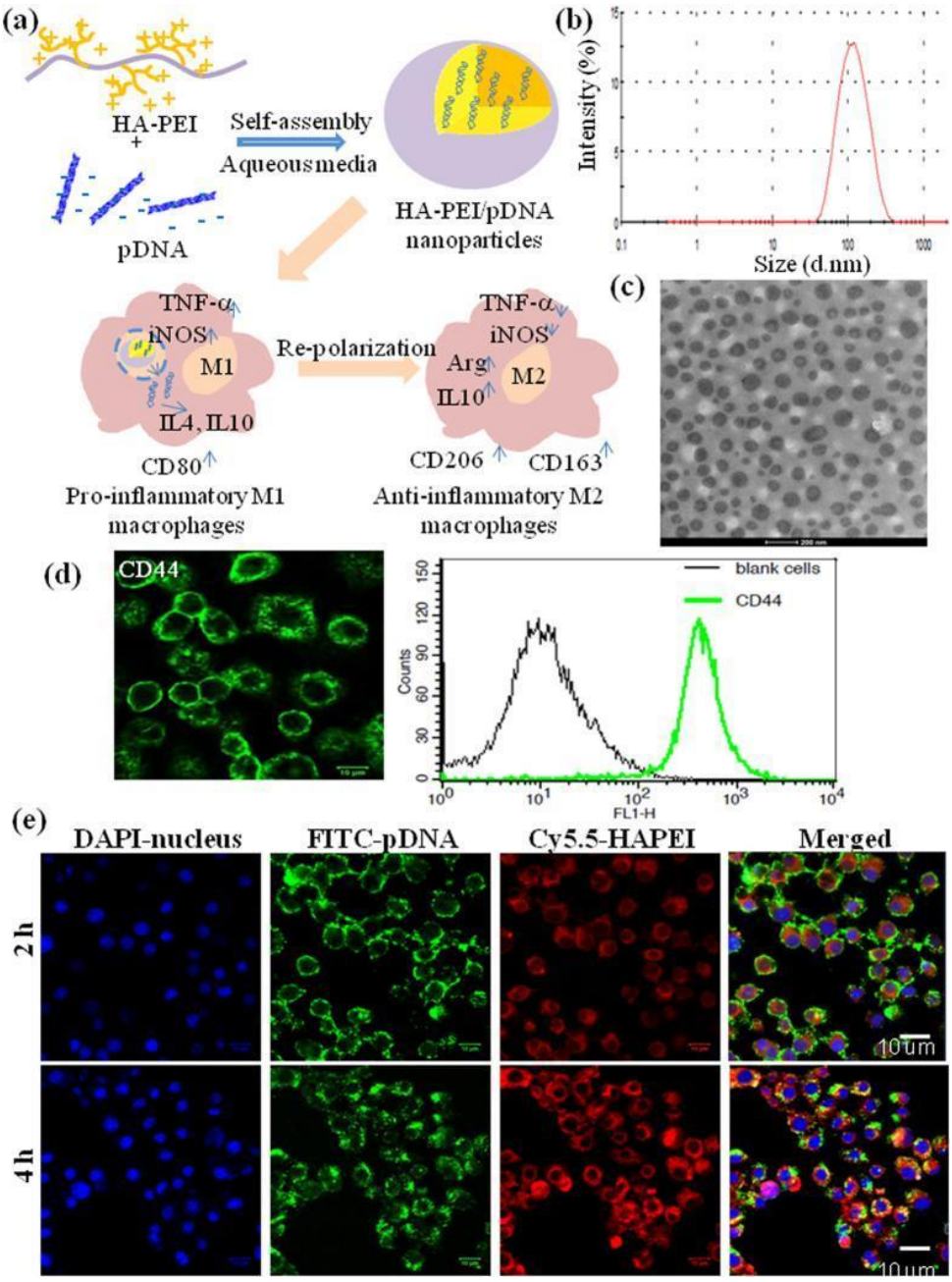

Figure 6. (a) Schematic illustration of pDNA encapsulation into HA-PEI nanoparticles for re-polarization of pro-inflammatory M1 macrophages to anti-inflammatory M2 macrophages. (b) Size distribution of HA-PEI/pDNA (9:1) in PBS by DLS. (c) TEM image of HA-PEI/pDNA in PBS (9:1). (d) Confocal microscopy and FACS analysis of CD44 expression in J774A.1 macrophages. (e) Uptake of HA-PEI/pDNA nanoparticles in J774A.1 macrophages. Reprinted with permission from [91].

Xie *et al* used HA-containing ethosomes (ES) for the delivery of rhodamine B for TDD [94]. Ethosomes are a kind of liposomal vesicles that are known for increasing skin

permeability, drug accumulation and targeting drug delivery [95–97] to avoid systemic toxicity. A 150 kDa HA was used for enhancing the drug entrapment in the ES using amphiphilic modifications in the HA backbone. Different ratios of HA:ES were tested for optimization, 2.5:1, 5:1 and 10:1. The increase in the ratio of HA led to an increase in the size of the drug delivery system with a range of 593-916 nm as per dynamic light scattering (DLS), however, transmission electron microscopy (TEM) detected the size of the system <100 nm. This difference can be because TEM analysis is conducted on a dry sample and DLS is performed in water which leads to swelling of the particles. High HA concentration also led to an increase in the quantity of the encapsulated drug. *In vivo* tests were conducted which noted skin permeation within 30 minutes of administration. HA was also noted to increase the effectiveness of the system by 30% as compared to the drug delivery system without HA. Therefore, the 5:1 ratio was concluded to be optimal.

The specific targeting ability of HA and its transdermal absorption is paramount in its use of TDD [98]. HA is a major synovial fluid component and artificially administered HA provides temporary relief for OA [99]. Zerrillo *et al* decided to take advantage of the low pH conditions in the synovial fluid and synthesize HA-loaded pH-responsive poly(lactic-co-glycolic acid) (PLGA) nanoparticles with a triggered burst release for OA [100]. The therapeutic approach of HA on OA partly includes reducing the inflammation at the OA site. The burst release of drug in this study was triggered by the ammonium bicarbonate loaded in the PLGA nanoparticles. The 750-1000 kDa HA was injected into the PLGA nanoparticles that showed a size of 202 nm and 28% encapsulation efficiency. *In vitro* studies showed that PLGA-HA nanoparticles had a faster uptake than only PLGA nanoparticles. *In vivo* studies were also conducted that showed that pH-responsive nanoparticles had a faster cargo release than non-pH-responsive nanoparticles. Fluorescence showed the presence of the nanoparticles in the knee even after 35 days of administration. The group concluded that a combined therapy of pH-responsive and non-pH-responsive nanoparticles would have a synergistic effect for optimal therapeutic conditions. Therefore, pH-responsive nanoparticles would have a burst release and non-pH-responsive nanoparticles would have a gradual steady release of the drug.

Zerrillo *et al* conducted another study where they tested HA-grafted PLGA nanoparticles for OA therapy [101]. Conventional HA therapy has a rapid clearance and short retention

time. Grafting is used as a method to overcome these issues. In this case, a 20 kDa HA is used to make a PLGA copolymer and further into PLGA-HA nanoparticles. The nanoparticles showed a size of 200 nm. Near-infrared dye tests showed that PLGA-HA nanoparticles had a 20% lower release rate after 10 days. There was a 2-fold increase in the *in vitro* binding studies for PLGA-HA nanoparticles. The intra-articular injection was used for *in vivo* tests. After 48 hours, PLGA-HA nanoparticles were noted to have penetrated the cartilage, unlike PLGA nanoparticles without HA.

Histochemical immunostaining has reported OA synovium to have a higher number of CD44 receptors than normal. This leads to an increase in inflammation due to the active presence of pro-inflammatory cytokines. This has further led to the increased targeting of CD44 as therapy for OA using HA, a well-known CD44 ligand [102–105].

3.3. Self-Assembling Nanosystems

The molecular arrangement of disorganised components into ordered structures as a response to external stimulus is known as self-assembly. It is a phenomenon often found in nature. Biological nanostructures come self-assembled to form DNA double helix, cell membranes, peptide chains, etc [106–108].

Vafaei *et al* tested budesonide (BDS) loaded self-assembled HA nanosystem as a therapeutic agent for inflamed intestinal mucosa caused by inflammatory bowel disease (IBD) [109]. The self-assembling effect was enhanced by amphiphilic chemical modifications to the HA backbone. The 10 and 25 kDa HA were tested and the thin film hydration method was used to load BDS. The human colon carcinoma cell line was used for *in vitro* tests. The increased degree of chemical modification showed a decrease in the size of nanoparticles. The size for 10 kDa HA decreased by 97 nm and for 25 kDa HA the size decreased by 61 nm.

Mota *et al* synthesized a PLGA-loaded HA hybrid system for viscosupplementation in OA [110]. The group used 1500-1800 kDa HA, 45-75 kDa PLGA and a modified-spontaneous emulsification/solvent diffusion method for synthesis. Oleic acid was also used to propagate long-term controlled drug release and provide stability to the nanosystem. DLS was used to check the size of HA-loaded PLGA particles (373 nm) and oleic acid-modified particles (4561 nm). The increase in the size of particles with oleic acid was attributed to particle agglomeration. Since DLS cannot differentiate between particle

agglomeration and large size, atomic force microscopy (AFM) was used to check the size for oleic acid-modified particles which showed a particle size of 409 nm. The use of the hybrid system for HA administration increased the drug release rate to up to 8 hours, as compared to the instant dissolution of free HA. *In vivo* anti-inflammatory effect was tested for free HA solution (76.9%) and HA-PLGA particles (82.6%).

Currently, the most common commercially available treatment method of OA is the intra-articular injection of HMW HA. The therapy shows results but is short-lived owing to the fact that HMW HA is prone to active HYAL-mediated degradation [48,53,111]. Kang *et al* realised the potential of using self-assembling HA nanoparticles as an alternative therapy for OA [111] (Figure 7). The group chemically modified the backbone of 10kDa HA with cholanic acid to create amphiphilic HA nanoparticles. The 221 nm nanoparticles were tested *in vivo* and *in vitro* where they showed remarkable improvement to conventional HMW HA OA therapy. *In vitro* studies noted that HA-nanoparticles had a larger CD44-mediated uptake and cartilage penetration up to 41 μm than free HA. Intra-articular injections were used for *in vivo* studies where it was observed that HA-nanoparticles blocked the CD44 receptor and prevented further cartilage degeneration in OA-induced mice, unlike free HMW HA. Attenuated NF-κB pathway activity was also noted to prevent pro-inflammatory cytokine expression. The group concluded that empty amphiphilic HA-nanoparticles had a higher resistance to HYAL degradation than free HA. This study has much potential to be continued with loading HA-nanoparticles to increase efficacy.

El-Refaie *et al* also tested the use of hyalusomes, however, they made them self-assembling TDD hyalusomes to be used for OA [112]. The film hydration technique was used to make 1% w/v HA (8-11.7 kDa) hyalusomes. The elasticity of the system was increased by the addition of ethanol. Ethanol-modified gel-core hyalusomes showed a size of 226 nm with an encapsulation efficiency of 32.6%. *Ex vivo* results showed that the skin permeability of gel-core hyalusomes was increased by 5.5-fold as compared to 1% HA solution. *In vivo* results also favoured the increase in HA in joint tissues by 6-fold after gel-core hyalusome administration.

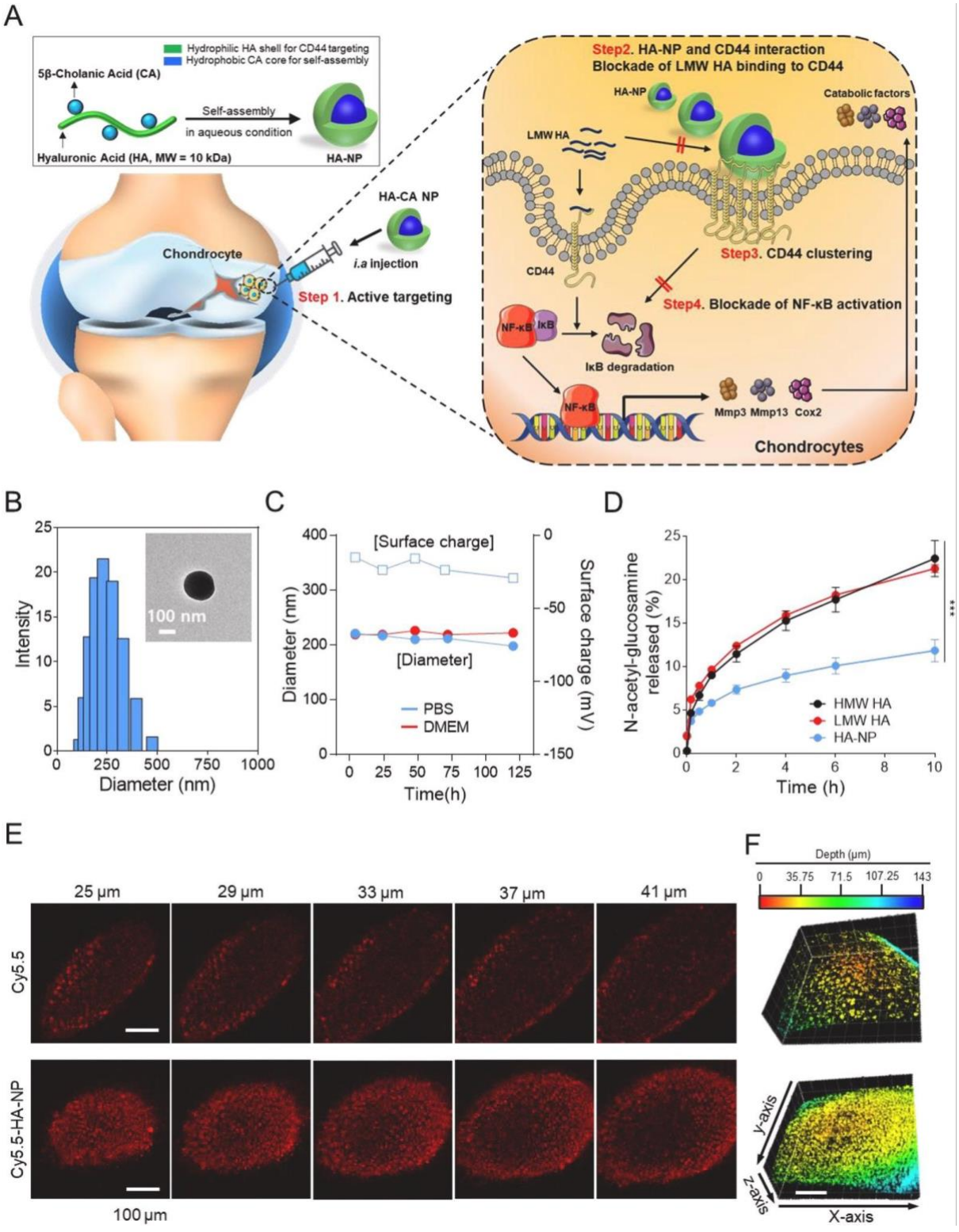

Figure 7. Characteristics of HA-NPs. (A) Schematic illustration of HA-NPs for treatment of OA. (B) TEM images and size distribution of HA-NP. Scale bar, 100 nm. (C) Time-dependent changes in particle size and surface charge of HA-NP in PBS and DMEM. Data are presented as mean ± SEM (n = 5). (D) Generation of N-acetyl-glucosamine after treatment of 1 mg/ml free HAs (10 kDa LMW and 2000 kDa HMW) or HA-NP with 100 IU/ml

HYAL-II. Data are presented as mean ± SEM (n = 4). ***P < 0.001. (E) Representative serial images (25–41 μm depth at intervals of 4 μm) from the femoral cartilages after i.a. injection of Cy5.5 and Cy5.5-labeled HA-NP into normal mice. Scale bars, 100 μm. (F) Three-dimensional lateral view of the femoral cartilages after i.a. injection of Cy5.5 and Cy5.5-labeled HA-NP into normal mice. Scale bars, 100 μm. Reprinted with permission from [111].

4. Hyaluronic Acid Nanosystems, Study Gaps and Future Directions

The active involvement of HA in inflammation makes it a top contender in being used as a nanosized drug carrier. However, it is also its negative charge that is critical for *in vivo* use. Several studies have reported that positively charged particles are more prone to causing the secretion of cytokines, inducing more T-cell proliferation that causes the recruitment of cytotoxic T cells directly damaging the erythrocyte membrane, and eliciting an immune response [113–118].

The rapid evolution of nanotechnology has changed the fundamental chemical, physical and physiological aspects of a successful drug delivery system [119]. Nanosystems come in different shapes and sizes, like nanohydrogels, nanoparticles, nanocomposites, and self-assembling nanoparticles, among others. With their high drug encapsulation efficiency and biological efficacy, they have become the top contenders for research in therapeutics, diagnostics and imaging. Table 1 summarises the HA-based nanosystems referred to in this review.

In this review, we highlight the recent advancements in HA-based nanosystems being developed for antinociceptive and anti-inflammatory activities. With an overview of the mechanism of action of pain and inflammation, we consolidated some of how HA-based nanosystems are being used as drugs and encapsulating agents to target CD44 receptor on macrophages for therapy for various disorders, such as gastritis [90], IBD [109], breast cancer [68], glioblastoma [69], inflammatory joint disease [70,112], wound healing [82], local anaesthetic [87], OA [100,101,110–112] and skin lesions [83,84]. These drug-encapsulating nanosystems have shown increased pharmacokinetic properties as compared to solo drug administration due to their biological versatility and targeting ability.

The size of the nanosystem is important for successful targeted drug delivery action. Nanosystems <100 nm are rapidly cleared by the RES and macromolecules are cleared

by the kidney and the spleen. The HA-based nanosystems mentioned above fall between the preferred range of drug delivery systems that can favourably avoid clearance by the body. The hydrophilicity of HA provides the nanosystem with a stealth effect that avoids opsonization [120].

Along with the advantages of using HA, it is also important not to overlook the challenges that come along with it. The effect of the molecular weight of HA on inflammation is not completely understood. Broadly it is accepted that HMW HA holds anti-inflammatory properties and LMW HA is pro-inflammatory [55,56]. However, Zerrillo *et al* found anti-inflammatory results with LMW HA [100,101]. In designing and synthesising nanosystems, LMW HA is given a preference due to the ease of working with it. LMW HA also produces smaller size nanosystems that are more effectively hidden against clearance by the immune system. As Kang *et al* reported, HMW HA is degraded by HYAL, which is avoided with LMW HA [111]. Further studies are required to clearly lay out the role of different MWs of HA in the functioning of the human body.

The delivery method of the nanosystem to the target area also affects the drug design. Therapeutics is moving more and more toward simpler, non-invasive drug delivery designs. This, however, can pose a limitation on synthesising the nanosystem. For instance, more and more research is being conducted on the advancement of TDD systems. The anionic nature of HA poses a problem in this case. The hydrophilicity of HA reduces its rate of skin permeability [121,122]. Although this can be overcome by either performing hydrophobic modifications of the HA chain or coating it with a hydrophobic compound (like chitosan), it still poses a challenge as it may not be a feasible step for the proposed function of the nanosystem.

Most of the nanosystems mentioned in this review are in the concept stage. Some have only undergone *in vitro* experimentation, while others conclude that further *in vivo* studies are required. No conclusive result can be stated until more research is conducted. There is a gap in understanding the working of pro and anti-inflammatory cytokines that control macrophage polarisation. Getting a clearer picture of the biological mechanisms involved will help optimise the nanosystems for more targeted action. Furthermore, the preclinical drug delivery models need to be tested for biodegradability for reduced toxicity, absorbability and high retention rate for a prolonged effect.

Translating biomaterials from laboratory experiments to commercial development takes decades [123,124]. Newer inventions must undergo a longer safety protocol to get approved. It is far easier to have a medical device that is "substantially equivalent" to one already on the market than a newer one to get Food and Drug Administration (FDA) approved [125–127]. So, while lab experiments continue to give positive results, they need to undergo further rigorous testing for years to be commercially available.

Table 1. Summary of HA-based nanosystems discussed in the review.

Nanosystem	**HA in nanosystem**	**Administration Route**	**Formulation Method**	**Characterisation**	**Drug**	**Therapy**	**Reference**
Drug Delivery Systems							
HA-nanogel loading quercetin	200 kDa Sodium hyaluronate	-	Solvent-non solvent method	Size: 211.3 nm ζ: -35.8±1.3 mV	quercetin	Anti-inflammatory effect in breast cancer tumour cells	[68]
HA-nanogel loading quercetin	200 kDa Sodium hyaluronate	-	Solvent-non solvent method	Size: 197.3 ± 3.3 nm ζ: -31.3±1.1 mV	quercetin	Anti-inflammatory effect in glioblastoma tumour cells	[69]

Non-crosslinked HA-fibrin hydrogels containing HA-shell nanocapsules co-loaded with dexamethasone and galectin-3 inhibitor	40 kDa, 700 kDa, 1.5 MDa Sodium hyaluronate	Intra-articular	Solvent displacement method	Size: 122-135 nm ζ: -29±5 mV	dexamethasone and galectin-3 inhibitor	Therapy for inflammatory joint diseases	[70]
HA nanocrystal hydrogels loading baicalin	800-1000 kDa Sodium hyaluronate	TDD system	Homogenization	Size: 189.21±0.36 nm	baicalin	anti-inflammation	[79]
Thioether-grafted HA nanofibrous hydrogel	1400 kDa Sodium hyaluronate, thioether modified and crosslinked with Fe^{3+}	TDD system	Electrospinning	Size: 60±11 nm	HMW HA	wound healing in diabetic conditions	[82]

HA-based mangiferin nanoemulsion	40-50 kDa and 1-1.2 MDa HA	TDD system	Emulsion method	Size: 296 nm ζ: -30 mV	mangiferin	Anti-inflammation for skin lesions	[83]
Curcumin-loaded HA-nanovesicles	200-400 kDa Sodium Hyaluronate	TDD system	Organic solvent-free dispersion method	Size: 157-166 nm ζ: 24±4 mV	curcumin	Anti-inflammation for skin lesions	[84]
HA nanostructured lipid carriers loading ropivacaine and dexmedetomidine	3 kDa HA, PEG-DSPE modified	TDD system	Solvent diffusion method	Size: 108.2±3.3 nm ζ: -30.7±2.8 mV	Ropivacaine and dexmedetomidine	Local analgesic	[85]
HA-modified nanostructured lipid carriers loading bupivacaine	300 kDa HA	Local administration	Emulsification and solvent injection methods	Size: 154.6±5.1 nm ζ: -40.1±3.9 mV	bupivacaine	Local anaesthetic	[87]
HA-chondroiti	-	Oral delivery	-	-	Esoxx®	Gastritis	[88]

n sulfate medical device (Esoxx)							
Macrophage Targeting Nanosystems							
HA-polylactide nanoparticles encapsulating curcumin	20 kDa Sodium hyaluronate	-	Solvent evaporation method	Size: 102.5 nm ζ: -24.5±2.2 mV	Curcumin	Macrophage repolarisation	[43]
HA-chitosan lipid nanostructures loading lidocaine (layer-by-layer)	-	TDD system	Melt-emulsification method	Size: 181.2 nm ζ: +37.6±4.2 mV	Lidocaine	Local anaesthesia	[89]
HA-nanoparticles loading pDNA	20 kDa Sodium hyaluronate	*in vitro* transfection	Coupling reaction	Size: 185.9 nm ζ: -11.6mV	pDNA	Macrophage repolarisation	[91]

HA-nanoparticles encapsulating siTNFα	20 kDa Sodium hyaluronate	Transfection	-	Size: 85-110 nm	TNF-α specific small interfering RNA	Inhibiting LPS-induced inflammation	[93]
HA containing ethosomes encapsulating rhodamine	150 kDa Sodium hyaluronate	TDD system	Homogenization	Size: 593.8 nm ζ: +10 mV	Rhodamine	Quick, high efficiency TDD system	[94]
pH-responsive HA-loaded PLGA nanoparticles	750-1000 kDa Sodium hyaluronate	Intra-articular injection	Single-emulsion solvent evaporation method	Size: 202.7±2.3 nm ζ: -21.0 mV	HMW HA	Osteoarthritis	[100]
HA decorated on PLGA nanoparticle surface	21-40 kDa Sodium hyaluronate	Intra-articular injection	Double-emulsion solvent method	Size: 200±2 nm ζ: -23±2 mV	HMW HA	Osteoarthritis	[101]
Self-Assembling Nanosystems							

HA-nanoparticles loading BDS	10-25 kDa Sodium hyaluronate, DA modified for amphiphilicity	*in vitro* dynamic dialysis drug release study	Thin film hydration method	Size: 207±11 nm ζ: -14.56±0.22 mV	Budesonide	IBD induced pain/inflammation	[109]
HA-PLGA hybrid systems	1.5-1.8 MDa Sodium hyaluronate	Viscosupplementation	Spontaneous emulsification solvent diffusion method	Size: 373±270 nm ζ: -16.65 mV	HMW HA	Osteoarthritis	[110]
Amphiphilic HA-nanoparticles	10 kDa HA	Intra-articular injection	Chemical conjugation	Size: 221±1 nm ζ: 15.08±0.83mV	LMW HA	OA treatment	[111]
Gel-core HA nanovesicles	8-11.7 kDa HA	TDD system	Thin layer evaporation technique	Size: 232.8±7.2 nm ζ: -45.1±8.3 mV	HMW HA	OA therapy	[112]

5. Conclusion

HA presents multiple beneficial characteristics like biocompatibility, hydrophilicity, biodegradability, non-toxicity, and binding ability with CD44 receptor, that make it an optimal choice for usage in anti-inflammatory drug delivery systems. Studies have shown that it can be formulated as a hydrogel, nanocomposite, nanoparticle or

superficially and chemically modified for wider targetability. Combining it with other compounds (PLGA, chitosan, etc.), enhances its chemical (amphiphilicity) and biological (resistance to HYAL degradation) properties, improves the efficacy of the nanosystems, and increases its *in vivo* half-life leading to prolonged drug release [128,129]. While there still needs much testing and designing in the proposed nanosystems, the results have been fairly positive with HA displaying high anti-inflammatory properties and CD44 targeting ability.

Funding: This research was funded by European Commission H2020-MSCA-ITN-2020-PIANO, grant number 956477.

Conflicts of Interest: The authors declare no conflict of interest.

6. References

(1) Pinho-Ribeiro, F. A.; Verri, W. A.; Chiu, I. M. Nociceptor Sensory Neuron–Immune Interactions in Pain and Inflammation. *Trends Immunol* 2017, *38* (1), 5–19. https://doi.org/10.1016/J.IT.2016.10.001.

(2) Kashem, S. W.; Riedl, M. S.; Yao, C.; Honda, C. N.; Vulchanova, L.; Kaplan, D. H. Nociceptive Sensory Fibers Drive Interleukin-23 Production from CD301b+ Dermal Dendritic Cells and Drive Protective Cutaneous Immunity. *Immunity* 2015, *43* (3), 515–526. https://doi.org/10.1016/J.IMMUNI.2015.08.016.

(3) Calil, I. L.; Zarpelon, A. C.; Guerrero, A. T. G.; Alves-Filho, J. C.; Ferreira, S. H.; Cunha, F. Q.; Cunha, T. M.; Verri, W. A. Lipopolysaccharide Induces Inflammatory Hyperalgesia Triggering a TLR4/MyD88-Dependent Cytokine Cascade in the Mice Paw. *PLoS One* 2014, *9* (3), e90013. https://doi.org/10.1371/JOURNAL.PONE.0090013.

(4) Gabanyi, I.; Muller, P. A.; Feighery, L.; Oliveira, T. Y.; Costa-Pinto, F. A.; Mucida, D. Neuro-Immune Interactions Drive Tissue Programming in Intestinal Macrophages. *Cell* 2016, *164* (3), 378–391. https://doi.org/10.1016/J.CELL.2015.12.023.

(5) Kurashige, C.; Hosono, K.; Matsuda, H.; Tsujikawa, K.; Okamoto, H.; Majima, M. Roles of Receptor Activity-Modifying Protein 1 in Angiogenesis and Lymphangiogenesis during Skin Wound Healing in Mice. *The FASEB Journal* 2014, *28* (3), 1237–1247. https://doi.org/10.1096/FJ.13-238998.

(6) Kiguchi, N.; Kobayashi, Y.; Maeda, T.; Fukazawa, Y.; Tohya, K.; Kimura, M.; Kishioka, S. Epigenetic Augmentation of the Macrophage Inflammatory Protein 2/C-X-C Chemokine Receptor Type 2 Axis through Histone H3 Acetylation in Injured Peripheral Nerves Elicits Neuropathic Pain. *Journal of Pharmacology and Experimental Therapeutics* 2012, *340* (3), 577–587. https://doi.org/10.1124/JPET.111.187724.

(7) Kobayashi, Y.; Kiguchi, N.; Fukazawa, Y.; Saika, F.; Maeda, T.; Kishioka, S. Macrophage-T Cell Interactions Mediate Neuropathic Pain through the Glucocorticoid-Induced Tumor Necrosis Factor Ligand System. *Journal of Biological Chemistry* 2015, *290* (20), 12603–12613. https://doi.org/10.1074/JBC.M115.636506.

(8) Old, E. A.; Nadkarni, S.; Grist, J.; Gentry, C.; Bevan, S.; Kim, K. W.; Mogg, A. J.; Perretti, M.; Malcangio, M. Monocytes Expressing CX3CR1 Orchestrate the Development of Vincristine-Induced Pain. *J Clin Invest* 2014, *124* (5), 2023–2036. https://doi.org/10.1172/JCI71389.

(9) Chen, O.; Donnelly, C. R.; Ji, R.-R. Regulation of Pain by Neuro-Immune Interactions between Macrophages and Nociceptor Sensory Neurons. *Curr Opin Neurobiol* 2020, *62*, 17–25. https://doi.org/10.1016/j.conb.2019.11.006.

(10) Shepherd, A. J.; Mickle, A. D.; Golden, J. P.; Mack, M. R.; Halabi, C. M.; De Kloet, A. D.; Samineni, V. K.; Kim, B. S.; Krause, E. G.; Gereau, R. W.; Mohapatra, D. P. Macrophage Angiotensin II Type 2 Receptor Triggers Neuropathic Pain. *Proc Natl Acad Sci U S A* 2018, *115* (34), E8057–E8066. https://doi.org/10.1073/PNAS.1721815115.

(11) Shutov, L. P.; Warwick, C. A.; Shi, X.; Gnanasekaran, A.; Shepherd, A. J.; Mohapatra, D. P.; Woodruff, T. M.; David Clark, J.; Usachev, Y. M. The Complement System Component C5a Produces Thermal Hyperalgesia via Macrophage-to-Nociceptor Signaling That Requires NGF and TRPV1. *Journal of Neuroscience* 2016, *36* (18), 5055–5070. https://doi.org/10.1523/JNEUROSCI.3249-15.2016.

(12) Zhu, Y.; Xian, X.; Wang, Z.; Bi, Y.; Chen, Q.; Han, X.; Tang, D.; Chen, R. Research Progress on the Relationship between Atherosclerosis and Inflammation. *Biomolecules 2018, Vol. 8, Page 80* 2018, *8* (3), 80. https://doi.org/10.3390/BIOM8030080.

(13) Beurel, E.; Toups, M.; Nemeroff, C. B. The Bidirectional Relationship of Depression and Inflammation: Double Trouble. *Neuron* 2020, *107* (2), 234–256. https://doi.org/10.1016/J.NEURON.2020.06.002.

(14) Newcombe, E. A.; Camats-Perna, J.; Silva, M. L.; Valmas, N.; Huat, T. J.; Medeiros, R. Inflammation: The Link between Comorbidities, Genetics, and Alzheimer's Disease. *Journal of Neuroinflammation 2018 15:1* 2018, *15* (1), 1–26. https://doi.org/10.1186/S12974-018-1313-3.

(15) Deng, T.; Lyon, C. J.; Bergin, S.; Caligiuri, M. A.; Hsueh, W. A. Obesity, Inflammation, and Cancer. *https://doi.org/10.1146/annurev-pathol-012615-044359* 2016, *11*, 421–449. https://doi.org/10.1146/ANNUREV-PATHOL-012615-044359.

(16) Liu, M.; Huang, Q.; Zhu, Y.; Chen, L.; Li, Y.; Gong, Z.; Ai, K. Harnessing Reactive Oxygen/Nitrogen Species and Inflammation: Nanodrugs for Liver Injury. *Mater Today Bio* 2022, *13*. https://doi.org/10.1016/J.MTBIO.2022.100215.

(17) Sun, Q.; Ma, H.; Zhang, J.; You, B.; Gong, X.; Zhou, X.; Chen, J.; Zhang, G.; Huang, J.; Huang, Q.; Yang, Y.; Ai, K.; Bai, Y. A Self-Sustaining Antioxidant Strategy for Effective Treatment of Myocardial Infarction. *Advanced Science* 2023, *10* (5), 2204999. https://doi.org/10.1002/ADVS.202204999.

(18) Antonelli, M.; Kushner, I. It's Time to Redefine Inflammation. *FASEB Journal* 2017, *31* (5), 1787–1791. https://doi.org/10.1096/FJ.201601326R.

(19) Park, K. H.; Zaichenko, L.; Peter, P.; Davis, C. R.; Crowell, J. A.; Mantzoros, C. S. Diet Quality Is Associated with Circulating C-Reactive Protein but Not Irisin Levels in Humans. *Metabolism* 2014, *63* (2), 233–241. https://doi.org/10.1016/J.METABOL.2013.10.011.

(20) Wu, W. Te; Tsai, S. S.; Shih, T. S.; Lin, M. H.; Chou, T. C.; Ting, H.; Wu, T. N.; Liou, S. H. The Impact of Obstructive Sleep Apnea on High-Sensitivity C-Reactive Protein in Subjects with or without Metabolic Syndrome. *Sleep Breath* 2015, *19* (4), 1449–1457. https://doi.org/10.1007/S11325-015-1166-2.

(21) Heffner, K. L.; Waring, M. E.; Roberts, M. B.; Eaton, C. B.; Gramling, R. Social Isolation, C-Reactive Protein, and Coronary Heart Disease Mortality among Community-Dwelling Adults. *Soc Sci Med* 2011, *72* (9), 1482–1488. https://doi.org/10.1016/J.SOCSCIMED.2011.03.016.

(22) Varbanova, M.; Frauenschläger, K.; Malfertheiner, P. Chronic Gastritis – An Update. *Best Pract Res Clin Gastroenterol* 2014, *28* (6), 1031–1042. https://doi.org/10.1016/J.BPG.2014.10.005.

(23) Mateen, S.; Zafar, A.; Moin, S.; Khan, A. Q.; Zubair, S. Understanding the Role of Cytokines in the Pathogenesis of Rheumatoid Arthritis. *Clinica Chimica Acta* 2016, *455*, 161–171. https://doi.org/10.1016/J.CCA.2016.02.010.

(24) Brown, G. C. The Endotoxin Hypothesis of Neurodegeneration. *Journal of Neuroinflammation 2019 16:1* 2019, *16* (1), 1–10. https://doi.org/10.1186/S12974-019-1564-7.

(25) Nedeva, C.; Menassa, J.; Puthalakath, H. Sepsis: Inflammation Is a Necessary Evil. *Front Cell Dev Biol* 2019, *7* (JUN), 108. https://doi.org/10.3389/FCELL.2019.00108/BIBTEX.

(26) Netea, M. G.; Balkwill, F.; Chonchol, M.; Cominelli, F.; Donath, M. Y.; Giamarellos-Bourboulis, E. J.; Golenbock, D.; Gresnigt, M. S.; Heneka, M. T.; Hoffman, H. M.; Hotchkiss, R.; Joosten, L. A. B.; Kastner, D. L.; Korte, M.; Latz, E.; Libby, P.; Mandrup-Poulsen, T.; Mantovani, A.; Mills, K. H. G.; Nowak, K. L.; O'Neill, L. A.; Pickkers, P.; Van Der Poll, T.; Ridker, P. M.; Schalkwijk, J.; Schwartz, D. A.; Siegmund, B.; Steer, C. J.; Tilg, H.; Van Der Meer, J. W. M.; Van De Veerdonk, F. L.; Dinarello, C. A. A Guiding Map for Inflammation. *Nature Immunology 2017 18:8* 2017, *18* (8), 826–831. https://doi.org/10.1038/ni.3790.

(27) McWhorter, F. Y.; Wang, T.; Nguyen, P.; Chung, T.; Liu, W. F. Modulation of Macrophage Phenotype by Cell Shape. *Proceedings of the National Academy of Sciences* 2013, *110* (43), 17253–17258. https://doi.org/10.1073/PNAS.1308887110.

(28) Mukhtar, M.; Ali, H.; Ahmed, N.; Munir, R.; Talib, S.; Khan, A. S.; Ambrus, R. Drug Delivery to Macrophages: A Review of Nano-Therapeutics Targeted Approach for Inflammatory Disorders and Cancer. *Expert Opinion on Drug Delivery*. Taylor and Francis Ltd September 1, 2020, pp 1239–1257. https://doi.org/10.1080/17425247.2020.1783237.

(29) Sang, Y.; Miller, L. C.; Blecha, F. Macrophage Polarization in Virus-Host Interactions. *J Clin Cell Immunol* 2015, *6* (2). https://doi.org/10.4172/2155-9899.1000311.

(30) Schleicher, U.; Paduch, K.; Debus, A.; Obermeyer, S.; König, T.; Kling, J. C.; Ribechini, E.; Dudziak, D.; Mougiakakos, D.; Murray, P. J.; Ostuni, R.; Körner, H.; Bogdan, C. TNF-Mediated Restriction of Arginase 1 Expression in Myeloid Cells Triggers Type 2 NO Synthase Activity at the Site of Infection. *Cell Rep* 2016, *15* (5), 1062–1075. https://doi.org/10.1016/J.CELREP.2016.04.001.

(31) Vannella, K. M.; Barron, L.; Borthwick, L. A.; Kindrachuk, K. N.; Narasimhan, P. B.; Hart, K. M.; Thompson, R. W.; White, S.; Cheever, A. W.; Ramalingam, T. R.; A. Wynn, T.

Incomplete Deletion of IL-4Rα by LysMCre Reveals Distinct Subsets of M2 Macrophages Controlling Inflammation and Fibrosis in Chronic Schistosomiasis. *PLoS Pathog* 2014, *10* (9), e1004372. https://doi.org/10.1371/JOURNAL.PPAT.1004372.

(32) Jain, N. K.; Mishra, V.; Mehra, N. K. Targeted Drug Delivery to Macrophages. *http://dx.doi.org/10.1517/17425247.2013.751370* 2013, *10* (3), 353–367. https://doi.org/10.1517/17425247.2013.751370.

(33) Dreaden, E. C.; Morton, S. W.; Shopsowitz, K. E.; Choi, J. H.; Deng, Z. J.; Cho, N. J.; Hammond, P. T. Bimodal Tumor-Targeting from Microenvironment Responsive Hyaluronan Layer-by-Layer (LbL) Nanoparticles. *ACS Nano* 2014, *8* (8), 8374–8382. https://doi.org/10.1021/NN502861T/SUPPL_FILE/NN502861T_SI_001.PDF.

(34) Xiao, B.; Xu, Z.; Viennois, E.; Zhang, Y.; Zhang, Z.; Zhang, M.; Han, M. K.; Kang, Y.; Merlin, D. Orally Targeted Delivery of Tripeptide KPV via Hyaluronic Acid-Functionalized Nanoparticles Efficiently Alleviates Ulcerative Colitis. *Molecular Therapy* 2017, *25* (7), 1628–1640. https://doi.org/10.1016/J.YMTHE.2016.11.020.

(35) Dahiya, P.; Kamal, R. Hyaluronic Acid: A Boon in Periodontal Therapy. *N Am J Med Sci* 2013, *5* (5), 309–315. https://doi.org/10.4103/1947-2714.112473.

(36) Bhattacharya, D. S.; Svechkarev, D.; Souchek, J. J.; Hill, T. K.; Taylor, M. A.; Natarajan, A.; Mohs, A. M. Impact of Structurally Modifying Hyaluronic Acid on CD44 Interaction †. *J. Mater. Chem. B* 2017, *5*, 8183. https://doi.org/10.1039/c7tb01895a.

(37) Lee-Sayer, S. S. M.; Dong, Y.; Arif, A. A.; Olsson, M.; Brown, K. L.; Johnson, P. The Where, When, How, and Why of Hyaluronan Binding by Immune Cells. *Front Immunol* 2015, *6* (MAR). https://doi.org/10.3389/fimmu.2015.00150.

(38) Dicker, K. T.; Gurski, L. A.; Pradhan-Bhatt, S.; Witt, R. L.; Farach-Carson, M. C.; Jia, X. Hyaluronan: A Simple Polysaccharide with Diverse Biological Functions. *Acta Biomater* 2014, *10* (4), 1558–1570. https://doi.org/10.1016/J.ACTBIO.2013.12.019.

(39) Choi, J. U.; Lee, S. W.; Pangeni, R.; Byun, Y.; Yoon, I. S.; Park, J. W. Preparation and in Vivo Evaluation of Cationic Elastic Liposomes Comprising Highly Skin-Permeable Growth Factors Combined with Hyaluronic Acid for Enhanced Diabetic Wound-Healing Therapy. *Acta Biomater* 2017, *57*, 197–215. https://doi.org/10.1016/J.ACTBIO.2017.04.034.

(40) Mitsi, E.; Kamng'ona, R.; Rylance, J.; Solórzano, C.; Jesus Reiné, J.; Mwandumba, H. C.; Ferreira, D. M.; Jambo, K. C. Human Alveolar Macrophages Predominately Express

Combined Classical M1 and M2 Surface Markers in Steady State. *Respir Res* 2018, *19* (1), 1–4. https://doi.org/10.1186/S12931-018-0777-0/FIGURES/1.

(41) Monzon, M. E.; Fregien, N.; Schmid, N.; Falcon, N. S.; Campos, M.; Casalino-Matsuda, S. M.; Forteza, R. M. Reactive Oxygen Species and Hyaluronidase 2 Regulate Airway Epithelial Hyaluronan Fragmentation. *Journal of Biological Chemistry* 2010, *285* (34), 26126–26134. https://doi.org/10.1074/jbc.M110.135194.

(42) Rios de la Rosa, J. M.; Tirella, A.; Gennari, A.; Stratford, I. J.; Tirelli, N. The CD44-Mediated Uptake of Hyaluronic Acid-Based Carriers in Macrophages. *Adv Healthc Mater* 2017, *6* (4). https://doi.org/10.1002/adhm.201601012.

(43) Farajzadeh, R.; Zarghami, N.; Serati-Nouri, H.; Momeni-Javid, Z.; Farajzadeh, T.; Jalilzadeh-Tabrizi, S.; Sadeghi-Soureh, S.; Naseri, N.; Pilehvar-Soltanahmadi, Y. Macrophage Repolarization Using CD44-Targeting Hyaluronic Acid–Polylactide Nanoparticles Containing Curcumin. *Artif Cells Nanomed Biotechnol* 2017, *46* (8), 1–9. https://doi.org/10.1080/21691401.2017.1408116.

(44) Kwon, S. S.; Kong, B. J.; Park, S. N. Physicochemical Properties of PH-Sensitive Hydrogels Based on Hydroxyethyl Cellulose-Hyaluronic Acid and for Applications as Transdermal Delivery Systems for Skin Lesions. *Eur J Pharm Biopharm* 2015, *92*, 146–154. https://doi.org/10.1016/J.EJPB.2015.02.025.

(45) Yu, M.; Zheng, J. Clearance Pathways and Tumor Targeting of Imaging Nanoparticles. *ACS Nano* 2015, *9* (7), 6655–6674. https://doi.org/10.1021/ACSNANO.5B01320/SUPPL_FILE/NN5B01320_SI_001.PDF.

(46) Ernsting, M. J.; Murakami, M.; Roy, A.; Li, S. D. Factors Controlling the Pharmacokinetics, Biodistribution and Intratumoral Penetration of Nanoparticles. *Journal of Controlled Release* 2013, *172* (3), 782–794. https://doi.org/10.1016/J.JCONREL.2013.09.013.

(47) Cowman, M. K.; Lee, H. G.; Schwertfeger, K. L.; McCarthy, J. B.; Turley, E. A. The Content and Size of Hyaluronan in Biological Fluids and Tissues. *Front Immunol* 2015, *6* (JUN), 261. https://doi.org/10.3389/FIMMU.2015.00261/BIBTEX.

(48) Rayahin, J. E.; Buhrman, J. S.; Zhang, Y.; Koh, T. J.; Gemeinhart, R. A. High and Low Molecular Weight Hyaluronic Acid Differentially Influence Macrophage Activation. *ACS Biomater Sci Eng* 2015, *1* (7). https://doi.org/10.1021/acsbiomaterials.5b00181.

(49) Lee, B. M.; Park, S. J.; Noh, I.; Kim, C.-H. The Effects of the Molecular Weights of Hyaluronic Acid on the Immune Responses. *Biomater Res* 2021, *25* (1), 27. https://doi.org/10.1186/s40824-021-00228-4.

(50) Scaturro, D.; Vitagliani, F.; Terrana, P.; Tomasello, S.; Falco, V.; Cuntrera, D.; Spoto, I.; Midiri, M.; Mauro, G. L. Hybrid Hyaluronic Acid versus High Molecular Weight Hyaluronic Acid for the Treatment of Hip Osteoarthritis in Overweight/Obese Patients. *J Funct Morphol Kinesiol* 2022, *7* (1). https://doi.org/10.3390/jfmk7010020.

(51) Sharath, S. S.; Ramu, J.; Nair, S. V.; Iyer, S.; Mony, U.; Rangasamy, J. Human Adipose Tissue Derivatives as a Potent Native Biomaterial for Tissue Regenerative Therapies. *Tissue Engineering and Regenerative Medicine*. 2020. https://doi.org/10.1007/s13770-019-00230-x.

(52) Yoon, J. Y.; Kim, D. W.; Ahn, J. H.; Choi, E. J.; Kim, Y. H.; Jeun, M.; Kim, E. J. Propofol Suppresses LPS-Induced Inflammation in Amnion Cells via Inhibition of NF-KB Activation. *Tissue Eng Regen Med* 2019, *16* (3). https://doi.org/10.1007/s13770-019-00194-y.

(53) Erickson, M.; Stern, R. Chain Gangs: New Aspects of Hyaluronan Metabolism. *Biochemistry Research International*. 2012. https://doi.org/10.1155/2012/893947.

(54) Bala, E.; Hazarika, R. A Biological Overview of Hyaluronidase: A Venom Enzyme and Its Inhibition with Plants Materials. *Mater Today Proc* 2018, *5*, 6406–6412.

(55) Misra, S.; Hascall, V. C.; Markwald, R. R.; Ghatak, S. Interactions between Hyaluronan and Its Receptors (CD44, RHAMM) Regulate the Activities of Inflammation and Cancer. *Frontiers in Immunology*. 2015. https://doi.org/10.3389/fimmu.2015.00201.

(56) Chernos, M.; Grecov, D.; Kwok, E.; Bebe, S.; Oladunni Babsola, •; Anastassiades, T. Rheological Study of Hyaluronic Acid Derivatives. *Biomed Eng Lett 7*. https://doi.org/10.1007/s13534-017-0010-y.

(57) Dhapte, V.; Pokharkar, V. Nanosystems for Drug Delivery: Design, Engineering, and Applications. *Green Synthesis, Characterization and Applications of Nanoparticles* 2019, 321–345. https://doi.org/10.1016/B978-0-08-102579-6.00013-7.

(58) Baeva, L. F.; Lyle, D. B.; Rios, M.; Langone, J. J.; Lightfoote, M. M. Different Molecular Weight Hyaluronic Acid Effects on Human Macrophage Interleukin 1β Production. *J Biomed Mater Res A* 2014, *102* (2). https://doi.org/10.1002/jbm.a.34704.

(59) Agas, D.; Laus, F.; Lacava, G.; Marchegiani, A.; Deng, S.; Magnoni, F.; Silva, G. G.; Di Martino, P.; Sabbieti, M. G.; Censi, R. Thermosensitive Hybrid Hyaluronan/p(HPMAm-

Lac)-PEG Hydrogels Enhance Cartilage Regeneration in a Mouse Model of Osteoarthritis. *J Cell Physiol* 2019, *234* (11), 20013–20027. https://doi.org/10.1002/JCP.28598.

(60) Isa, I. L. M.; Srivastava, A.; Tiernan, D.; Owens, P.; Rooney, P.; Dockery, P.; Pandit, A. Hyaluronic Acid Based Hydrogels Attenuate Inflammatory Receptors and Neurotrophins in Interleukin-1β Induced Inflammation Model of Nucleus Pulposus Cells. *Biomacromolecules* 2015, *16* (6), 1714–1725. https://doi.org/10.1021/acs.biomac.5b00168.

(61) Chistyakov, D. V.; Astakhova, A. A.; Azbukina, N. V.; Goriainov, S. V.; Chistyakov, V. V.; Sergeeva, M. G. High and Low Molecular Weight Hyaluronic Acid Differentially Influences Oxylipins Synthesis in Course of Neuroinflammation. *International Journal of Molecular Sciences 2019, Vol. 20, Page 3894* 2019, *20* (16), 3894. https://doi.org/10.3390/IJMS20163894.

(62) Quazi, M. Z.; Park, N. Nanohydrogels: Advanced Polymeric Nanomaterials in the Era of Nanotechnology for Robust Functionalization and Cumulative Applications. *International Journal of Molecular Sciences*. MDPI February 1, 2022. https://doi.org/10.3390/ijms23041943.

(63) Mayumi, K.; Liu, C.; Yasuda, Y.; Ito, K. Softness, Elasticity, and Toughness of Polymer Networks with Slide-Ring Cross-Links. *Gels* 2021, *7* (3). https://doi.org/10.3390/GELS7030091.

(64) Qian, Z. Y.; Fu, S. Z.; Feng, S. S. Nanohydrogels as a Prospective Member of the Nanomedicine Family. *Nanomedicine* 2013, *8* (2), 161–164. https://doi.org/10.2217/NNM.13.1/FORMAT/EPUB.

(65) Suhail, M.; Rosenholm, J. M.; Minhas, M. U.; Badshah, S. F.; Naeem, A.; Khan, K. U.; Fahad, M. Nanogels as Drug-Delivery Systems: A Comprehensive Overview. *https://doi.org/10.4155/tde-2019-0010* 2019, *10* (11), 697–717. https://doi.org/10.4155/TDE-2019-0010.

(66) Soni, K. S.; Desale, S. S.; Bronich, T. K. Nanogels: An Overview of Properties, Biomedical Applications and Obstacles to Clinical Translation. *Journal of Controlled Release* 2016, *240*, 109–126. https://doi.org/10.1016/J.JCONREL.2015.11.009.

(67) Sivaram, A. J.; Rajitha, P.; Maya, S.; Jayakumar, R.; Sabitha, M. Nanogels for Delivery, Imaging and Therapy. *Wiley Interdiscip Rev Nanomed Nanobiotechnol* 2015, *7* (4), 509–533. https://doi.org/10.1002/WNAN.1328.

(68) Quagliariello, V.; Iaffaioli, R. V.; Armenia, E.; Clemente, O.; Barbarisi, M.; Nasti, G.; Berretta, M.; Ottaiano, A.; Barbarisi, A. Hyaluronic Acid Nanohydrogel Loaded With Quercetin Alone or in Combination to a Macrolide Derivative of Rapamycin RAD001 (Everolimus) as a New Treatment for Hormone-Responsive Human Breast Cancer. *J Cell Physiol* 2017, *232* (8), 2063–2074. https://doi.org/10.1002/jcp.25587.

(69) Barbarisi, M.; Iaffaioli, R. V.; Armenia, E.; Schiavo, L.; De Sena, G.; Tafuto, S.; Barbarisi, A.; Quagliariello, V. Novel Nanohydrogel of Hyaluronic Acid Loaded with Quercetin Alone and in Combination with Temozolomide as New Therapeutic Tool, CD44 Targeted Based, of Glioblastoma Multiforme. *J Cell Physiol* 2018, *233* (10), 6550–6564. https://doi.org/10.1002/jcp.26238.

(70) Storozhylova, N.; Crecente-Campo, J.; Cabaleiro, D.; Lugo, L.; Dussouy, C.; Simões, S.; Monteiro, M.; Grandjean, C.; Alonso, M. J. An In Situ Hyaluronic Acid-Fibrin Hydrogel Containing Drug-Loaded Nanocapsules for Intra-Articular Treatment of Inflammatory Joint Diseases. *Regen Eng Transl Med* 2020, *6* (2), 201–216. https://doi.org/10.1007/s40883-020-00154-2.

(71) Han, T.; Das, D. B. Potential of Combined Ultrasound and Microneedles for Enhanced Transdermal Drug Permeation: A Review. *Eur J Pharm Biopharm* 2015, *89*, 312–328. https://doi.org/10.1016/J.EJPB.2014.12.020.

(72) Schoellhammer, C. M.; Blankschtein, D.; Langer, R. Skin Permeabilization for Transdermal Drug Delivery: Recent Advances and Future Prospects. *https://doi.org/10.1517/17425247.2014.875528* 2014, *11* (3), 393–407. https://doi.org/10.1517/17425247.2014.875528.

(73) Gupta, S.; Bansal, R.; Gupta, S.; Jindal, N.; Jindal, A. Nanocarriers and Nanoparticles for Skin Care and Dermatological Treatments. *Indian Dermatol Online J* 2013, *4* (4), 267. https://doi.org/10.4103/2229-5178.120635.

(74) Nunes, D.; Andrade, S.; Ramalho, M. J.; Loureiro, J. A.; Pereira, M. C. Polymeric Nanoparticles-Loaded Hydrogels for Biomedical Applications: A Systematic Review on In Vivo Findings. *Polymers (Basel)* 2022, *14* (5). https://doi.org/10.3390/POLYM14051010.

(75) Jiang, Y.; Krishnan, N.; Heo, J.; Fang, R. H.; Zhang, L. Nanoparticle–Hydrogel Superstructures for Biomedical Applications. *Journal of Controlled Release* 2020, *324*, 505–521. https://doi.org/10.1016/J.JCONREL.2020.05.041.

(76) Carbinatto, F. M.; de Castro, A. D.; Evangelista, R. C.; Cury, B. S. F. Insights into the Swelling Process and Drug Release Mechanisms from Cross-Linked Pectin/High Amylose Starch Matrices. *Asian J Pharm Sci* 2014, *9* (1), 27–34. https://doi.org/10.1016/J.AJPS.2013.12.002.

(77) Ko, S. W.; Lee, J. Y.; Lee, J.; Son, B. C.; Jang, S. R.; Aguilar, L. E.; Oh, Y. M.; Park, C. H.; Kim, C. S. Analysis of Drug Release Behavior Utilizing the Swelling Characteristics of Cellulosic Nanofibers. *Polymers (Basel)* 2019, *11* (9). https://doi.org/10.3390/POLYM11091376.

(78) Hezaveh, H.; Muhamad, I. I.; Noshadi, I.; Shu Fen, L.; Ngadi, N. Swelling Behaviour and Controlled Drug Release from Cross-Linked -Carrageenan/NaCMC Hydrogel by Diffusion Mechanism. *J Microencapsul* 2012, *29* (4), 368–379. https://doi.org/10.3109/02652048.2011.651501.

(79) Wei, S.; Xie, J.; Luo, Y.; Ma, Y.; Tang, S.; Yue, P.; Yang, M. Hyaluronic Acid Based Nanocrystals Hydrogels for Enhanced Topical Delivery of Drug: A Case Study. *Carbohydr Polym* 2018, *202*, 64–71. https://doi.org/10.1016/j.carbpol.2018.08.112.

(80) Fan, M.; Ma, Y.; Zhang, Z.; Mao, J.; Tan, H.; Hu, X. Biodegradable Hyaluronic Acid Hydrogels to Control Release of Dexamethasone through Aqueous Diels–Alder Chemistry for Adipose Tissue Engineering. *Materials Science and Engineering: C* 2015, *56*, 311–317. https://doi.org/10.1016/J.MSEC.2015.04.004.

(81) Tan, H.; Fan, M.; Ma, Y.; Qiu, J.; Li, X.; Yan, J. Injectable Gel Scaffold Based on Biopolymer Microspheres via an Enzymatic Reaction. *Adv Healthc Mater* 2014, *3* (11), 1769–1775. https://doi.org/10.1002/ADHM.201400123.

(82) Liu, S.; Zhang, Q.; Yu, J.; Shao, N.; Lu, H.; Guo, J.; Qiu, X.; Zhou, D.; Huang, Y.; Liu, S.; Zhang, Q.; Yu, J.; Shao, N.; Lu, H.; Zhou, D.; Huang, Y.; Qiu, X. Absorbable Thioether Grafted Hyaluronic Acid Nanofibrous Hydrogel for Synergistic Modulation of Inflammation Microenvironment to Accelerate Chronic Diabetic Wound Healing. 2020. https://doi.org/10.1002/adhm.202000198.

(83) Pleguezuelos-Villa, M.; Nácher, A.; Hernández, M. J.; Ofelia Vila Buso, M. A.; Ruiz Sauri, A.; Díez-Sales, O. Mangiferin Nanoemulsions in Treatment of Inflammatory Disorders and Skin Regeneration. *Int J Pharm* 2019, *564*, 299–307. https://doi.org/10.1016/j.ijpharm.2019.04.056.

(84) Manca, M. L.; Castangia, I.; Zaru, M.; Nácher, A.; Valenti, D.; Fernàndez-Busquets, X.; Fadda, A. M.; Manconi, M. Development of Curcumin Loaded Sodium Hyaluronate Immobilized Vesicles (Hyalurosomes) and Their Potential on Skin Inflammation and Wound Restoring. *Biomaterials* 2015, *71*, 100–109. https://doi.org/10.1016/j.biomaterials.2015.08.034.

(85) Yang, Y.; Qiu, D.; Liu, Y.; Chao, L. Topical Anesthetic Analgesic Therapy Using the Combination of Ropivacaine and Dexmedetomidine: Hyaluronic Acid Modified Long-Acting Nanostructured Lipid Carriers Containing a Skin Penetration Enhancer. *Drug Des Devel Ther* 2019, *13*, 3307–3319. https://doi.org/10.2147/DDDT.S211443.

(86) Chauhan, I.; Yasir, M.; Verma, M.; Singh, A. P. Nanostructured Lipid Carriers: A Groundbreaking Approach for Transdermal Drug Delivery. *Adv Pharm Bull* 2020, *10* (2), 150. https://doi.org/10.34172/APB.2020.021.

(87) Yue, Y.; Zhao, D.; Yin, Q. Hyaluronic Acid Modified Nanostructured Lipid Carriers for Transdermal Bupivacaine Delivery: In Vitro and in Vivo Anesthesia Evaluation. *Biomedicine & Pharmacotherapy* 2018, *98*, 813–820. https://doi.org/10.1016/j.biopha.2017.12.103.

(88) Iannitti, T.; Morales-Medina, J. C.; Merighi, A.; Boarino, V.; Laurino, C.; Vadalà, M.; Palmieri, B. A Hyaluronic Acid- and Chondroitin Sulfate-Based Medical Device Improves Gastritis Pain, Discomfort, and Endoscopic Features. *Drug Deliv Transl Res* 2018, *8* (5), 994–999. https://doi.org/10.1007/s13346-018-0531-7.

(89) Zhang, L.; Wang, J.; Chi, H.; Wang, S. Local Anesthetic Lidocaine Delivery System: Chitosan and Hyaluronic Acid-Modified Layer-by-Layer Lipid Nanoparticles. *Drug Deliv* 2016, *23* (9), 3529–3537. https://doi.org/10.1080/10717544.2016.1204569.

(90) Deng, Y.; Ren, J.; Chen, G.; Li, G.; Wu, X.; Wang, G.; Gu, G.; Li, J. Injectable in Situ Cross-Linking Chitosan-Hyaluronic Acid Based Hydrogels for Abdominal Tissue Regeneration. *Sci Rep* 2017, *7* (1). https://doi.org/10.1038/S41598-017-02962-Z.

(91) Tran, T. H.; Rastogi, R.; Shelke, J.; Amiji, M. M. Modulation of Macrophage Functional Polarity towards Anti-Inflammatory Phenotype with Plasmid DNA Delivery in CD44 Targeting Hyaluronic Acid Nanoparticles. *Sci Rep* 2015, *5*. https://doi.org/10.1038/srep16632.

(92) Ganesh, S.; Iyer, A. K.; Morrissey, D. V.; Amiji, M. M. Hyaluronic Acid Based Self-Assembling Nanosystems for CD44 Target Mediated SiRNA Delivery to Solid Tumors.

Biomaterials 2013, *34* (13), 3489–3502. https://doi.org/10.1016/J.BIOMATERIALS.2013.01.077.

(93) Kosovrasti, V. Y.; Nechev, L. V.; Amiji, M. M. Peritoneal Macrophage-Specific TNF-α Gene Silencing in LPS-Induced Acute Inflammation Model Using CD44 Targeting Hyaluronic Acid Nanoparticles. *Mol Pharm* 2016, *13* (10), 3404–3416. https://doi.org/10.1021/ACS.MOLPHARMACEUT.6B00398/SUPPL_FILE/MP6B00398_SI_001.PDF.

(94) Xie, J.; Ji, Y.; Xue, W.; Ma, D.; Hu, Y. Hyaluronic Acid-Containing Ethosomes as a Potential Carrier for Transdermal Drug Delivery. *Colloids Surf B Biointerfaces* 2018, *172*, 323–329. https://doi.org/10.1016/j.colsurfb.2018.08.061.

(95) Hussain, A.; Haque, W.; Kumar, S.; Farhan, S. &; Ahmed, J.; Singh, S. K.; Ahmed, F. J. Optimized Permeation Enhancer for Topical Delivery of 5-Fluorouracil-Loaded Elastic Liposome Using Design Expert: Part II. *https://doi.org/10.3109/10717544.2015.1124473* 2015, *23* (4), 1242–1253. https://doi.org/10.3109/10717544.2015.1124473.

(96) Li, Y.; Xu, F.; Li, X.; Chen, S. Y.; Huang, L. Y.; Bian, Y. Y.; Wang, J.; Shu, Y. T.; Yan, G. J.; Dong, J.; Yin, S. P.; Gu, W.; Chen, J. Development of Curcumin-Loaded Composite Phospholipid Ethosomes for Enhanced Skin Permeability and Vesicle Stability. *Int J Pharm* 2021, *592*, 119936. https://doi.org/10.1016/J.IJPHARM.2020.119936.

(97) Nainwal, N.; Jawla, S.; Singh, R.; Saharan, V. A. Transdermal Applications of Ethosomes – a Detailed Review. *https://doi.org/10.1080/08982104.2018.1517160* 2018, *29* (2), 103–113. https://doi.org/10.1080/08982104.2018.1517160.

(98) Gao, Y.; Cheng, X.; Wang, Z.; Wang, J.; Gao, T.; Li, P.; Kong, M.; Chen, X. Transdermal Delivery of 10,11-Methylenedioxycamptothecin by Hyaluronic Acid Based Nanoemulsion for Inhibition of Keloid Fibroblast. *Carbohydr Polym* 2014, *112*, 376–386. https://doi.org/10.1016/J.CARBPOL.2014.05.026.

(99) Brun, P.; Zavan, B.; Vindigni, V.; Schiavinato, A.; Pozzuoli, A.; Iacobellis, C.; Abatangelo, G. In Vitro Response of Osteoarthritic Chondrocytes and Fibroblast-like Synoviocytes to a 500-730 KDa Hyaluronan Amide Derivative. *J Biomed Mater Res Part B: Appl Biomater* 2012, *100*, 2073–2081. https://doi.org/10.1002/jbm.b.32771.

(100) Zerrillo, L.; Que, I.; Vepris, O.; Morgado, L. N.; Chan, A.; Bierau, K.; Li, Y.; Galli, F.; Bos, E.; Censi, R.; Di Martino, P.; van Osch, G. J. V. M.; Cruz, L. J. PH-Responsive Poly(Lactide-Co-Glycolide) Nanoparticles Containing near-Infrared Dye for Visualization and

Hyaluronic Acid for Treatment of Osteoarthritis. *Journal of Controlled Release* 2019, *309*, 265–276. https://doi.org/10.1016/j.jconrel.2019.07.031.

(101) Zerrillo, L.; Gigliobianco, M. R.; D'atri, D.; Garcia, J. P.; Baldazzi, F.; Ridwan, Y.; Fuentes, G.; Chan, A.; Creemers, L. B.; Censi, R.; Martino, P. Di; Cruz, L. J. PLGA Nanoparticles Grafted with Hyaluronic Acid to Improve Site-Specificity and Drug Dose Delivery in Osteoarthritis Nanotherapy. *Nanomaterials* 2022, *12* (13). https://doi.org/10.3390/nano12132248.

(102) Mobarak, M.; Badghaish, O.; Noor, G.; Qorban, M.; Albaqami, A. S.; Nemer, A. A.; Alali, A. J.; Fouad, R.; Al Yaqoub, H.; Alshamrani, H. A.; Hasan Badahman, O.; Ansaif, R. A.; Alasmari, A.; Alghamdi, A. Y.; Ahmad, H.; Alshareef, S.; Aljadeed, A. M.; Almohammed, A. A.; Filmban, D. M.; Alaql, A. S. Rheumatoid Arthritis, Pathophysiology and Management. *Egypt J Hosp Med* 2018, *70* (11), 1898–1903. https://doi.org/10.12816/0044839.

(103) Gorantla, S.; Gorantla, G.; Saha, R. N.; Singhvi, G. CD44 Receptor-Targeted Novel Drug Delivery Strategies for Rheumatoid Arthritis Therapy. *https://doi.org/10.1080/17425247.2021.1950686* 2021, *18* (11), 1553–1557. https://doi.org/10.1080/17425247.2021.1950686.

(104) Altman, R. D.; Manjoo, A.; Fierlinger, A.; Niazi, F.; Nicholls, M. The Mechanism of Action for Hyaluronic Acid Treatment in the Osteoarthritic Knee: A Systematic Review. *BMC Musculoskeletal Disorders 2015 16:1* 2015, *16* (1), 1–10. https://doi.org/10.1186/S12891-015-0775-Z.

(105) Dosio, F.; Arpicco, S.; Stella, B.; Fattal, E. Hyaluronic Acid for Anticancer Drug and Nucleic Acid Delivery. *Adv Drug Deliv Rev* 2016, *97*, 204–236. https://doi.org/10.1016/J.ADDR.2015.11.011.

(106) Yadav, S.; Sharma, A. K.; Kumar, P. Nanoscale Self-Assembly for Therapeutic Delivery. *Front Bioeng Biotechnol* 2020, *8*, 127. https://doi.org/10.3389/FBIOE.2020.00127/BIBTEX.

(107) Mendes, A. C.; Baran, E. T.; Reis, R. L.; Azevedo, H. S. Self-Assembly in Nature: Using the Principles of Nature to Create Complex Nanobiomaterials. *Wiley Interdiscip Rev Nanomed Nanobiotechnol* 2013, *5* (6), 582–612. https://doi.org/10.1002/WNAN.1238.

(108) Stoffelen, C.; Huskens, J. Soft Supramolecular Nanoparticles by Noncovalent and Host–Guest Interactions. *Small* 2016, *12* (1), 96–119. https://doi.org/10.1002/SMLL.201501348.

(109) Vafaei, S. Y.; Esmaeili, M.; Amini, M.; Atyabi, F.; Ostad, S. N.; Dinarvand, R. Self Assembled Hyaluronic Acid Nanoparticles as a Potential Carrier for Targeting the Inflamed Intestinal Mucosa. *Carbohydr Polym* 2016, *144*, 371–381. https://doi.org/10.1016/j.carbpol.2016.01.026.

(110) Mota, A. H.; Direito, R.; Carrasco, M. P.; Rijo, P.; Ascensão, L.; Viana, A. S.; Rocha, J.; Eduardo-Figueira, M.; Rodrigues, M. J.; Custódio, L.; Kuplennik, N.; Sosnik, A.; Almeida, A. J.; Gaspar, M. M.; Reis, C. P. Combination of Hyaluronic Acid and PLGA Particles as Hybrid Systems for Viscosupplementation in Osteoarthritis. *Int J Pharm* 2019, *559*, 13–22. https://doi.org/10.1016/j.ijpharm.2019.01.017.

(111) Kang, L.-J.; Yoon, J.; Rho, J. G.; Han, H. S.; Lee, S.; Oh, Y. S.; Kim, H.; Kim, E.; Kim, S. J.; Lim, Y. T.; Park, J. H.; Song, W. K.; Yang, S.; Kim, W. Self-Assembled Hyaluronic Acid Nanoparticles for Osteoarthritis Treatment. *Biomaterials* 2021, *275*, 120967. https://doi.org/10.1016/j.biomaterials.2021.120967.

(112) El-Refaie, W. M.; Elnaggar, Y. S. R.; El-Massik, M. A.; Abdallah, O. Y. Novel Self-Assembled, Gel-Core Hyaluosomes for Non-Invasive Management of Osteoarthritis: In-Vitro Optimization, Ex-Vivo and In-Vivo Permeation. *Pharmaceutical Research 2015 32:9* 2015, *32* (9), 2901–2911. https://doi.org/10.1007/S11095-015-1672-8.

(113) Della Sala, F.; Longobardo, G.; Fabozzi, A.; Di Gennaro, M.; Borzacchiello, A. Hyaluronic Acid-Based Wound Dressing with Antimicrobial Properties for Wound Healing Application. *Applied Sciences 2022, Vol. 12, Page 3091* 2022, *12* (6), 3091. https://doi.org/10.3390/APP12063091.

(114) Romanò, C. L.; Vecchi, E. De; Bortolin, M.; Morelli, I.; Drago, L. Hyaluronic Acid and Its Composites as a Local Antimicrobial/Antiadhesive Barrier. *J Bone Jt Infect* 2017, *2* (1), 63–72. https://doi.org/10.7150/JBJI.17705.

(115) Zamboni, F.; Okoroafor, C.; Ryan, M. P.; Pembroke, J. T.; Strozyk, M.; Culebras, M.; Collins, M. N. On the Bacteriostatic Activity of Hyaluronic Acid Composite Films. *Carbohydr Polym* 2021, *260*, 117803. https://doi.org/10.1016/J.CARBPOL.2021.117803.

(116) Sinh, P.; Fiocchi, C.; Achkar, J. P. Immune Based Therapies for Inflammatory Bowel Disease. *Immune Rebalancing: The Future of Immunosuppression* 2016, 37–61. https://doi.org/10.1016/B978-0-12-803302-9.00003-8.

(117) Naahidi, S.; Jafari, M.; Edalat, F.; Raymond, K.; Khademhosseini, A.; Chen, P. Biocompatibility of Engineered Nanoparticles for Drug Delivery. *Journal of Controlled Release* 2013, *166* (2), 182–194. https://doi.org/10.1016/J.JCONREL.2012.12.013.

(118) Liu, P. S.; Fan, G. M.; Liu, Y. H.; Miao, Z.; Cao, Y.; Lv, X.; Wang, Y.; Ding, W.; Wang, F.; Zhang, J.; Guo, Y.; Ju, S.; Wang, H. A Novel Local Anti-Colorectal Cancer Drug Delivery System: Negative Lipidoid Nanoparticles with a Passive Target via a Size-Dependent Pattern. *Nanotechnology* 2013, *24* (37), 375101. https://doi.org/10.1088/0957-4484/24/37/375101.

(119) Chen, M.; Li, L.; Wang, Z.; Li, P.; Feng, F.; Zheng, X. High Molecular Weight Hyaluronic Acid Regulates P. Gingivalis–Induced Inflammation and Migration in Human Gingival Fibroblasts via MAPK and NF-KB Signaling Pathway. *Arch Oral Biol* 2019, *98*, 75–80. https://doi.org/10.1016/J.ARCHORALBIO.2018.10.027.

(120) Salmaso, S.; Caliceti, P. Stealth Properties to Improve Therapeutic Efficacy of Drug Nanocarriers. *J Drug Deliv* 2013, *2013*, 1–19. https://doi.org/10.1155/2013/374252.

(121) Payne, W. M.; Svechkarev, D.; Kyrychenko, A.; Mohs, A. M. The Role of Hydrophobic Modification on Hyaluronic Acid Dynamics and Self-Assembly. *Carbohydr Polym* 2018, *182*, 132–141. https://doi.org/10.1016/J.CARBPOL.2017.10.054.

(122) Choi, W. Il; Lee, J. H.; Kim, J. Y.; Kim, J. C.; Kim, Y. H.; Tae, G. Efficient Skin Permeation of Soluble Proteins via Flexible and Functional Nano-Carrier. *Journal of Controlled Release* 2012, *157* (2), 272–278. https://doi.org/10.1016/J.JCONREL.2011.08.013.

(123) Gallo, N.; Nasser, H.; Salvatore, L.; Natali, M. L.; Campa, L.; Mahmoud, M.; Capobianco, L.; Sannino, A.; Madaghiele, M. Hyaluronic Acid for Advanced Therapies: Promises and Challenges. *Eur Polym J* 2019, *117*, 134–147. https://doi.org/10.1016/J.EURPOLYMJ.2019.05.007.

(124) Prestwich, G. D.; Bhatia, S.; Breuer, C. K.; Dahl, S. L. M.; Mason, C.; McFarland, R.; McQuillan, D. J.; Sackner-Bernstein, J.; Schox, J.; Tente, W. E.; Trounson, A. What Is the Greatest Regulatory Challenge in the Translation of Biomaterials to the Clinic? *Sci Transl Med* 2012, *4* (160), 160–174. https://doi.org/10.1126/SCITRANSLMED.3004915/ASSET/F3E619A5-BAE7-41BE-B88F-963904926805/ASSETS/GRAPHIC/4160CM14-F3.JPEG.

(125) Pai, D. B. Mapping the Genealogy of Medical Device Predicates in the United States. *PLoS One* 2021, *16* (10), e0258153. https://doi.org/10.1371/JOURNAL.PONE.0258153.

(126) Curfman, G. D.; Redberg, R. F. Medical Devices - Balancing Regulation and Innovation. *The Ethical Challenges of Emerging Medical Technologies* 2020, 49–52. https://doi.org/10.4324/9781003074984-4/MEDICAL-DEVICES-BALANCING-REGULATION-INNOVATION-GREGORY-CURFMAN-RITA-REDBERG.

(127) Bauman, J. The "Déjà Vu Effect:" Evaluation of United States Medical Device Legislation, Regulation, and the Food and Drug Administration's Contentious 510(k) Program. *Food Drug Law J* 2012, *67* (3), 337–361.

(128) Mero, A.; Pasqualin, M.; Campisi, M.; Renier, D.; Pasut, G. Conjugation of Hyaluronan to Proteins. *Carbohydr Polym* 2013, *92* (2), 2163–2170. https://doi.org/10.1016/J.CARBPOL.2012.11.090.

(129) Zhang, H.; Huang, S.; Yang, X.; Zhai, G. Current Research on Hyaluronic Acid-Drug Bioconjugates. *European Journal of Medicinal Chemistry*. Elsevier Masson SAS October 30, 2014, pp 310–317. https://doi.org/10.1016/j.ejmech.2014.08.067.

Chapter 3

Enabling Anti-Inflammatory Activity Through Hyaluronan-Coated PLGA Nanoparticles Loaded With Carvacrol

Abstract

Chronic inflammation leads to excessive inflammatory cytokine production and macrophage infiltration, contributing to the development of chronic diseases. Carvacrol (CVL), a phenolic compound derived from oregano, activates the PPAR-γ gene to suppress inflammatory cyclooxygenase-2 cytokine production. To address both the cytotoxicity and the volatility of free carvacrol (CVL), which limits its bioavailability and certain administration routes (e.g., intravenous), poly(lactic-co-glycolic) acid (PLGA)-based nanoparticles (CP) were formulated, achieving a size of 155±3 nm and a zeta potential of +16.70±1.1 mV. For targeted drug delivery, 1.5% w/v hyaluronic acid (HA) was coated onto the PLGA nanoparticles, forming CHP nanoparticles, with a final size of 225±18 nm and a zeta potential of -26.70±2.2 mV. HA, a natural ligand of the CD44 receptor abundantly expressed on pro-inflammatory macrophages, enhanced CHP nanoparticle internalization by +41.2% compared to uncoated CP nanoparticles. The encapsulation efficiency of CVL reached 90.8±5.2%, with a loading capacity of 26.0±6.6%, and a sustained drug release profile was observed, with complete release over 66 days. In lipopolysaccharide-induced macrophages, CHP nanoparticles significantly increased anti-inflammatory cytokine production, with IL-1ra, IL-4, and IL-10 levels rising by +258%, +260%, and +40%, respectively, compared to untreated cells. Meanwhile, pro-inflammatory cytokine levels were reduced, with IL-1α, IL-1β, and TNF-α decreasing by -25%, -36%, and -36%, respectively, relative to untreated cells. These findings highlight the potential of HA-coated PLGA nanoparticles as an effective targeted delivery system for CVL, offering a promising strategy for combating chronic inflammation-related diseases.

1. Introduction

Under adverse conditions, inflammation serves as the body first line of defense and as innate immune response, primarily regulated by macrophages [1,2]. These macrophages exhibit remarkable plasticity, which determines the intensity and progression of inflammation through cytokine release. Macrophage plasticity encompasses a spectrum of phenotypes rather than a strict dichotomy between pro- and anti-inflammatory states. While macrophages are often categorized into pro-inflammatory (M1-m) and anti-inflammatory (M2-m) phenotypes, this classification represents only two extremes within a highly dynamic and context-dependent continuum. In response to various microenvironmental cues, macrophages can adopt intermediate or hybrid states that exhibit overlapping functional properties. Acute inflammation, typically driven by macrophages with an M1-like phenotype, plays a crucial role in maintaining homeostasis and protecting tissues from infection or injury [3]. However, the resolution of inflammation is a tightly regulated process involving multiple macrophage subsets with anti-inflammatory and tissue-repair functions. A failure to properly transition through these phenotypic states, particularly an inadequate shift toward pro-resolving macrophages, can result in chronic inflammation, leading to persistent tissue damage and contributing to diseases such as chronic pain [4].

Carvacrol (2-methyl-5-(1-methylethyl) phenol, CVL) is a phenolic monoterpene derived from oregano (*Origanum vulgare* L.) and thyme (*Thymus vulgaris*) [5], and it is widely recognized for its antibacterial [6], antimicrobial [7] and anti-inflammatory properties [8]. CVL anti-inflammatory action is mediated through the activation of peroxisome proliferator-activated receptor-γ (PPARγ), leading to the suppression of inflammatory cytokines like cyclooxygenase-2 (COX-2) production [9,10] and interleukin-6 (IL-6), as proved in literature [11–13]. Despite its therapeutic potential, direct administration of free CVL may cause cytotoxicity in healthy cells, limiting its clinical applicability[14–16]. Yammine *et al*. reported reduced toxicity of encapsulated CVL as compared to its free counterpart [17]. Therefore, encapsulation of CVL within nanoparticles has emerged as a promising strategy to mitigate this cytotoxicity by improving its biocompatibility and therefore effectively harnessing the anti-inflammatory mechanism of action [18].

One therapeutic strategy to resolve chronic inflammation involves the polarization of pro-inflammatory M1-m to anti-inflammatory M2-m [19]. To achieve this, such therapeutic nanosystem must specifically target M1 macrophages (M1-m) to ensure high efficacy. Hyaluronic acid (HA), a naturally occurring ligand, binds directly to the cluster of differentiation 44 (CD44) receptor, which is abundantly expressed on the surface of M1-m. This interaction facilitates receptor-mediated uptake of the nanosystem by M1-m [20]. Furthermore, the HA is extensively utilized in scientific research due to its versatility, with application in nanoparticles [21] and nanocarriers [22] synthesis, often in combination with polymers [23], for the targeted delivery of therapeutic agents. To mention, the role of HA in the modulation of inflammation is widely acknowledged, however, it remains a subject of scientific debate. Indeed, while some studies suggest that low molecular weight (LMW) HA promotes inflammatory responses and high molecular weight (HMW) HA exhibits anti-inflammatory effects, other research presents conflicting evidence, challenging this dichotomy [24]. Nevertheless, HA remains a hot topic in nano drug delivery methods for cancer [22,25,26] and inflammatory diseases [27–29].

The intrinsic electrostatic properties of HA, characterized by its negative charge, allow it to be efficiently coated onto polymeric nanoparticles such as poly(lactic-co-glycolic acid) (PLGA) with the assistance of charged surfactants like cetyltrimethylammonium bromide (CTAB). This coating enhances the delivery of poorly water-soluble drugs by improving stability, bioavailability, and target specificity [30]. Polymeric nanoparticles offer a promising strategy to reduce the cytotoxicity but also overcome the volatility associated with the delivery of free drugs, allowing for their administration through various routes and enhancing their therapeutic potential [31,32]. CVL, being a volatile compound with low stability [33], benefits from encapsulation in PLGA nanoparticles, which provide enhanced stability and enable controlled, sustained release [34], thereby minimizing the risk of degradation [35].

In this study, we developed a novel PLGA nanoparticle system encapsulating CVL to investigate its ability to target inflammation while preserving a hydrophobic environment for CVL loading. Furthermore, the HA coating on PLGA nanoparticles was performed to enable precise targeting of inflamed tissue, and macrophage uptake was evaluated. The impact of this system on inflammatory response modulation was evaluated through macrophage polarization and cytokine suppression. Overall, this study represents the

first exploration of this targeted nanotherapeutic platform, providing new insights into its potential for inflammation management by demonstrating, for the first time, the combined effect of HA-coated and CVL-loaded PLGA nanoparticles on macrophage uptake and inflammatory response modulation.

2. Materials and Methods

2.1 Materials

Poly(lactic-co-glycolic acid) (PLGA) with a molecular weight of 17 kDa and acid-terminated structure (PURASORB PDLG 5002A) was obtained from Corbion (Amsterdam, the Netherlands). Carvacrol (CVL) with a purity greater than 98.0% was purchased from TCI EUROPE N.V. (Zwijndrecht, Belgium). Hyaluronic acid (23 kDa) was supplied by ContiPro (Dolní Dobrouč, Czech Republic). Cetyltrimethylammonium bromide (CTAB) and bovine serum albumin (BSA) were sourced from Sigma-Aldrich (St. Louis, Missouri, United States). Dichloromethane (DCM), stabilized with ethanol, was provided by Carlo Erba (Milan, Italy). Distilled water (DI) was obtained with the apparatus RO 60 TS demi2 water deionizer provided by Gamma 3 Ecologia (Castelverde Costa Sant'abramo, Italy). The phosphate-buffered saline (PBS) used for the experiments wass based on the 150 mM buffer solution at pH 7.4 of NaCl (136.9 mM), KH_2PO_4 (1.7 mM), and Na_2HPO_4 (13.4 mM).

For macrophage isolation, NCTC clone L-929 mouse fibroblasts cell line was obtained from ATCC (distributed by LGC, Milan, Italy) and cultured using Eagle Minimum Essential Medium (EMEM) (LGC, Milan, Italy). Additional reagents including fetal bovine serum (FBS, Gibco, Life Technologies, Milan, Italy), penicillin, streptomycin, and Roswell Park Memorial Institute (RPMI) 1640 Medium were purchased by Gibco, Life Technologies (Milan, Italy).

2.2 Hyaluronic acid-coated PLGA nanoparticles

The protocol for formulating PLGA nanoparticles was adapted and modified from Pradhan *et al.* [36]. Oil/water solvent evaporation method was used to synthesize PLGA nanoparticles where CTAB was used as a surfactant dissolved in the water phase (Scheme 1a). Briefly, a solution of 100 mg of PLGA dissolved in 3 mL of DCM was

gradually added dropwise to an aqueous phase consisting of 18 mL of 0.5% w/v CTAB solution. To mention, CTAB is a quaternary ammonium surfactant with a positive charge, which enables it to conjugate to the surface of PLGA nanoparticles, thereby imparting a net positive surface charge to the nanoparticles. This positive charge facilitates the addition of HA, a negatively charged polysaccharide at physiological pH, by enabling electrostatic interactions with the cationic regions of the CTAB molecules. Afterwards, the emulsion was homogenized (T 25 digital ULTRA-TURRAX®) at 11000 rpm for 15 minutes and left to stir at 500 rpm overnight in order to allow the solvent evaporation. To prepare HA-coated PLGA nanoparticles (Scheme 1a), 10 mL of a 1.5% w/v HA solution was added dropwise to the PLGA nanoparticles suspension. The resulting HA-coated PLGA nanoparticles were stirred for 15 min at 600 rpm and centrifuged at 3000 g and at 4˚ C for 20 minutes, favoring the removal of uncoated HA. The empty HA-coated PLGA nanoparticles (namely HP) were then collected [36,37].

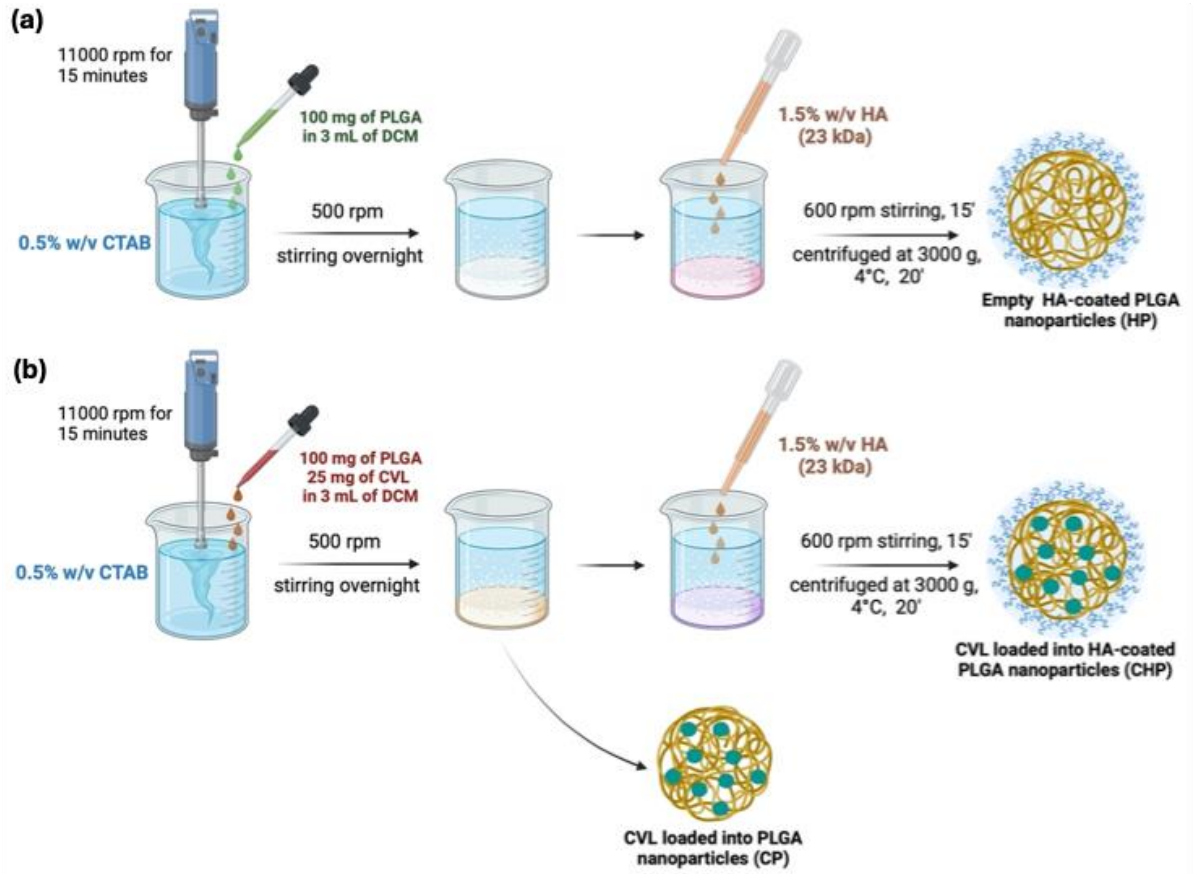

Scheme 1. Schematic representation of (a) HA-coated PLGA empty (HP) nanoparticles, and (b) CVL-loaded uncoated PLGA (CP) nanoparticles and CVL-loaded HA-coated PLGA (CHP) nanoparticles. Partially created with BioRender.com.

2.3 Carvacrol-loaded nanoparticles

For the loading of CVL, 25 mg of CVL was dissolved in the organic phase mixture containing PLGA and DCM, and then added dropwise into the aqueous phase following the protocol described in section 2.2 (Scheme 1b). The resulting nanoparticles, CVL-loaded PLGA-nanoparticles (namely CP) and CVL-loaded HA-coated PLGA-nanoparticles (namely CHP) were dried and stored in the freezer (-20 °C) until further use.

2.4 Nanoparticles characterization

2.4.1 Size, PDI and Zeta Potential

The hydrodynamic diameter, polydispersity index (PDI) and zeta potential (ζ) of the formed nanoparticles were determined by Dynamic Light Scattering (DLS) technique with the Zetasizer Nano equipped with 633nm HeNe (Malvern Instruments, Malvern, UK). For the measurements, 5 mg of freeze-dried HP, CP or CHP nanoparticles, prepared following sections 2.2 and 2.3, were suspended in 1 mL of DI water at 25°C and an angle of 90°. All measurements were performed at 25 ˚ C and in triplicates. Data were corrected for viscosity using the Malvern Zetasizer software (version 8.01).

2.4.2 Scanning Electron Microscopy

The morphology of the CHP nanoparticles (formulation described in section 2.3), was evaluated by a field emission-scanning electron microscope ZEISS SIGMA 300 FESEM equipped with the Gemini column (1.2 nm @ 15 kV) (SEM, Zeiss Sigma 300, Zeiss, Germany). The dried CHP nanoparticles sample was sputtered under vacuum with a chromium layer of approximately 100 Å thickness (Quorum Q150T ES, Quorum Technologies, Lewes, UK) before analysis. Conductive thin films (chromium and graphite) were deposited on the samples with the QUORUM Q150T.

2.4.3 Fourier-Transform Infrared Attenuated Total Reflectance (FT-IR ATR) spectroscopy

To highlight the presence of the HA coating on the PLGA nanoparticles, the chemical composition of the nanoparticles and the HA polymer was evaluated using FT-IR ATR analysis, performed with a PerkinElmer FT-IR spectrometer (Spectrum Two UATR) equipped with a ZnSe crystal (Waltham, Massachusetts, United States). The measurements were processed by a PerkinElmer data manager SpectrumTM 10 Software in a 400-4000 cm^{-1} range at a 2 cm^{-1} resolution and 4 scans.

2.4.4 CVL encapsulation efficiency and loading capacity

Gas Chromatography-Mass Spectrometry (GC-MS, Agilent GC-MS 8890 5790B, Milan, Italy) was used to calculate drug encapsulation efficiency (EE%) and loading capacity (LC%) following the Equation 1 and Equation 2 respectively:

$$Encapsulation\ Efficiency\ (EE\%) = \frac{Amount\ of\ drug\ encapsulated}{Total\ drug\ added} \times\ 100 \quad Equation\ 1$$

$$Loading\ Capacity\ (LC\%) = \frac{Amount\ of\ drug\ encapsulated}{Total\ weight\ of\ nanoparticles} \times 100 \qquad Equation\ 2$$

To prepare the samples for EE% and LC% analyses, 1 mL of acetone was added to 100 µL of the supernatant obtained from freshly prepared nanoparticles. The mixture was then centrifuged at 3000×g for 10 minutes at 4°C [38]. The supernatant was then collected and analyzed with GC-MS to estimate the non-encapsulated CVL. For further verification, CP nanoparticles were mixed with 1 mL of acetone, centrifuged at 3000 g for 10 minutes at 4 ˚ C, and analyzed with GC-MS for measuring the amount of encapsulated CVL within the CP nanoparticles. It is important to note that CHP nanoparticles with a hyaluronic acid (HA) coating were not tested due to the hydrophilicity of HA and its incompatibility with the GC-MS system.

2.5 *In vitro* drug release studies

The release studies were conducted on CHP nanoparticles in phosphate-buffered saline (PBS, pH 7.4 composition given in section 2.1) containing 4.5% w/v bovine serum

albumin (BSA). Prior to release, the CVL solubility in 150 mM PBS + 4.5% w/v BSA was evaluated. For this, 1 mg of CVL was added to 4,6,8 and 10 mL of PBS + 4.5% w/v BSA solution and incubated at 37˚ C overnight. Then, 500 µL of each sample was centrifuged at 10000 rpm, 22˚ C for 20 minutes. Afterwards, 1 volume of supernatant (100 µL) was added to 10x the amount of acetone and centrifuged at 5000 rpm for 10 minutes at 22˚ C. The samples were then tested with GC-MS. Based on the results, 8 mL of the media (PBS + 4.5% w/v BSA) per 1 mg of CVL was chosen for the release study.

To perform the release study, 3.85 mg of CHP (corresponding to 1 mg of encapsulated CVL) was added to 28 mL of PBS + 4.5% w/v BSA solution and incubated at 37˚ C while continuously shaking (350 rpm) using an IKA vortex 4 digital (IKA®-Werke GmbH & Co. KG, Janke & Kunkel-Str. 10 79219 Staufen, Germany). Sink conditions were maintained in the compartment during release studies. Aliquots were collected at different time points and prepared for GC-MS analysis as previously described.

To investigate the mechanism of CVL release, the time-dependent cumulative release percentage of CVL from HA-coated PLGA nanoparticles was analyzed using a zero-order kinetics model, as shown in Equation 3 [39,40]:

$$Q = kt \qquad Equation\ 3$$

where Q is the fraction of drug released at time t; and k is the kinetic rate constant.

2.6 *In vitro* anti-inflammatory activity

2.7.1 Bone marrow derived macrophages studies

Cell studies were performed with bone marrow derived macrophages (BMDMs) harvested from 3-month-old C57BL/6J Balb-c mice (Envigo, Indiana, United States), sacrificed by carbon dioxide euthanasia and cervical dislocation. Then, femurs and tibia were surgically removed, and the bone marrow was flushed by injecting RPMI 1460 medium (Thermo Fisher Scientific, Monza, Italy) into the bone cavity. BMDMs were then filtered using falcon cell strainers to remove any pieces of bone or muscles and subsequently centrifuged and resuspended in the RPMI 1460 medium.

Macrophages isolation was performed by growing the BMCs on coverslip in RPMI 1460 medium containing 30% of the L-929 culture supernatant, 10% of FBS, penicillin and

streptomycin, and enriched with the macrophage colony-stimulating factor (M-CSF) at the concentration of 10 ng/mL. The purpose of adding M-CSF is to stimulate monocytes to differentiate into neutral macrophages (M0), as previously demonstrated[41].

Cells were then let grow in the humidified incubator at 5% CO_2 and at 37° for a week, changing the medium every 3 days. Subsequently, nanoparticles were added to cultures of untreated macrophages and macrophages previously inflamed with lipopolysaccharide (LPS, 100 ng/mL) to induce polarization toward the M1 phenotype. Specifically, M0 and M1 macrophages were incubated with 1 mL of HP and CHP nanoparticles at two different concentrations (5 µg/mL and 10 µg/mL). Only CHP nanoparticles contained CVL, with 1.3 µg and 2.6 µg of CVL, respectively. Additionally, 1 mL free CVL (2.6 µg/mL and 10 µg/mL) was tested to assess polarization and cytokine release. The nanoparticles compositions are described in section 2.3.

2.7.2 Immunofluorescence assay

After 4 days of incubation with the nanoparticles and free CVL, cells were washed with PBS (150 mM at pH 7.4) for 3 times. Then, cells were fixed in 4% paraformaldehyde (PFA) diluted in PBS for 20 minutes. After washing with PBS cells were permeabilized with 0.3 %v/v Triton X-100 for 20 minutes. A method to study the M1 and M2 macrophages phenotype can be based on the evaluation of the expression of their specific markers through immunofluorescence analysis. Thus, cultures were incubated for 2 h with the following primary antibodies: anti-rabbit CD86 (diluted 1:100) and anti-mouse iNOS (diluted 1:50) to evaluate the expression of M1 markers; anti-mouse CD206 (diluted 1:50) and an anti-rabbit CD163 (diluted 1:50) to study the expression of M2 markers. After 3 washing with PBS (150 mM, pH 7.4), cells were incubated with the secondary antibodies Alexa fluor 488 chicken anti-mouse and Alexa fluor 594 goat anti-rabbit, both diluted 1:80, for 2 h. Since CD206 antibody is conjugated with the 488 fluorochrome, it was added together with secondary antibodies. Cells were then washed 2 times with PBS and incubated for 45 minutes with DAPI (diluted 1:1000) at 37°C. Finally, all cultures were washed 3 times with PBS and coverslips were mounted on slides in PBS/Glycerol 1:1. The slides were analyzed with a C2 Plus confocal laser scanning microscope (CLSM,

Nikon Instruments, Florence, Italy). The microscope images were processed using NIS-Elements imaging software (Nikon Instrument, Florence, Italy).

2.7.3 Nanoparticle internalization

Coating the nanoparticles with HA is motivated by its reported capability to bind to the CD44 receptor on M1 macrophages, facilitating enhanced cellular internalization[20,42]. To observe the efficacy of HA-coated nanoparticles (CHP nanoparticles) to internalize in M1-m, as compared to uncoated CP, nanoparticle uptake was visualized by staining CHP and CP with Nile red [43]. A Nile red stock solution of 1 mg/mL was prepared, out of which 10 µL was added to the PLGA organic phase. The nanoparticles were further synthesized like stated in Sections 2.2 and 2.3. For the cell analyses, LPS-treated and untreated BMDMs were incubated with 1mL of working nanoparticle (CP and CHP) concentration of 10 µg/mL for 24 hours. The uptake was studied by quantifying the fluorescence signal of Nile red. Specifically, the mean fluorescence intensity (MFI) was measured using NIS-Elements imaging software (Nikon Instrument, Florence, Italy).

2.7.4 Analyzing macrophage polarization and cytokine production

LPS-treated and untreated BMDMs were cultured in a 24-well plate with 1 mL of 10 µg/mL CHP and HP nanoparticles, along with 2.6 µg/mL of free CVL, following the protocol in Section 2.7.1. The uptake was quantified by the expression of macrophage specific markers CD86 and iNOS for M1-m and CD163 and CD206 for M2-m, and the total MFI was calculated as described on section 2.7.3 [44,45]. To further verify the anti-inflammatory effect of CVL, the expressions of certain inflammatory cytokines was also analyzed. The cells were treated as in Section 2.7.2, and the supernatant was collected after 24 hours. The amount of different pro- (IL-1α/1β and TNF- α) and anti- (IL-1ra/4/10) inflammatory cytokines was tested with Mouse Cytokine Array Panel A kit (R&D Systems). Immunoreactive spots were quantitated densitometrically using ImageJ software.

2.8 Statistical analysis

The p values were determined by a Student's test with two-tailed distribution performed with the software GraphPad Prism 9 (GraphPad Software Inc., La Jolla, California), where p values < 0.05 are considered statistically significant (*p < 0.05, **p < 0.01).

3. Results and Discussion

3.1 Nanoparticles characterization

The hydrodynamic diameter of the formulated nanoparticles was characterized using dynamic light scattering (DLS), as summarized in Figure 1. The size of the empty PLGA nanoparticles was determined to be 162±2 nm with a low polydispersity index (PDI) of 0.09±0.03, indicating a narrow size distribution. Consistent with previous studies [36,37], the incorporation of hyaluronic acid (HA) led to a significant increase in HA-coated PLGA (HP) nanoparticles size, reaching 285±17 nm (PDI 0.39±0.01). This trend aligns with findings by Pradhan *et al*. [36], who reported a size increase proportional to the concentration of HA. Additional details on the effects of varying HA concentrations and molecular weights on nanoparticle size optimization are provided in the supplementary materials accompanying this paper (Figure S1, Supporting Information). Encapsulation of carvacrol (CVL) into PLGA resulted in CP nanoparticles with a mean hydrodynamic size of 155±3 nm and a low PDI of 0.07±0.03, indicating a uniform size distribution. Also in this case, HA-coated CP nanoparticles (CHP) increased the size to 225±18 nm with a higher PDI of 0.34±0.12, reflecting a broader size distribution. Morphological analysis using scanning electron microscopy (SEM) revealed an overall smaller CHP nanoparticle distribution size than the one determined by DLS (Figure 1). This discrepancy is likely due to differences in measurement conditions between the two techniques. The larger size observed in DLS measurements can be attributed to sample preparation, where nanoparticles are suspended in water. This suspension can lead to water absorption by the highly hydrophilic hyaluronan coating and subsequent swelling of the nanoparticles. The swelling effect is particularly pronounced due to the hygroscopic nature of HA, whose negatively charged subunits promote water retention [46]. This phenomenon highlights the influence of surface modification on nanoparticle behavior in aqueous environments and suggests that the hydrodynamic size measured by DLS may more closely reflect the functional state of nanoparticles in biological conditions [47]. In contrast,

SEM analysis requires dried samples, which eliminates the possibility of nanoparticle swelling due to water absorption. Consequently, the smaller size of the nanoparticles observed in SEM images reflects their dehydrated state, minimizing the influence of HA-induced water retention.

The surface charge (ζ-potential) of empty PLGA nanoparticles was measured at +57.7±1.3 mV, attributed to the addition of CTAB as a surfactant. However, upon coating with HA, the ζ-potential of HP nanoparticles decreased significantly to -25.5±0.3 mV. This shift in charge can be attributed to the anionic nature of HA, stemming from its carboxyl groups. Similarly, the ζ-potential of CHP nanoparticles was measured at -26.7±2.2 mV, which aligns with the expected negative surface charge conferred by HA. These findings underscore the significant impact of HA coating on both particle size and surface charge, which are critical parameters influencing nanoparticle stability and interaction with biological systems.

CVL is known for its high encapsulation efficiency profile in polymers [48,49]. Using Equation 1, the encapsulated CVL accounted for 90.8±5.2%, with a loading capacity (LC%) of 26.0±6.6%, as calculated using Equation 2. These results demonstrate the effectiveness of the single-emulsion solvent evaporation method used in this study. Furthermore, even after lyophilization, carvacrol remains within the nanoparticles, indicating that encapsulation effectively reduces the volatility of the molecule. This, in turn, enhances its stability over time and extends its potential shelf life.

In comparison, a previous study reported a CVL encapsulation efficiency of ~26% in PLGA nanoparticles prepared using the solvent displacement method [6]. In contrast, our method demonstrated a substantial improvement, tripling the encapsulation efficiency (~90%). Also, the LC% increased from their reported ~21% to ~26% in our formulation, this improvement is related by the significant enhancement in EE%. This improvement highlights the advantages of the single-emulsion solvent evaporation method, which appears to provide a more favorable environment for the efficient encapsulation of CVL. These findings are promising for the development of polymer-based drug delivery systems with high encapsulation efficiency.

(a)

Sample	Size (nm)	PDI	ζ-potential (mV)
PLGA	162±2	0.09±0.03	57.7±1.3
HP	285±17	0.39±0.01	-25.5±0.3
CP	155±3	0.07±0.03	16.7±1.1
CHP	225±18	0.34±0.12	-26.7±2.2

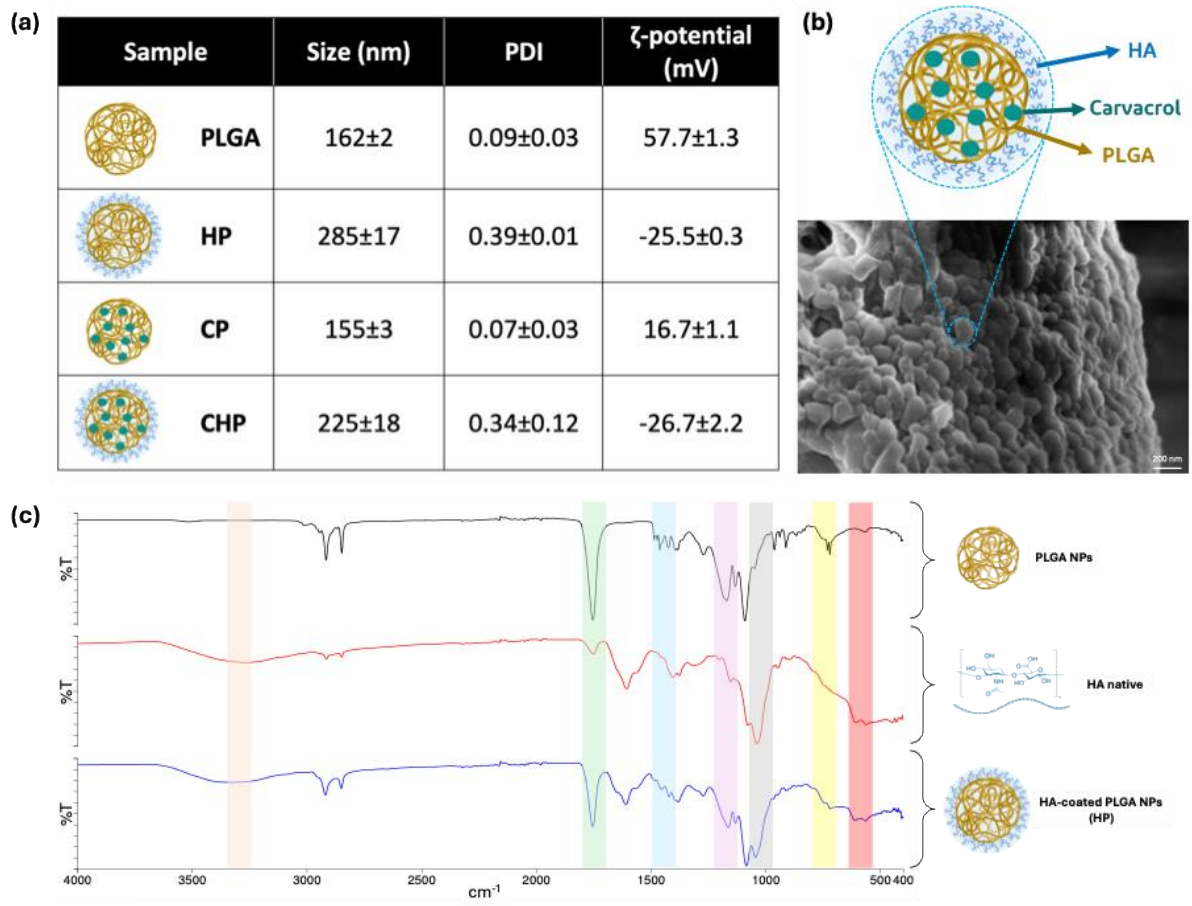

Figure 1. a) Size, PDI, and zeta potential (ζ) of all the synthesized nanoparticles; (b) SEM analysis of CHP nanoparticles, highlighting the smaller nanoparticle size observed compared to DLS measurements (n=3, mean ± SD); (c) FT-IR spectra of PLGA nanoparticles (black), native hyaluronic acid (HA) (red), and HA-coated PLGA nanoparticles (HP) (blue), confirming the successful coating of PLGA with HA through characteristic peaks.

Furthermore, the FT-IR spectra confirm the successful coating of PLGA nanoparticles with hyaluronic acid (HA) by displaying characteristic peaks from both components. The spectrum of PLGA nanoparticles (black) shows distinct absorption bands, including a strong C=O stretching vibration at ~1750 cm^{-1}, characteristic of ester bonds, C-O stretching in the range of 1180–1080 cm^{-1}, and C-H stretching near 2990–2940 cm^{-1}. Native HA (red) exhibits key peaks such as a broad O-H stretching vibration between 3300–3400 cm^{-1}, indicative of hydroxyl groups, as well as amide I (1650 cm^{-1}) and amide II (1550 cm^{-1}) bands, which correspond to the amide bonds in HA. Additionally, C-O-C stretching vibrations around 1070–1030 cm^{-1} confirm the polysaccharide structure of

HA. The HA-coated PLGA nanoparticles (blue) spectrum retains the key features of both PLGA and HA, demonstrating successful coating. The presence of the broad O-H stretching (3300–3400 cm^{-1}), amide I and II bands (~1650 cm^{-1} and ~1550 cm^{-1}), and C-O-C stretching near 1070–1030 cm^{-1} confirms the presence of HA, while the retained C=O stretching at ~1750 cm^{-1} indicates the integrity of the PLGA core. These findings align with literature values and confirm the successful functionalization of PLGA nanoparticles with HA, which is essential for applications such as targeted drug delivery and biomaterial engineering.

In addition, shelf life is a critical parameter in therapeutic nanosystems, as it directly impacts the practicality of large-scale production by reducing the frequency of synthesis and ensuring consistent formulation quality. To evaluate stability, all formulations were lyophilized and stored at -22°C. After 4 months of storage, HP nanoparticles exhibited a mean size of 201±2 nm with a PDI of 0.17±0.01, indicating a stable size distribution. However, by 6 months, the particle size increased significantly to 649±43 nm with a PDI of 0.75±0.20, suggesting the onset of aggregation or instability. In contrast, CHP nanoparticles demonstrated less stability, indeed their size was already 661±114 nm and 0.55±0.19 PDI after 2 months of storage at -22°C. These results suggest that while the synthesized empty HP nanoparticles maintain stability for up to 4 months under the tested conditions, drug-loaded CHP formulations exhibit reduced shelf life. This reduction in stability is likely due to additional stress on the nanoparticle matrix from the encapsulated CVL, potentially exacerbating aggregation or degradation processes[50]. Future optimization of the formulation or storage conditions may help mitigate this issue and enhance the shelf life of drug-loaded nanosystems.

3.2 Carvacrol release studies

The release profile of CVL from HA-coated PLGA nanoparticles was monitored over 66 days in PBS + 4.5% w/v BSA media under sink conditions (Figure 2). BSA is included in the release medium to simulate physiological conditions and enhance the solubility of hydrophobic compounds, ensuring accurate measurement of its release kinetics. The release graph illustrates a sustained drug release profile with an initial burst release in the first 7 hours and a subsequent zero-order release pattern. The burst release phase

exhibits a 36±3% CVL release, whereas the remaining ~64% of the drug undergoes release over the next 65.7 days. The first part of CVL release stems from the amount of drug encapsulated close to the surface of PLGA nanoparticles or drug adsorbed to the external surface, which characterizes the burst release phenomenon. Specifically, 26±3% of the drug is liberated immediately at the first time point (1 hour), as the drug located on the surface becomes rapidly stripped away in an uncontrolled manner by the release medium. Between 25% and 40% release, the drug requires approximately 6 hours to dissolve, following a zero-order kinetic profile with a slope coefficient of 35.5 (R^2=0.99). This fraction of the drug release results from desorption, meaning the breakdown of weak interactions between the polymer matrix and carvacrol.

Following this, the real zero-order kinetics phase initiates, governed by PLGA degradation, with a slope coefficient of 0.8 (R^2=0.99), which remains lower than that of the desorption phase. In this final phase, drug release relies on the gradual degradation of the polymeric nanoparticles, ensuring a sustained and controlled delivery over time. Indeed, PLGA is a well-known drug carrier for its biodegradability but notorious for its slow-release profile [51–54]. The review by Fredenberg *et al*. [54] described the various mechanisms of drug release from PLGA noting many studies that reported the adsorbance of BSA on PLGA and subsequent delayed drug release. Moreover, a strong drug-polymer interaction can also cause a slow release [55,56]. Considering that the nanoparticles were coated with a highly hydrophilic HA, it is possible that the initial burst release noticed may have been due to the release of the CVL close to the surface of PLGA caused by diffusion through water absorbed by the HA. Once this was over, the subsequent drug release would have to be from deep inside the core of the nanoparticles, this would require erosion of the nanoparticle and/or release of the cargo from the polymer by further water absorption. Either of these mechanisms would take longer than usual due to slow degrading characteristic of PLGA.

Hence, the hydrophilicity of HA and hydrophobicity of PLGA provided a challenge for the nanoparticles to dissolve. This resulted in a long-prolonged release of CVL that lasted 66 days. A similar slow drug release profile of CVL from chitosan nanoparticles was also reported by Keawchaoon *et al* [57]. The study reported triphasic release profiles in different pH media for over a span of two months. A more acidic buffer (pH 3) was observed with the highest release rate of 52%, while pH 7-11 reported release rates of 22-33%. This is

in line with our studies where BSA was used in the release media which has a reported pH range of 4-9. While our study employed PLGA nanoparticles and HA, it can be said that CVL has an inherent nature of a slow-release profile.

Moreover, the slow PLGA nanoparticle erosion is validated using Equation 3, where the mechanism is attributed to the controlled release phenomenon where a potential gradient is developed, and nanoparticle erosion is witnessed in stress conditions.

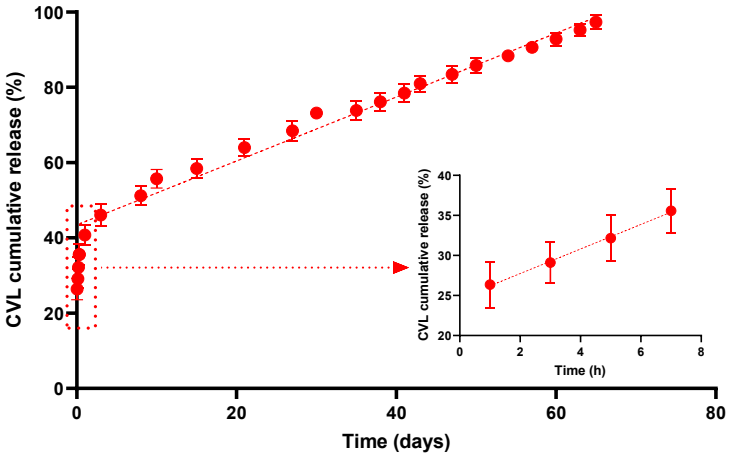

Figure 2. The cumulative release profile of CVL from CHP nanoparticles in PBS with 4.5% w/v BSA was analyzed using GC-MS. A burst release of CVL was observed in the first 7 hours, followed by a sustained zero-order release until day 66, leading to complete drug release. Data are presented as mean ± SD (n = 3)

3.3 Nanoparticle uptake by M1 macrophages

A targeted drug delivery system is essential for maximizing therapeutic efficacy while minimizing unintended effects. By reducing damage to nearby healthy cells, such systems improve patient outcomes and reduce adverse effects. In this study, HA was utilized to enhance the precision of CVL-loaded PLGA nanoparticles delivery specifically to M1 macrophages (M1-m). This targeted approach is crucial, as it ensures that the therapeutic effects are concentrated solely on the intended cells. The difference in cellular uptake after 24 hours of incubation of PLGA nanoparticles co-loaded with CVL and Nile red, with and without HA coating, is depicted in Figure 3. Before nanoparticles

incubation, M1-m cells were pre-treated with lipopolysaccharide (LPS). LPS pretreatment is crucial for nanoparticle uptake studies involving M1 macrophages because it polarizes the macrophages toward a pro-inflammatory state, mimicking conditions seen in infection or disease. M1 macrophages, characterized by their heightened phagocytic activity and cytokine production, provide a realistic and physiologically relevant model to evaluate how nanoparticles interact with activated immune cells. This step ensures accurate assessment of nanoparticle efficacy, targeting potential, and safety under inflammatory conditions, which are often the therapeutic focus in drug delivery or immunomodulation research.

Notably, LPS-treated M1-m incubated with HA-coated CVL-loaded PLGA nanoparticles (CHP NPs) exhibited a significant increase in total mean fluorescence intensity (MFI) compared to uncoated CVL-loaded PLGA nanoparticles (CP NPs). Nile red, a hydrophobic fluorescent dye, was chosen to label the nanoparticles due to its strong affinity for lipid-rich environments and co-loaded with CVL. It shares the same hydrophobic nature as CVL, making it an ideal marker for tracking the distribution and uptake of CVL-loaded nanoparticles. Specifically, the MFI recorded was 33,453±3,599 a.u. for CHP NPs while a signal of 47,055±4,544 a.u. was noted for CP NPs. This represented approximately a +41% higher fluorescence signal when the nanoparticles were coated with HA, indicating enhanced uptake. The observed increase is attributed to HA functioning as a direct ligand for the CD44 receptor on the M1-m surface, facilitating receptor-mediated endocytosis and improving nanoparticle internalization. The observed increase in uptake due to HA coating aligns with previous studies[1, 51], further validating the role of HA in enhancing macrophage-specific targeting. These findings underscore the potential of HA-functionalized nanoparticles as a robust platform for targeted drug delivery, offering a compelling strategy to improve therapeutic outcomes.

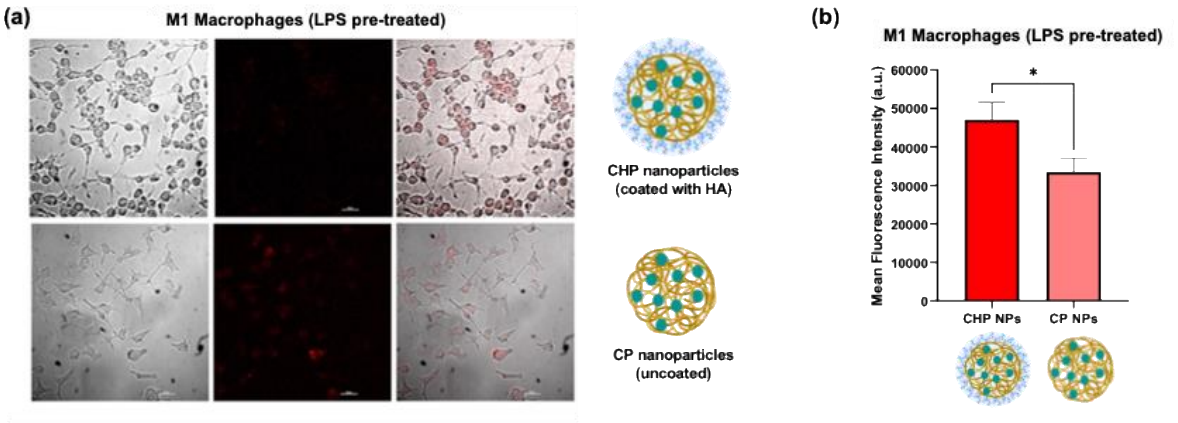

Figure 3. Uptake of PLGA (CP) and HA-coated PLGA (CHP) nanoparticles (NPs) co-loaded with CVL and Nile red by M1 macrophages (M1-m). (a) Confocal laser scanning microscopy (CLSM) images of M1-m monocultures after 24 hours of incubation with CP and CHP NPs at 37 °C, showing intracellular NPs localization. (b) Quantification of total mean fluorescence intensity (MFI) as described in section 2.3.7, indicating the extent of NPs uptake. Data are presented as mean ± SD (n = 6), with *p < 0.05. Scale bar = 20 µm.

3.4 Macrophage polarization

Macrophages exhibit remarkable plasticity, enabling them to polarize into either a pro-inflammatory (M1) or an anti-inflammatory (M2) phenotype in response to environmental stimuli. This dynamic polarization plays a critical role in immune regulation and has significant implications for the development of targeted therapies for inflammatory diseases. In this study, LPS treatment was employed to polarize macrophages into the M1 phenotype effectively, as evidenced by the significantly higher expression of M1 markers CD86 and iNOS compared to M2 markers CD163 and CD206. This polarization model provided a robust framework to evaluate the effects of CVL-loaded HA-coated PLGA nanoparticles (CHP) on macrophage phenotype modulation.

The study revealed that treating M1-polarized macrophages with 5 µg/mL of CHP nanoparticles (containing 1.3 µg of CVL) led to a modest increase in the M2 marker CD163 (+93%), indicating limited polarization resistance at this concentration (Figure 4). However, when the CHP concentration was increased to 10 µg/mL (containing 2.6 µg/mL of CVL), the effects became striking. Specifically, M1 markers CD86 and iNOS were drastically reduced (-83% and -84%, respectively), while M2 markers CD163 and CD206 were significantly elevated (+321% and +399%, respectively). These results demonstrate

a clear dose-dependent effect, reinforcing the potency of CHP nanoparticles in shifting macrophages from a pro-inflammatory to an anti-inflammatory state. This underscores the importance of optimizing CHP concentrations for effective therapeutic outcomes.

To further investigate the synergistic effects of CVL and HA-coated PLGA nanoparticles, parallel experiments were conducted using equivalent (2.6 µg/mL) and higher (10 µg/mL) concentrations of naked CVL and unloaded HA-PLGA nanoparticles (HP). In all the control groups (Figure 5), the formulations showed negligible effects on macrophage polarization, with minimal changes in M1 and M2 markers. At CVL 10 µg/mL, naked CVL-treated macrophages exhibited an ambiguous phenotype, with moderate reductions in CD86 (-40%) and iNOS (-38%) but only limited increases in CD163 (+115%) and CD206 (+189%), indicating a lack of strong polarization in either direction. Similarly, treatment with HP nanoparticles at 10 µg/mL failed to elicit a significant M2 response. Overall, these findings highlight the critical role of HA-mediated targeting and sustained CVL release in maximizing therapeutic efficacy. Unlike naked CVL and placebo HP nanoparticles, which displayed only partial or inconsistent effects, CHP nanoparticles effectively suppressed pro-inflammatory M1 markers while robustly enhancing M2 polarization. This underscores the novel synergistic potential of CHP in immune modulation, paving the way for its application in inflammation-related therapies. Therefore, the HA coating of the PLGA nanoparticles plays a pivotal role in targeting macrophages and enhancing therapeutic outcomes. HA affinity for CD44 receptors, which are overexpressed on activated macrophages, facilitates selective uptake of CHP by the target cells. This targeted delivery mechanism likely contributes to the enhanced anti-inflammatory effects observed with CHP treatment. Additionally, the HA coating may improve nanoparticle stability and biodistribution, further augmenting their efficacy.

An important observation was the dose-dependent toxicity associated with higher concentrations of CVL and CHP (Figures 4-5), necessitating the exclusion of higher doses from the study to maintain cell viability. While 10 µg/mL of CHP nanoparticles was identified as an effective concentration for macrophage polarization, higher doses led to significant cytotoxicity, underscoring the delicate balance between therapeutic efficacy and safety in nanoparticle-based drug delivery systems (data not shown). This finding highlights the importance of optimizing nanoparticle formulations and dosing regimens to minimize off-target effects while maximizing therapeutic benefits.

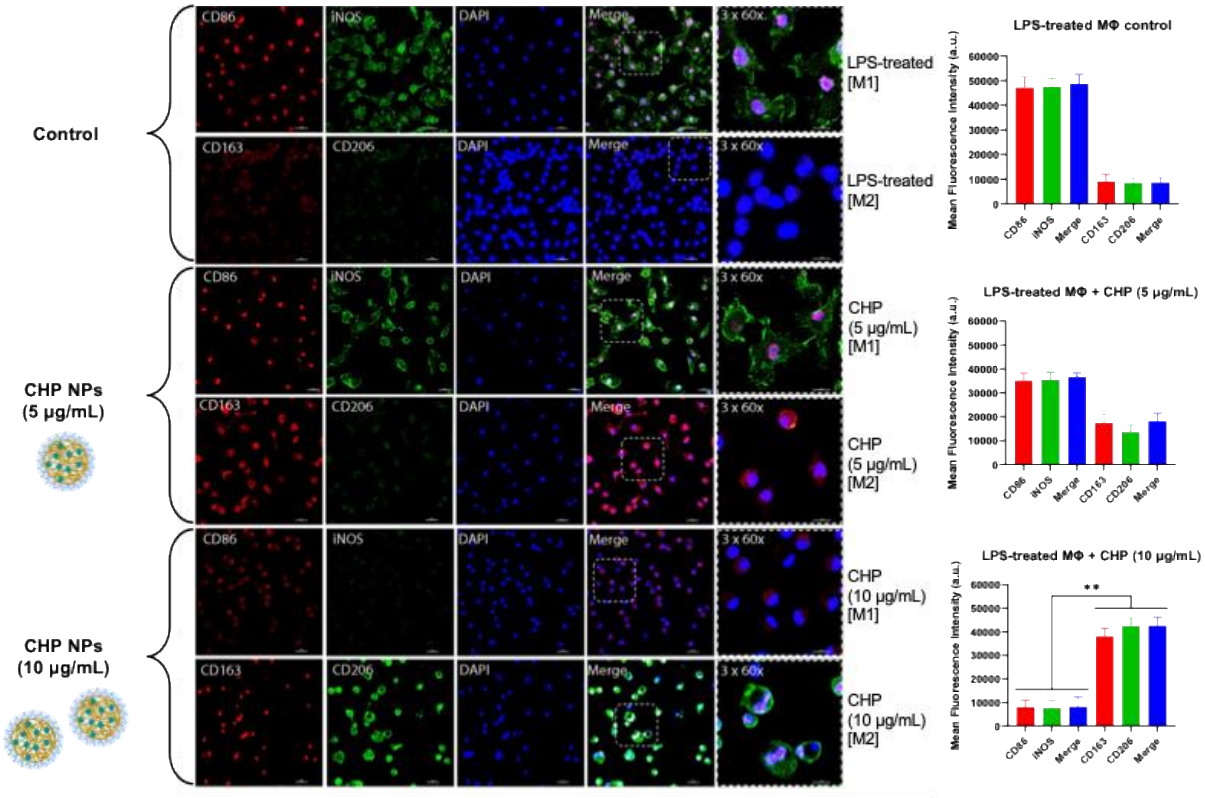

Figure 4. LPS pre-treated macrophages (M were incubated with different concentrations of CHP nanoparticles (CHP NPs). CHP nanoparticles with 5 µg/mL concentration showed a lower polarization of M1 macrophages to M2 marcophages, as compared to a higher CHP nanoparticle concentration of 10 µg/mL. The total MFI was calculated as described in section 2.3.7. All values are expressed as mean ± SD (n =3).

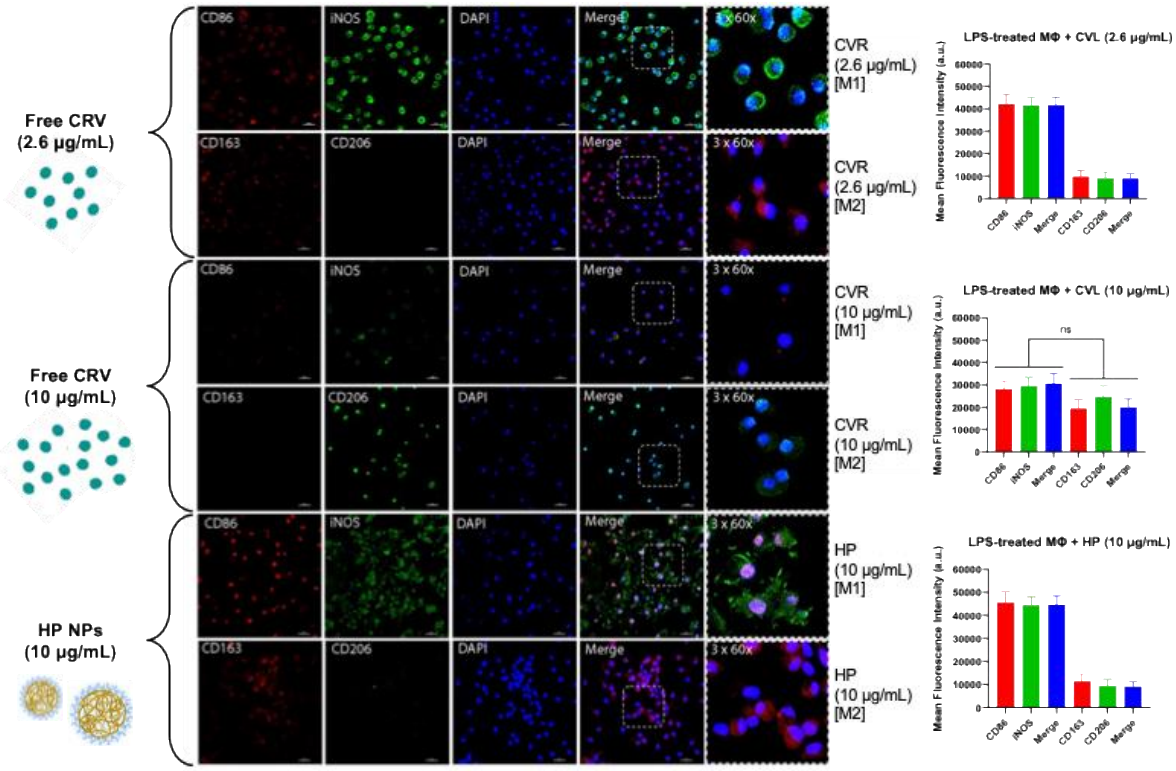

Figure 5. LPS-treated cells were incubated with different concentrations of CVL and HP, to observe the difference in the marker expressions of M1-m and M2-m. Failure to see a significant increase in the M2-m marker expressions on incubation with HP and free CVL, confirm the anti-inflammatory effect of CVL in CHP. The total MFI calculated as described in section 2.3.7. All values are expressed as mean ± SD (n =6).

3.5 Modulation of inflammatory cytokine production

The production of inflammatory cytokines plays a pivotal role in regulating the inflammatory response at the site of injury or infection. These signaling molecules orchestrate the activation, resolution, or amplification of the immune response, and their balance is critical in determining the progression of inflammation. To better understand the therapeutic potential of the CHP nanoparticles (NPs), the cytokines expression profile of LPS-treated macrophages was analyzed for both pro-inflammatory cytokines (IL-1α, IL-1β, TNF-α) and anti-inflammatory cytokines (IL-1ra, IL-4, IL-10). The detailed results are illustrated in Figure 6. In LPS-stimulated macrophages, a hallmark of inflammation is the robust production of pro-inflammatory cytokines such as IL-1α, IL-1β, and TNF-α [27,59,60]. After treatment with 10 µg/mL of CHP NPs, a substantial reduction in these pro-inflammatory mediators was observed. Specifically, IL-1α expression

decreased by -25%, IL-1β by -36%, and TNF-α by -36%, as shown in Figure 6a-c. These reductions highlight the ability of CHP to suppress key inflammatory pathways, likely due to the sustained release of CVL and HA-mediated targeted delivery. TNF-α, a pivotal cytokine that amplifies the inflammatory cascade, was notably reduced, indicating that CHP could effectively disrupt the inflammation feedback loop. Similarly, IL-1α and IL-1β, which contribute to tissue damage and immune cell recruitment, were significantly downregulated, reinforcing the broad anti-inflammatory potential of CHP treatment. In addition to reducing pro-inflammatory cytokines, CHP treatment markedly increased the levels of anti-inflammatory cytokines. As depicted in Figure 6d-f, IL-1ra expression increased by +258%, IL-4 by +260%, and IL-10 by +40% following CHP administration. These cytokines play essential roles in resolving inflammation and promoting tissue repair, further supporting the therapeutic potential of CHP nanoparticles.

Taken together, these findings underscore the powerful dual action of CHP nanoparticles in both suppressing pro-inflammatory pathways and enhancing anti-inflammatory responses. The HA-mediated targeted delivery and sustained release of CVL enable effective macrophage reprogramming, making CHP a promising strategy for inflammation modulation and tissue regeneration. For example, IL-1ra acts as a natural antagonist to IL-1α/β, competitively inhibiting their pro-inflammatory effects, while IL-4 and IL-10 are key regulators of M2 macrophage polarization and immune homeostasis. The dramatic upregulation of these cytokines indicates that CHP not only suppresses inflammation but also actively promotes resolution and repair processes.

The dual action of CHP, by downregulating pro-inflammatory and upregulating anti-inflammatory cytokines, points to a sophisticated mechanism of immune modulation. The HA coating facilitates targeted delivery to inflammatory macrophages, which are abundant in receptors for hyaluronic acid, ensuring that the nanoparticles reach their intended site of action. Once internalized, the slow and controlled release of CVL enables sustained suppression of inflammatory mediators while preventing macrophage activation from rebounding. Moreover, the enhanced expression of IL-4 and IL-10 suggests that CVL influences the signaling pathways that drive macrophage polarization from the pro-inflammatory M1 phenotype to the anti-inflammatory M2 phenotype, as demonstrated previously. To mention, also in this case, the control groups did not show any effect on the cytokine modulation levels.

These findings are particularly significant given the challenges associated with current anti-inflammatory therapies, which often lack specificity and have systemic side effects. By selectively targeting inflammatory macrophages and modulating their cytokine production, CHP presents a novel therapeutic approach. The ability to simultaneously suppress harmful inflammation while enhancing reparative processes sets this system apart as an advanced and potentially transformative treatment for inflammatory diseases, including those involving chronic or excessive immune activation. Given the potent effects observed in cytokine modulation, CHP has the potential to be adapted for a variety of clinical applications. Beyond the scope of this study, its use could be extended to conditions such as rheumatoid arthritis, inflammatory bowel disease, and even neuroinflammatory disorders. Furthermore, the platform's versatility allows for modification with other bioactive agents, expanding its utility across a broad range of inflammatory and degenerative diseases.

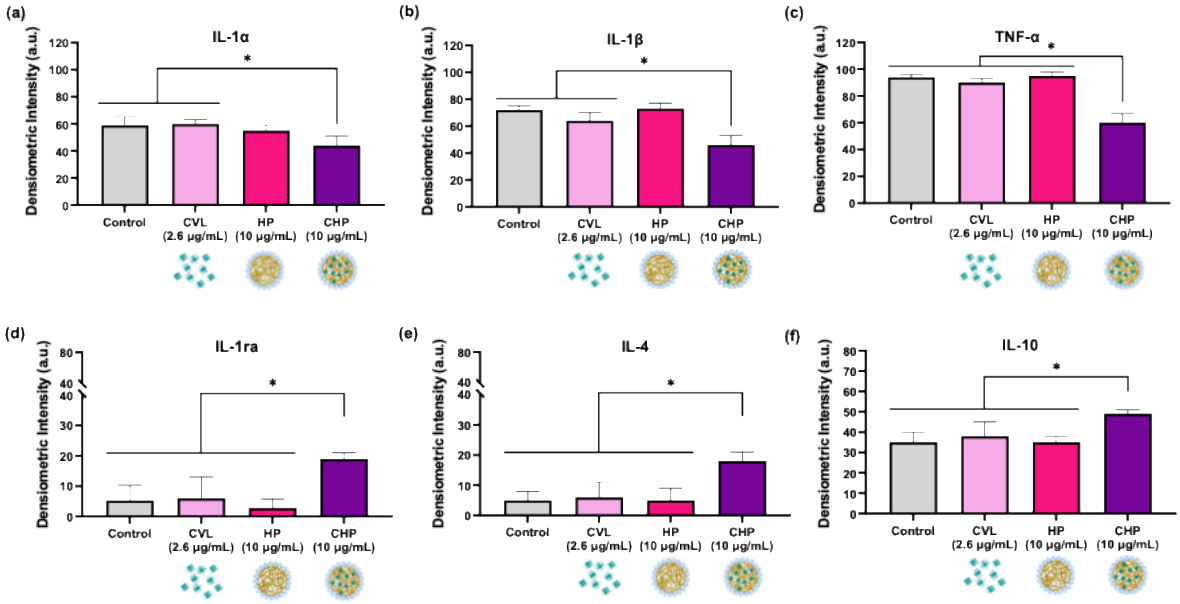

Figure 6. The difference in the cytokine expressions in LPS-treated macrophages. (a) Decrease in pro-inflammatory cytokines, IL-1α/β and TNF-α, on treatment with CHP and (b) increase in the anti-inflammatory cytokine expressions of IL-1ra/4/10. Immunoreactive spots were quantitated densitometrically using ImageJ software. Error bars represent ± standard error (*$p < 0.05$).

4. Conclusion

This study introduces a novel HA-coated PLGA (CHP) nanoparticle system for sustained CVL delivery, demonstrating its potent anti-inflammatory potential. CHP nanoparticles achieve high CVL encapsulation efficiency while enabling targeted release, minimizing drug volatility and cytotoxicity. Following an initial burst, CVL release follows zero-order kinetics, extending over 66 days. Uniquely, CHP nanoparticles downregulate pro-inflammatory cytokines (IL-1α/β, TNF-α) while upregulating anti-inflammatory markers (IL-1ra, IL-4, IL-10), promoting a significant shift of macrophages from the inflammatory M1 state to the anti-inflammatory M2 state. Furthermore, the controlled release of CVL from the nanoparticles prolongs its anti-inflammatory effects and mitigates its rapid biological degradation. These findings highlight a highly efficient, novel nanosystem capable of targeting inflammation through cytokine modulation and macrophage polarization, with potential for transformative applications in inflammation-related diseases and pain management.

5. References

(1) Farajzadeh, R.; Zarghami, N.; Serati-Nouri, H.; Momeni-Javid, Z.; Farajzadeh, T.; Jalilzadeh-Tabrizi, S.; Sadeghi-Soureh, S.; Naseri, N.; Pilehvar-Soltanahmadi, Y. Macrophage Repolarization Using CD44-Targeting Hyaluronic Acid–Polylactide Nanoparticles Containing Curcumin. *Artif Cells Nanomed Biotechnol* **2017**, *46* (8), 1–9. https://doi.org/10.1080/21691401.2017.1408116.

(2) Pan, M. H.; Lai, C. S.; Ho, C. T. Anti-Inflammatory Activity of Natural Dietary Flavonoids. *Food Funct* **2010**, *1* (1), 15–31. https://doi.org/10.1039/C0FO00103A.

(3) Chamorro, Á.; Hallenbeck, J. The Harms and Benefits of Inflammatory and Immune Responses in Vascular Disease. *Stroke* **2006**, *37* (2), 291–293. https://doi.org/10.1161/01.STR.0000200561.69611.F8.

(4) Jiang, W.; Zhang, L. X.; Tan, X. Y.; Yu, P.; Dong, M. Inflammation and Histone Modification in Chronic Pain. *Front Immunol* **2023**, *13*, 1087648. https://doi.org/10.3389/FIMMU.2022.1087648/BIBTEX.

(5) Campos, E. V. R.; Proença, P. L. F.; Oliveira, J. L.; Pereira, A. E. S.; De Morais Ribeiro, L. N.; Fernandes, F. O.; Gonçalves, K. C.; Polanczyk, R. A.; Pasquoto-Stigliani, T.; Lima, R.; Melville, C. C.; Della Vechia, J. F.; Andrade, D. J.; Fraceto, L. F. Carvacrol

and Linalool Co-Loaded in β-Cyclodextrin-Grafted Chitosan Nanoparticles as Sustainable Biopesticide Aiming Pest Control. *Scientific Reports 2018 8:1* **2018**, *8* (1), 1–14. https://doi.org/10.1038/s41598-018-26043-x.

(6) Iannitelli, A.; Grande, R.; di Stefano, A.; di Giulio, M.; Sozio, P.; Bessa, L. J.; Laserra, S.; Paolini, C.; Protasi, F.; Cellini, L. Potential Antibacterial Activity of Carvacrol-Loaded Poly(DL-Lactide-Co-Glycolide) (PLGA) Nanoparticles against Microbial Biofilm. *International Journal of Molecular Sciences 2011, Vol. 12, Pages 5039-5051* **2011**, *12* (8), 5039–5051. https://doi.org/10.3390/IJMS12085039.

(7) Ben Arfa, A.; Combes, S.; Preziosi-Belloy, L.; Gontard, N.; Chalier, P. Antimicrobial Activity of Carvacrol Related to Its Chemical Structure. *Lett Appl Microbiol* **2006**, *43* (2), 149–154. https://doi.org/10.1111/J.1472-765X.2006.01938.X.

(8) Lima, M. D. S.; Quintans-Júnior, L. J.; De Santana, W. A.; Martins Kaneto, C.; Pereira Soares, M. B.; Villarreal, C. F. Anti-Inflammatory Effects of Carvacrol: Evidence for a Key Role of Interleukin-10. *Eur J Pharmacol* **2013**, *699* (1–3), 112–117. https://doi.org/10.1016/J.EJPHAR.2012.11.040.

(9) Simmons, D. L.; Botting, R. M.; Hla, T. Cyclooxygenase Isozymes: The Biology of Prostaglandin Synthesis and Inhibition. *Pharmacol Rev* **2004**, *56* (3), 387–437. https://doi.org/10.1124/PR.56.3.3.

(10) Hotta, M.; Nakata, R.; Katsukawa, M.; Hori, K.; Takahashi, S.; Inoue, H. Carvacrol, a Component of Thyme Oil, Activates PPARα and γ and Suppresses COX-2 Expression. *J Lipid Res* **2010**, *51* (1), 132–139. https://doi.org/10.1194/jlr.M900255-JLR200.

(11) Yan, C.; Kuang, W.; Jin, L.; Wang, R.; Niu, L.; Xie, C.; Ding, J.; Liao, Y.; Wang, L.; Wan, H.; Ma, G.; Liang, J. Carvacrol Protects Mice against LPS-Induced Sepsis and Attenuates Inflammatory Response in Macrophages by Modulating the ERK1/2 Pathway. *Scientific Reports* | **123AD**, *13*, 12809. https://doi.org/10.1038/s41598-023-39665-7.

(12) Mahmoodi, M.; Amiri, H.; Ayoobi, F.; Rahmani, M.; Taghipour, Z.; Ghavamabadi, R. T.; Jafarzadeh, A.; Sankian, M. Carvacrol Ameliorates Experimental Autoimmune Encephalomyelitis through Modulating Pro- and Anti-Inflammatory Cytokines. *Life Sci* **2019**, *219*, 257–263. https://doi.org/10.1016/j.lfs.2018.11.051.

(13) Wei, H. K.; Xue, H. X.; Zhou, Z. X.; Peng, J. A Carvacrol-Thymol Blend Decreased Intestinal Oxidative Stress and Influenced Selected Microbes without Changing the Messenger RNA Levels of Tight Junction Proteins in Jejunal Mucosa of Weaning Piglets. *Animal* **2017**, *11*, 193–201. https://doi.org/10.1017/S1751731116001397.

(14) Türkez, H.; Aydln, E. Investigation of Cytotoxic, Genotoxic and Oxidative Properties of Carvacrol in Human Blood Cells. *Toxicol Ind Health* **2016**, *32* (4), 625–633. https://doi.org/10.1177/0748233713506771.

(15) Sampaio, L. A.; Pina, L. T. S.; Serafini, M. R.; Tavares, D. dos S.; Guimarães, A. G. Antitumor Effects of Carvacrol and Thymol: A Systematic Review. *Frontiers in Pharmacology*. Frontiers Media S.A. July 2021. https://doi.org/10.3389/fphar.2021.702487.

(16) Llana-Ruiz-Cabello, M.; Gutiérrez-Praena, D.; Pichardo, S.; Moreno, F. J.; Bermúdez, J. M.; Aucejo, S.; Cameán, A. M. Cytotoxicity and Morphological Effects Induced by Carvacrol and Thymol on the Human Cell Line Caco-2. *Food and Chemical Toxicology* **2014**, *64*, 281–290. https://doi.org/10.1016/j.fct.2013.12.005.

(17) Yammine, J.; Gharsallaoui, A.; Fadel, A.; Mechmechani, S.; Karam, L.; Ismail, A.; Chihib, N. E. Enhanced Antimicrobial, Antibiofilm and Ecotoxic Activities of Nanoencapsulated Carvacrol and Thymol as Compared to Their Free Counterparts. *Food Control* **2023**, *143*. https://doi.org/10.1016/j.foodcont.2022.109317.

(18) Xu, J.; Zhou, F.; Ji, B. P.; Pei, R. S.; Xu, N. The Antibacterial Mechanism of Carvacrol and Thymol against Escherichia Coli. *Lett Appl Microbiol* **2008**, *47* (3), 174–179. https://doi.org/10.1111/J.1472-765X.2008.02407.X.

(19) Liu, Y. C.; Zou, X. B.; Chai, Y. F.; Yao, Y. M. Macrophage Polarization in Inflammatory Diseases. *Int J Biol Sci* **2014**, *10* (5), 520. https://doi.org/10.7150/IJBS.8879.

(20) Rios de la Rosa, J. M.; Tirella, A.; Gennari, A.; Stratford, I. J.; Tirelli, N. The CD44-Mediated Uptake of Hyaluronic Acid-Based Carriers in Macrophages. *Adv Healthc Mater* **2017**, *6* (4). https://doi.org/10.1002/adhm.201601012.

(21) Choi, K. Y.; Chung, H.; Min, K. H.; Yoon, H. Y.; Kim, K.; Park, J. H.; Kwon, I. C.; Jeong, S. Y. Self-Assembled Hyaluronic Acid Nanoparticles for Active Tumor Targeting.

Biomaterials **2010**, *31* (1), 106–114. https://doi.org/10.1016/J.BIOMATERIALS.2009.09.030.

(22) Wickens, J. M.; Alsaab, H. O.; Kesharwani, P.; Bhise, K.; Amin, M. C. I. M.; Tekade, R. K.; Gupta, U.; Iyer, A. K. Recent Advances in Hyaluronic Acid-Decorated Nanocarriers for Targeted Cancer Therapy. *Drug Discov Today* **2017**, *22* (4), 665–680. https://doi.org/10.1016/J.DRUDIS.2016.12.009.

(23) Yadav, A. K.; Mishra, P.; Mishra, A. K.; Mishra, P.; Jain, S.; Agrawal, G. P. Development and Characterization of Hyaluronic Acid–Anchored PLGA Nanoparticulate Carriers of Doxorubicin. *Nanomedicine* **2007**, *3* (4), 246–257. https://doi.org/10.1016/J.NANO.2007.09.004.

(24) Salathia, S.; Gigliobianco, M. R.; Casadidio, C.; Di Martino, P.; Censi, R. Hyaluronic Acid-Based Nanosystems for CD44 Mediated Anti-Inflammatory and Antinociceptive Activity. *International Journal of Molecular Sciences 2023, Vol. 24, Page 7286* **2023**, *24* (8), 7286. https://doi.org/10.3390/IJMS24087286.

(25) Liu, E.; Zhou, Y.; Liu, Z.; Li, J.; Zhang, D.; Chen, J.; Cai, Z. Cisplatin Loaded Hyaluronic Acid Modified TiO2 Nanoparticles for Neoadjuvant Chemotherapy of Ovarian Cancer. *J Nanomater* **2015**, *2015*. https://doi.org/10.1155/2015/390358.

(26) Pedrosa, S. S.; Pereira, P.; Correia, A.; Gama, F. M. Targetability of Hyaluronic Acid Nanogel to Cancer Cells: In Vitro and in Vivo Studies. **2017**. https://doi.org/10.1016/j.ejps.2017.03.045.

(27) Isa, I. L. M.; Srivastava, A.; Tiernan, D.; Owens, P.; Rooney, P.; Dockery, P.; Pandit, A. Hyaluronic Acid Based Hydrogels Attenuate Inflammatory Receptors and Neurotrophins in Interleukin-1β Induced Inflammation Model of Nucleus Pulposus Cells. *Biomacromolecules* **2015**, *16* (6), 1714–1725. https://doi.org/10.1021/acs.biomac.5b00168.

(28) Misra, S.; Hascall, V. C.; Markwald, R. R.; Ghatak, S. Interactions between Hyaluronan and Its Receptors (CD44, RHAMM) Regulate the Activities of Inflammation and Cancer. *Frontiers in Immunology*. 2015. https://doi.org/10.3389/fimmu.2015.00201.

(29) Manca, M. L.; Castangia, I.; Zaru, M.; Nácher, A.; Valenti, D.; Fernàndez-Busquets, X.; Fadda, A. M.; Manconi, M. Development of Curcumin Loaded Sodium Hyaluronate Immobilized Vesicles (Hyalurosomes) and Their Potential on Skin

Inflammation and Wound Restoring. *Biomaterials* **2015**, *71*, 100–109. https://doi.org/10.1016/j.biomaterials.2015.08.034.

(30) Kita, K.; Dittrich, C. Drug Delivery Vehicles with Improved Encapsulation Efficiency: Taking Advantage of Specific Drug-Carrier Interactions. *Expert Opin Drug Deliv* **2011**, *8* (3), 329–342. https://doi.org/10.1517/17425247.2011.553216.

(31) Kim, M. R.; Feng, T.; Zhang, Q.; Chan, H. Y. E.; Chau, Y. Co-Encapsulation and Co-Delivery of Peptide Drugs via Polymeric Nanoparticles. *Polymers (Basel)* **2019**, *11* (2). https://doi.org/10.3390/POLYM11020288.

(32) Klojdová, I.; Milota, T.; Smetanová, J.; Stathopoulos, C. Encapsulation: A Strategy to Deliver Therapeutics and Bioactive Compounds? *Pharmaceuticals* **2023**, *16* (3). https://doi.org/10.3390/PH16030362.

(33) Ayres Cacciatore, F.; Dalmás, M.; Maders, C.; Ataíde Isaía, H.; Brandelli, A.; da Silva Malheiros, P. Carvacrol Encapsulation into Nanostructures: Characterization and Antimicrobial Activity against Foodborne Pathogens Adhered to Stainless Steel. *Food Research International* **2020**, *133*, 109143. https://doi.org/10.1016/J.FOODRES.2020.109143.

(34) Schaffazick, S. R.; Guterres, S. S.; De Lucca Freitas, L.; Pohlmann, A. R. Caracterização e Estabilidade Físico-Química de Sistemas Poliméricos Nanoparticulados Para Administração de Fármacos. *Quim Nova* **2003**, *26* (5), 726–737. https://doi.org/10.1590/S0100-40422003000500017.

(35) Michiels, J.; Missotten, J.; Dierick, N.; Fremaut, D.; Maene, P.; De Smet, S. In Vitro Degradation and in Vivo Passage Kinetics of Carvacrol, Thymol, Eugenol and Trans-Cinnamaldehyde along the Gastrointestinal Tract of Piglets. *J Sci Food Agric* **2008**, *88* (13), 2371–2381. https://doi.org/10.1002/JSFA.3358.

(36) Pradhan, R.; Ramasamy, T.; Choi, J. Y.; Kim, J. H.; Poudel, B. K.; Tak, J. W.; Nukolova, N.; Choi, H. G.; Yong, C. S.; Kim, J. O. Hyaluronic Acid-Decorated Poly(Lactic-Co-Glycolic Acid) Nanoparticles for Combined Delivery of Docetaxel and Tanespimycin. *Carbohydr Polym* **2015**, *123*, 313–323. https://doi.org/10.1016/J.CARBPOL.2015.01.064.

(37) Cosco, D.; Mare, R.; Paolino, D.; Salvatici, M. C.; Cilurzo, F.; Fresta, M. Sclareol-Loaded Hyaluronan-Coated PLGA Nanoparticles: Physico-Chemical Properties

and in Vitro Anticancer Features. *Int J Biol Macromol* **2019**, *132*, 550–557. https://doi.org/10.1016/J.IJBIOMAC.2019.03.241.

(38) Sheybanifard, M.; Beztsinna, N.; Bagheri, M.; Buhl, E. M.; Bresseleers, J.; Varela-Moreira, A.; Shi, Y.; van Nostrum, C. F.; van der Pluijm, G.; Storm, G.; Hennink, W. E.; Lammers, T.; Metselaar, J. M. Systematic Evaluation of Design Features Enables Efficient Selection of Π Electron-Stabilized Polymeric Micelles. *Int J Pharm* **2020**, *584*, 119409. https://doi.org/10.1016/J.IJPHARM.2020.119409.

(39) Dash, S.; Murthy, P. N.; Nath, L.; Chowdhury, P. Kinetic Modeling on Drug Release from Controlled Drug Delivery Systems. *Acta Poloniae Pharmaceutica - Drug Research*. 2010, pp 217–223.

(40) Stulzer, H. K.; Tagliari, M. P.; Parize, A. L.; Silva, M. A. S.; Laranjeira, M. C. M. Evaluation of Cross-Linked Chitosan Microparticles Containing Acyclovir Obtained by Spray-Drying. *Materials Science and Engineering C* **2009**, *29*, 387–392. https://doi.org/10.1016/j.msec.2008.07.030.

(41) Brugger, W.; Kreutz, M.; Andreesen, R. Macrophage Colony-Stimulating Factor Is Required for Human Monocyte Survival and Acts as a Cofactor for Their Terminal Differentiation to Macrophages in Vitro. *J Leukoc Biol* **1991**, *49*, 483–488. https://doi.org/10.1002/jlb.49.5.483.

(42) Spadea, A.; Rios De La Rosa, J. M.; Tirella, A.; Ashford, M. B.; Williams, K. J.; Stratford, I. J.; Tirelli, N.; Mehibel, M. Evaluating the Efficiency of Hyaluronic Acid for Tumor Targeting via CD44. *Mol Pharm* **2019**, *16*, 2481–2493. https://doi.org/10.1021/acs.molpharmaceut.9b00083.

(43) MUKERJEE, A.; VISHWANATHA, J. K. Formulation, Characterization and Evaluation of Curcumin-Loaded PLGA Nanospheres for Cancer Therapy. *Anticancer Res* **2009**, *29* (10), 3867.

(44) Lisi, L.; Ciotti, G. M. P.; Braun, D.; Kalinin, S.; Currò, D.; Dello Russo, C.; Coli, A.; Mangiola, A.; Anile, C.; Feinstein, D. L.; Navarra, P. Expression of INOS, CD163 and ARG-1 Taken as M1 and M2 Markers of Microglial Polarization in Human Glioblastoma and the Surrounding Normal Parenchyma. *Neurosci Lett* **2017**, *645*, 106–112. https://doi.org/10.1016/J.NEULET.2017.02.076.

(45) Lescoat, A.; Ballerie, A.; Jouneau, S.; Fardel, O.; Vernhet, L.; Jego, P.; Lecureur, V. M1/M2 Polarisation State of M-CSF Blood-Derived Macrophages in Systemic

Sclerosis. *Ann Rheum Dis* **2019**, *78* (11), e127–e127. https://doi.org/10.1136/ANNRHEUMDIS-2018-214333.

(46) Casadidio, C.; Mayol, L.; Biondi, M.; Scuri, S.; Cortese, M.; Hennink, W. E.; Vermonden, T.; De Rosa, G.; Di Martino, P.; Censi, R. Anionic Polysaccharides for Stabilization and Sustained Release of Antimicrobial Peptides. *Int J Pharm* **2023**, *636*. https://doi.org/10.1016/j.ijpharm.2023.122798.

(47) Dovedytis, M.; Liu, Z. J.; Bartlett, S. Hyaluronic Acid and Its Biomedical Applications: A Review. *Engineered Regeneration* **2020**, *1*, 102–113. https://doi.org/10.1016/J.ENGREG.2020.10.001.

(48) Tampau, A.; González-Martinez, C.; Chiralt, A. Carvacrol Encapsulation in Starch or PCL Based Matrices by Electrospinning. *J Food Eng* **2017**, *214*, 245–256. https://doi.org/10.1016/J.JFOODENG.2017.07.005.

(49) Gursul, S.; Karabulut, I.; Durmaz, G. Antioxidant Efficacy of Thymol and Carvacrol in Microencapsulated Walnut Oil Triacylglycerols. *Food Chem* **2019**, *278*, 805–810. https://doi.org/10.1016/J.FOODCHEM.2018.11.134.

(50) Sun, H.; Jiao, R.; An, G.; Xu, H.; Wang, D. Influence of Particle Size on the Aggregation Behavior of Nanoparticles: Role of Structural Hydration Layer. *J Environ Sci (China)* **2021**, *103*, 33–42. https://doi.org/10.1016/j.jes.2020.10.007.

(51) Lim, Y. W.; Tan, W. S.; Ho, K. L.; Mariatulqabtiah, A. R.; Kasim, N. H. A.; Abd. Rahman, N.; Wong, T. W.; Chee, C. F. Challenges and Complications of Poly(Lactic-Co-Glycolic Acid)-Based Long-Acting Drug Product Development. *Pharmaceutics* **2022**, *14* (3). https://doi.org/10.3390/PHARMACEUTICS14030614.

(52) Xu, Y.; Kim, C. S.; Saylor, D. M.; Koo, D. Polymer Degradation and Drug Delivery in PLGA-Based Drug–Polymer Applications: A Review of Experiments and Theories. *J Biomed Mater Res B Appl Biomater* **2017**, *105* (6), 1692–1716. https://doi.org/10.1002/JBM.B.33648.

(53) Li, J.; Pu, Y.; Wang, S.; Ding, M.; Chen, D.; Zhu, M. Pharmacokinetic Study and Effectiveness Evaluation of Slow-Release PLGA-5-Fluorouracil Microsphere. *Cancer Chemother Pharmacol* **2013**, *71* (2), 351–359. https://doi.org/10.1007/S00280-012-2016-6/METRICS.

(54) Fredenberg, S.; Wahlgren, M.; Reslow, M.; Axelsson, A. The Mechanisms of Drug Release in Poly(Lactic-Co-Glycolic Acid)-Based Drug Delivery Systems—A Review.

Int J Pharm **2011**, *415* (1–2), 34–52. https://doi.org/10.1016/J.IJPHARM.2011.05.049.

(55) Son, G. H.; Lee, B. J.; Cho, C. W. Mechanisms of Drug Release from Advanced Drug Formulations Such as Polymeric-Based Drug-Delivery Systems and Lipid Nanoparticles. *Journal of Pharmaceutical Investigation*. Springer Netherlands July 2017, pp 287–296. https://doi.org/10.1007/s40005-017-0320-1.

(56) Chen, Y.; Wang, S.; Wang, S.; Liu, C.; Su, C.; Hageman, M.; Hussain, M.; Haskell, R.; Stefanski, K.; Qian, F. Initial Drug Dissolution from Amorphous Solid Dispersions Controlled by Polymer Dissolution and Drug-Polymer Interaction. *Pharm Res* **2016**, *33*, 2445–2458. https://doi.org/10.1007/s11095-016-1969-2.

(57) Keawchaoon, L.; Yoksan, R. Preparation, Characterization and in Vitro Release Study of Carvacrol-Loaded Chitosan Nanoparticles. *Colloids Surf B Biointerfaces* **2011**, *84*, 163–171. https://doi.org/10.1016/j.colsurfb.2010.12.031.

(58) Tran, T. H.; Rastogi, R.; Shelke, J.; Amiji, M. M. Modulation of Macrophage Functional Polarity towards Anti-Inflammatory Phenotype with Plasmid DNA Delivery in CD44 Targeting Hyaluronic Acid Nanoparticles. *Scientific Reports 2015 5:1* **2015**, *5* (1), 1–15. https://doi.org/10.1038/srep16632.

(59) Kosovrasti, V. Y.; Nechev, L. V.; Amiji, M. M. Peritoneal Macrophage-Specific TNF-α Gene Silencing in LPS-Induced Acute Inflammation Model Using CD44 Targeting Hyaluronic Acid Nanoparticles. *Mol Pharm* **2016**, *13* (10), 3404–3416. https://doi.org/10.1021/ACS.MOLPHARMACEUT.6B00398/SUPPL_FILE/MP6B00398_SI_001.PDF.

(60) Schleicher, U.; Paduch, K.; Debus, A.; Obermeyer, S.; König, T.; Kling, J. C.; Ribechini, E.; Dudziak, D.; Mougiakakos, D.; Murray, P. J.; Ostuni, R.; Körner, H.; Bogdan, C. TNF-Mediated Restriction of Arginase 1 Expression in Myeloid Cells Triggers Type 2 NO Synthase Activity at the Site of Infection. *Cell Rep* **2016**, *15* (5), 1062–1075. https://doi.org/10.1016/J.CELREP.2016.04.001.

Supplementary Information

Table S1: Optimising HA coating % with respect to high molecular weight (HMW) and low molecular weight (LMW) for small size, optimal zeta potential (Z) and low polydispersity index (PI)

	HMW 350 kDa HA-coated PLGA				**LMW 23 kDa HA-coated PLGA**
	0.5%	1%	1.25%	1.5%	1.5%
Size (d.nm)	133	252	203	2618±127	285±17
PI	0.30	0.10	0.41	0.89±0.08	0.39±0.01
Z (mV)	15.16	18.25	31.26	-28.58±2.5	-25.5±0.3

IR for verification of successful HA coating

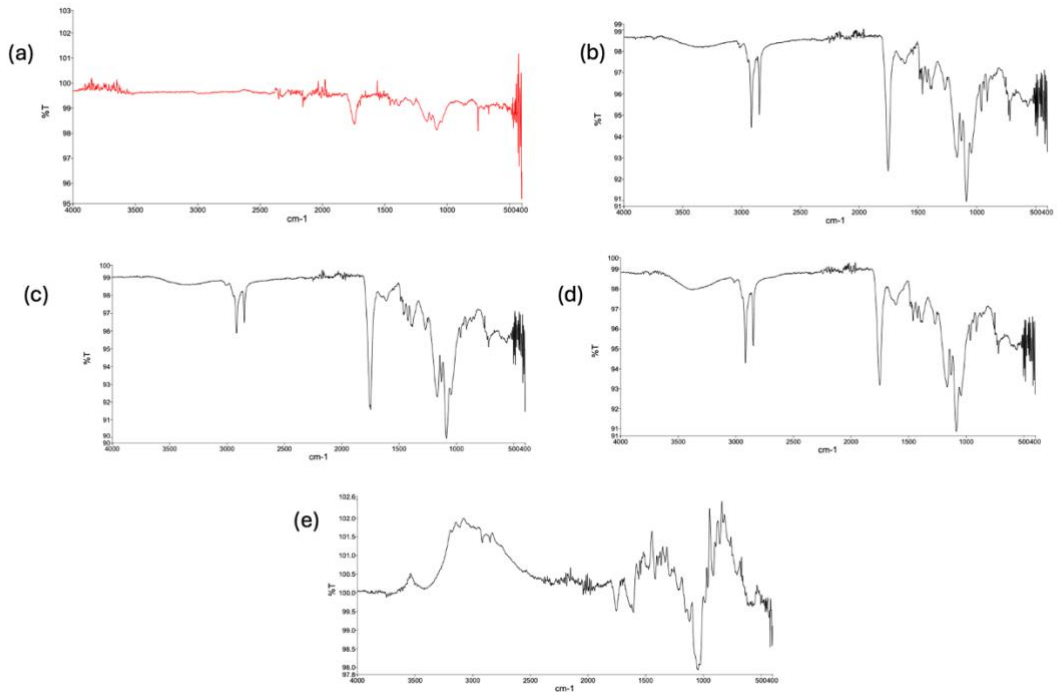

Figure S1: IR analysis of (a) PLGA; and HA-coated PLGA nanoparticles with HMW concentration (b) 0.5%; (c) 1%; (d) 1.25%; and (e) 1.5%. Slight IR bending characteristic of HA is noted at 3500 for (d) and majorly for (e) indicating the presence of HA on the surface of PLGA nanoparticles.

Chapter 4
Polyplexes for RNA Silencing: A New Frontier in Anti-Inflammatory and Neuroregenerative Therapies After Spinal Cord Injury

Abstract

Spinal cord injury (SCI) is a traumatic event that can lead to significant lifestyle changes and chronic pain in affected individuals. Antagomir (Amir) technology has gained increasing attention as a promising therapeutic approach for inflammation and pain management, by targeting endogenous microRNAs (miRNAs). Anti-inflammatory strategies typically focus on promoting the polarization of M1-macrophages (M1-m) to the anti-inflammatory M2-macrophage phenotype (M2-m), while antinociceptive treatments aim to regenerate neurons and modulate pain signals via astrocytes. In this study, we target lipopolysaccharide (LPS)-treated M1-macrophages to silence the inflammation-inducing miRNA-21 and modulate miRNA-155 expression in neurons and astrocytes using Amir-21 and Amir-155, respectively. The cationic polymer mPEG-pDMAEMA is used to form polyplexes with the Amirs (PA21 and PA155), and gold nanoparticles are incorporated into PA155 (resulting in GP155 nanoparticles) to enhance electrical conductivity for neuronal regeneration. *In vitro* results show that PA21 polyplexes induce a +30% increase in M2-m polarization and a -20% reduction in M1-m expression compared to controls. Additionally, dorsal horn cells treated with GP155 nanoparticles demonstrate a 1.24-fold increase in astrocyte uptake and a 12-fold increase in neuronal uptake, compared to naked Amir-155. A pilot *in vivo* study using female Sprague Dawley rats with compression-induced SCI involved the injection of 5 µL of a pNIPAM-based thermosensitive hydrogel containing GP155, control, or scramble sequences. The locomotion tests revealed a slight improvement in paw movement in the GP155-treated rats compared to controls and scramble groups at 3 days post-injury (dpi), although results from Randall-Selitto tests were inconclusive. Rats were euthanized at 14 dpi, and spinal cord samples were collected for further analysis.

1. Introduction

Spinal cord injury (SCI) is a traumatic event that can lead to a lifetime of suffering and chronic pain. Chronic pain involves a complex mechanism of action of immune and nervous systems acting co-dependently to induce inflammation and eventual pain. The recent advancements in nucleic acid (NA) therapies have proved to be efficient in SCI-derived pain models[1,2]. NA therapies, including siRNA, mRNA, pDNA, have been used to modify endogenous gene expression to get the desired effect. This therapeutic method has been used to treat Alzheimer's[3,4], cancer[5,6] and chronic pain[7,8].

However, these NA therapies come with their fair share of disadvantages as well. They undergo quick biodegradation, which can cause hindrance to their bioactivity and therapeutic longevity. Moreover, cations are more favourable to be uptaken by cells as compared to their negative counterparts, and NAs are anionic in nature at physiological pH. Viral vectors are usually used to counter the low permeability of NAs. Viruses, like adenovirus and retrovirus, provide high transfection efficiency, which comes at a cost of low loading capacity and insertion mutations. To avoid these major clinical concerns, cationic polymers are being used as carriers for anionic NAs, and the forming entity is called a polyplex. Polyplexes work by condensing the NAs into the polycationic polymer and providing protection against premature biodegradation and enhanced permeation through the physiological membrane [9]. In this study, the poly(2-(dimethylamino)ethyl methacrylate) (pDMAEMA) was used as cationic polymer for NA condensation. Since the polymer pDMAEMA is conjugated with a noncharged poly(ethylene glycol) (PEG) group, the resulting polyplex forms a core-shell structure, where the NA is condensed into the core and the PEG polymer chains act as a shell[10].

The novelty of this therapeutic approach was underscored by the use of antagomirs (Amirs), which are synthetic oligonucleotides designed to inhibit the activity of their endogenous microRNA (miRNA) counterparts[11]. Amirs are chemically modified single-stranded analogues of RNA, with cholesterol conjugation for stability, that act complementarily to target endogenous miRNAs for silencing. The mechanism of action of Amirs is based on the blocking of its complementary miRNA. Figure 1 describes the route of miRNA to its target for expression in a state of equilibrium, and when an Amir is

presented into the equation, the miRNA gets blocked by the complementary sequence of Amir and its target is left empty and expression is silenced.

To design the anti-inflammatory polyplexes, we turned our attention to microRNA-21 (miR-21) and microRNA-155 (miR-155). The miR-21 is a known promoter of inflammation and is induced by the activated response of Th1/2 cytokines [12]. Some studies have depicted the transfer of miR-21 packaged extracellular vesicles from injured dorsal root ganglia (DRG) neurons to macrophages for upregulation of inflammation [13–15]. On the other hand, miR-155 is highly responsive to macrophage-induced production of inflammatory cytokines, such as tumor necrosis factor alpha (TNF-α) and interleukin-1β/α (IL-1β/IL-1α). [16–20]. The nuclear factor-κB (NF- κB) inflammatory pathway is also dependent on miR-155 expression [21]. Targeting miR-21/155 with Amir-21/155 for down regulation of inflammation and pain has been demonstrated a potent therapeutic technology [22,23]. However, literature suggests that even though miR-21/155 promote inflammation through different pathways, these pathways counteract each other in the case of SCI[24,25]. A contusion SCI study by Lv *et al*, suggests that suppressing miR-21 expression leads to increased apoptosis of spinal cord tissue, whereas enhancing the miR-21 expression lowers the production of inflammatory cytokines [26]. Zhang *et al* also demonstrates the promotion of functional recovery of neurons due to miR-21, post-SCI [24]. Therefore, this enhances the need for two models to test the two Amir-21/155.

In this study, we presented a non-viral gene delivery method with mPEG-PDMAEMA-Amir21 and mPEG-PDMAEMA-Amir155 (respectively PA21 and PA155) polyplexes as antinociceptive, anti-inflammatory and regenerative therapies. PA21 was tested with cultured macrophages for analysing the polarization from inflammatory (M1) to anti-inflammatory (M2) phenotype. Furthermore, the PA155 polyplexes were conjugated with gold (Au) nanoparticles (yielding GP155 formulations) for increased biocompatibility and electrical conductivity for enhanced axonal regeneration in a SCI rat model [27,28]. The SCI rat models were developed using a compression model of injury and GP155 nanoparticles were loaded into a thermosensitive hydrogel before being injected onto the lesion site. Behavioural studies were performed on the subjects at different time intervals, including mechanical hyperalgesia and locomotion tests.

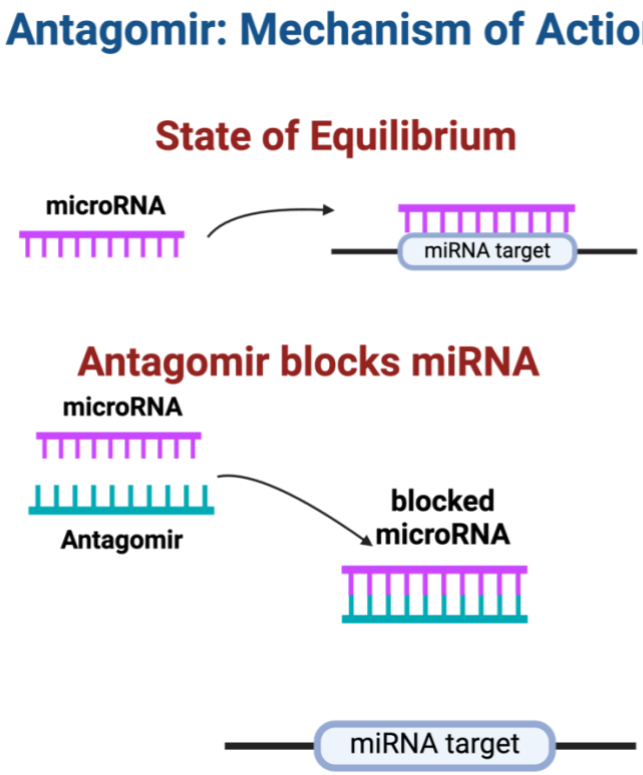

Figure 1. Mechanism of action of antagomirs to silence microRNA expression.

2. Materials and Methods

2.1 Materials

Methoxypoly(ethylene glycol) poly(2-(dimethylamino)ethyl methacrylate) (mPEG-PDMAEMA) diblock copolymer with a final MW of 35kDa (5.4 kDa PEG chain and 29.6 kDa PDMAEMA) was synthesized by RAFT (Reversible Addition Fragmentation Chain Transfer) polymerization), using a method previously reported[10]. The synthesis of the triblock copolymer consisting of a thermosensitive poly(N-isopropylacrylamide) (pNIPAM) and a hydrophilic PEG block, was performed following the Atom Transfer Radical Polymerization (ATRP)[29]. The M_n of the synthesized NPN triblock copolymer was 38 kDa while the M_n of the two pNIPAM blocks was 16 kDa. FAM-labelled miR-155-5p antagomir (Custom miRCURY LNA Power Inhibitor 5'-/FAM/CCCCTATCACAATTAGCATT, Qiagen Ltd. United Kingdom), FAM-labelled miR-21-5p antagomir (Custom miRCURY Power Inhibitor, 5'-/FAM/TCAGTCTGATAAGCT-3', Qiagen Srl, Italy), HEPES buffer, pcDNA3.1+N-eGFP (GenScript Biotech BV, Netherlands), tetrachloroauric (III) acid trihydrate (Thermo Scientific Chemicals, Italy), sodium borohydride (99%, Thermo Scientific Chemicals,

Italy), and distilled water (DI) was obtained with the apparatus RO 60 TS demi2 water deionizer provided by Gamma 3 Ecologia (Castelverde Costa Sant'abramo, Italy).

2.2 Synthesis of Gold Nanoparticles

The synthesis route for gold nanoparticles was adapted from Dinari *et al* [30]. Briefly, 0.001M $HAuCl_4$ was stirred in 100ml DI water at 100˚C at 300 rpm. Next, 10mg $NaBH_4$ was added to the solution and stirred for further 30 minutes before bringing it to room temperature. The solution was left undisturbed for 30 minutes at room temperature and the size and zeta potential (ZP) of the synthesized Au nanoparticles was tested by Dynamic Light Scattering (DLS) technique with Zetasizer Nano equipped with 633nm HeNe laser (Malvern Instruments, Malvern, UK). All measurements were performed at 25 ˚C and at least in triplicates.

2.3 Synthesis of Polyplexes

The synthesis route for polyplexes was divided into three stages, as described below.

2.3.1 Conjugation of Au NPs with PEG-pDMAEMA

Polyplexes are synthesised in terms of NP ratios, which refers to the nitrogen/phosphate (N/P) molar ratios of the polymer and NA, respectively. A 5mg/ml stock solution of polymer was prepared in 10mM HEPES buffer. The amount of polymer as per NP ratios of 1/5/10/20/30/50 was adjusted and accordingly added to Au nanoparticles, synthesised in section 2.3.2 as per 1:0.5 molar ratio. The polymer solution was mixed in the Au NPs solution and stirred for at least 6 hours at room temperature.

2.3.2 Polyplexes formulation

A 1mg/ml stock solution of Amir-21/155 was prepared in 10mM HEPES buffer. After the conjugation of Au NPs and polymer, the amount of Amir-155 was added to the solution to make gold-complexed polyplexes (GP155) as per the appropriate NP ratios of 10/30. The solution was vortexed for 10 seconds and left undisturbed at room temperature for 30 minutes. PA21 were synthesised similarly, where polymer solution was added to Amir-21 solution in NP ratios of 10/50. For screening purposes, pDNA-eGFP was used to

synthesize the polyplexes (NP 1/5/10/20/30) and these polyplexes were used to measure the size and ZP using DLS, as in section 2.2.

2.3.3 Thermosensitive Hydrogel Loading of Polyplexes

The administration of GP155 was conducted with PNIPAM-based thermosensitive hydrogel. Briefly, 20 w/v% of PNIPAM was dissolved in the GP155 polyplex dispersion and dissolved overnight at 4 ˚C. The resulting samples (GP) were kept on ice until injection.

2.4 *In Vitro* Studies

2.4.1 Macrophages

The bone marrow derived macrophages (BMDMs) were cultured as previously described in Chapter 3. Briefly, BMDMs were harvested from femurs and tibia of 3-month-old C57BL/6J Balb-c mice (Envigo, Indiana, United States). The cells were isolated and enriched with the macrophage colony-stimulating factor (M-CSF) for monocyte differentiation. PA21(NP10/50; 3µg/well) and naked free polymer (17µg/well; comparable to NP10) were added in the BMDM culture, in a 24-well plate with and without lipopolysaccharide (LPS) pre-treatment. Macrophage differentiation was measured by analysing the expressions of macrophage-specific markers, like CD86 and iNOS for M1-m and CD163 and CD206 for M2-m.

2.4.2 Dorsal Horn Culture

Dorsal horn cells were freshly harvested from prenatal mice. Briefly, animals were anesthetized with 5% isoflurane and sacrificed via decapitation. A ventral laminectomy was performed, and the dorsal horn strip of the spinal cord was collected in a solution of ice-cold HBSS + HEPES. The cords were then digested for 30 min in a CO_2 incubator at 37 ˚C. The tissue was washed with HBSS + HEPES twice. The liquid was discarded and replaced with culture media and a fire-polished tip was used to triturate the tissue for 6-7 times. The supernatant was collected with a cell strainer and the above steps repeated to collect 3ml of supernatant in total. The supernatant was centrifuged at 1000g for 5 min at 4 ˚C and the cells collected carefully. The cells were resuspended in cell culture media and incubated in a 24-well plate for 60 min. The media was changed after 1 day [31]. GP155 (NP10; 2µg/well) and naked Amir-155 (2µg/well) were added to the cells.

2.5 Primary Antibody Staining – Neurons and Glial Cells

To start, the cells were washed with PBS and then fixed with 4% paraformaldehyde (PFA) for 20 min at room temperature. The cells were again washed with a mix of PBS and 0.001% Triton X-100 (PBSX). PBSX (500µl per well) was then used to permeabilize the cells for 5 min. Further, a blocking solution with 5% goat serum was added and incubated with for 30 min at room temperature. The wells were then divided before staining with primary antibodies for neurons and astrocytes, separately. Primary antibodies - Glial Fibrillary Acidic Protein (GFAP) mouse (1:1000) and Beta III Tubulin (BIIIT) mouse (1:500) were used to incubate and mark the cells for astrocytes and neurons, respectively.

2.6 Mounting and Confocal Microscopy

A Zeiss LSM880 + Airyscan Inverted Confocal Microscope (diode 405nm, argon 458/488/514nm, DPSS 561nm, HeNe 633nm) was used for bioimaging. For sample preparation, a mounting media with DAPI was used to fix the coverslips on the slides. Briefly, 10µl of the media was applied on the slide, the coverslip was lifted from the well plate and blotted for removing excess media before being slowly placed on the slide. For placement, the coverslip was lowered carefully onto the media, to avoid bubbles. The slips were then sealed with nail polish and left in a dark chamber to dry before imaging.

2.7 Pilot *in Vivo* Studies

The pilot *in vivo* study was conducted with 20 female Sprague Dawley rats (Charles River Laboratories, Kingston, Pennsylvania), weighing 210-240 g. The animals were housed with 24-hour food and water and 12-hour day/night cycles. All animal procedures were approved by the UK Home Office and University of Leeds Animal Welfare and Ethics Committee, in accordance with UK Animals (Scientific Procedures) Act 1986.

After being acclimatized for 7 days, the rats were anesthetized with isoflurane (5% IsoFlo; (Zoetis UK Ltd, London, United Kingdom) at 2 L/min^{-1} O_2 flow induction and maintained with 2.5% isoflurane throughout surgery. Partial laminectomy was performed at the contusion level of the vertebra (T9-11). A contusion SCI was performed at T10 vertebral level with an Infinite Horizon impactor (Precision Systems & Instrumentation, Lexington,

Kentucky) at 200 kdyn. Immediately after the injury, a 5µl injection of CTRL/SCR/GP was injected at the site of injury. The injections were randomly assigned to the rats caged together in groups of 3, to maintain unbiases during the behavioural tests.

For the *in vivo* experiment, the animals were divided into 3 groups:

- Control (CTRL) – the CTRL group received an empty injection after the injury (n=6).

- Scramble (SCR) – for the SCR group, in the polyplex synthesis phase described in section 2(c(ii)), the Amir-155 added to the Au-polymer phase was replaced by its scrambled counterpart, to act as a negative control (n=6).

- therapeutic (GP) – the GP group of animals were administered with GP155 made with therapeutic Amir-155 (n=6).

After the injection, the animals were sutured and placed in an incubator until they regained consciousness and returned to their randomly assigned cages. Antibiotics (Baytril, 2.5 mg/kg), opioids (buprenorphine 0.015 mg/kg) and saline (10 ml) were subcutaneously administered at 0, 24 and 48 hours after the surgery. The bladders of the animals were manually expressed twice a day until sacrificed.

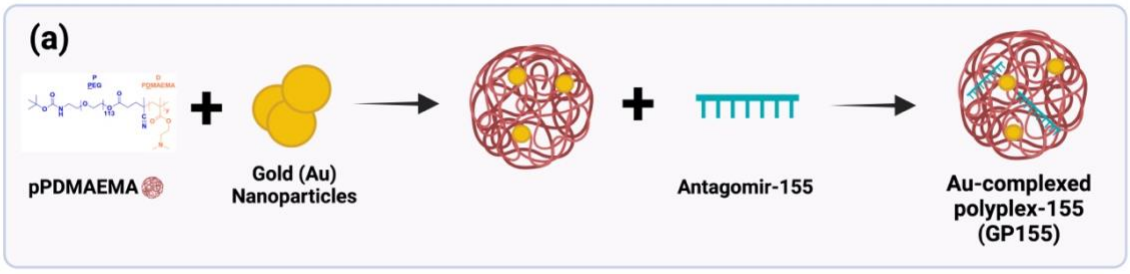

Figure 2. Synthesis mechanism of GP155 and administration of GP into the animals post-SCI. (a) conjugation of Au NPs onto pPDMAEMA and subsequent formation of GP155 by addition of Amir-155, (b) contusion injury model of SCI and injecting GP onto the lesion site.

2.8 Behavioural Tests

The Basso, Beattie, Bresnahan (BBB) test is a general locomotor activity test that was performed at 3-, 7- and 14-days post injury (dpi). The outcome of the injury wasassessed visually in an open field test as proposed by Basso *et al* [32]. The animals were tested blindly and scored on a 21-point scale.

The Randall-Selitto (RS) test was executed at 14dpi, and is a test performed as a measure of mechanical hyperalgesia [33]. The response thresholds of the animals were measured by a Digital Randall Selitto Paw Pressure Test with Pressure Applicator Model I-2500 (Campden Instruments, England).

2.9 Collection of Spinal Cords

At the end of 14dpi, the animals were sacrificed by a administering a dose of pentobarbital sodium 20% (Pentoject; Animalcare Ltd, York, United Kingdom) and perfused with PBS followed by a 4% PFA in 0.1 m phosphate buffer. Following that, the brains and spinal cords of the animals were collected and postfixed in 4% PFA solution at 4˚C overnight. The solution was then replaced by a 30% sucrose solution in which the samples were stored for at least 72 hours.

3. Results and Discussion

3.1 Polyplex Characterisation

Polyplexes were synthesized using pDNA-eGFP for screening purposes. Table 1 summarizes the size, zeta potential (ZP), and polydispersity index (PDI) of these polyplexes, both with and without the inclusion of gold nanoparticles (Au NPs). Dynamic Light Scattering (DLS) analysis revealed that polyplexes without Au NPs exhibited a size range of 118-550 nm. Notably, a decreasing trend in size was observed from NP1 to NP10, with the size reducing from 550 nm (NP1) to 338 nm (NP5), and finally to 118 nm (NP10).

However, after NP10, an increase in size was observed in NP20 and NP30, suggesting a threshold effect in the polyplex formation. This trend mirrors findings by Fliervoet et al., who reported a similar size reduction with increasing NP ratio, followed by an increase with higher NP concentrations [34]. This behavior is likely due to enhanced condensation of the polyplexes up to NP10, after which the excess polymer chains hinder further condensation of the pDNA, leading to an increase in particle size beyond this threshold [35,36]. Regarding PDI, except for NP1 (PDI = 0.75), no differences were observed across the polyplexes. The relatively high PDI of NP1 suggests incomplete condensation of the pDNA, which is consistent with the observed low zeta potential (ZP) of 3 mV. In contrast, an increasing trend in ZP was observed with the polyplexes, starting at 3 mV for NP1 and rising to 36 mV for NP20. The positive charge observed with NP20 may be indicative of charge shielding effects imparted by the polymer. However, after this point, a decline in ZP was noted, with NP30 showing a ZP of 28 mV, which can be attributed to reduced shielding efficacy by the cationic polymer at higher NP concentrations. Gold nanoparticles (Au NPs) were synthesized with a size of 42±22 nm and a negative ZP of -16 mV. The negative charge of Au NPs, when incorporated into the polyplexes, likely contributes to a reduction in the overall charge of the complexes. As shown in Table 1, the inclusion of Au NPs led to a sharp decrease in the zeta potential of the polyplexes, with values dropping to the range of 9-14 mV. This indicates a charge neutralization effect due to the interaction between the positively charged polyplexes and the negatively charged Au NPs.

Table 1: Size, PDI and Zeta Potential of Au NPs, and Polyplexes (with and without Au NPs)

	NP ratio	**Size (d.nm.)**	**PDI**	**ZP (mV)**
PEG-pDMAEMA-eGFP-pDNA polyplexes	**1**	550±65	0.75±0.12	3.81±2.26
	5	338±24	0.26±0.3	21.4±1.47
	10	118±2	0.26±0.20	30.79±1.72
	20	138±0.62	0.24±0.02	36.19±1.52
	30	276±20	0.23±0.01	28.50±1.27

Au-PDMAEMA polyplexes	**10**	377±7	0.28±0.01	11.52±0.37
	30	305±29	0.31±0.06	14.16±0.28
Au NPs	**n.a.**	42±22	0.24±0.05	-16.85±0.55

3.2 Macrophage Polarisation with PA21

Inflammation is intricately regulated by macrophages, which exhibit remarkable plasticity in response to inflammatory stimuli. The pro-inflammatory macrophages (M1-m) can be distinguished by their surface markers from their anti-inflammatory counterparts (M2-m), and their ability to switch between these phenotypes is a key mechanism in the resolution of inflammation. Modulating macrophage plasticity at the site of inflammation represents a promising strategy for controlling excessive inflammatory responses. Figure 3 illustrates the polarization of M1-m macrophages to M2-m in LPS-treated bone marrow-derived macrophages (BMDMs) upon exposure to free polymer and two polyplex formulations of NP10PA21 and NP50PA21, compared to control (no treatment). As anticipated, no significant polarization was observed in the macrophages cultured with free polymer, as shown in panels (c) and (d) of Figure 3. In contrast, treatment with NP10PA21 led to a notable +30% increase in CD206 expression, a hallmark of the M2-m phenotype, indicating successful polarization of M1-m macrophages to the anti-inflammatory M2-m phenotype. Additionally, a -20% reduction in M1-m markers was observed, further supporting the shift toward an anti-inflammatory state. However, when the NP50PA21 polyplex formulation was tested, the results were less favorable. Figure 3(g) reveals a significant -70% reduction in the macrophage population compared to the control, suggesting high toxicity at the elevated nanoparticle (NP) ratio. This toxicity is likely due to the increased cationic polymer content in the polyplexes, as the cytotoxic effects of cationic polymers are well-documented in the literature [34,35]. Despite this, the NP10PA21 formulation successfully silenced miRNA-21 in LPS-treated M1-m macrophages, providing an effective means to modulate inflammation. Supporting studies, such as the work by Lee et al., have demonstrated that silencing miRNA-21 with Amir-21 results in decreased levels of inflammatory cytokines like IL-4, IL-5, and IL-13 [37]. Similar findings were reported by Mirna et al., where the dysregulation of miRNA-21 by Amir-21 significantly reduced inflammation [38]. Given the

observed cytotoxicity with higher NP ratios, which is often correlated with reduced transfection efficiency [39], the NP10PA21 polyplexes were selected for subsequent experiments. These results underscore the importance of optimizing polyplex formulations to balance efficacy with biocompatibility.

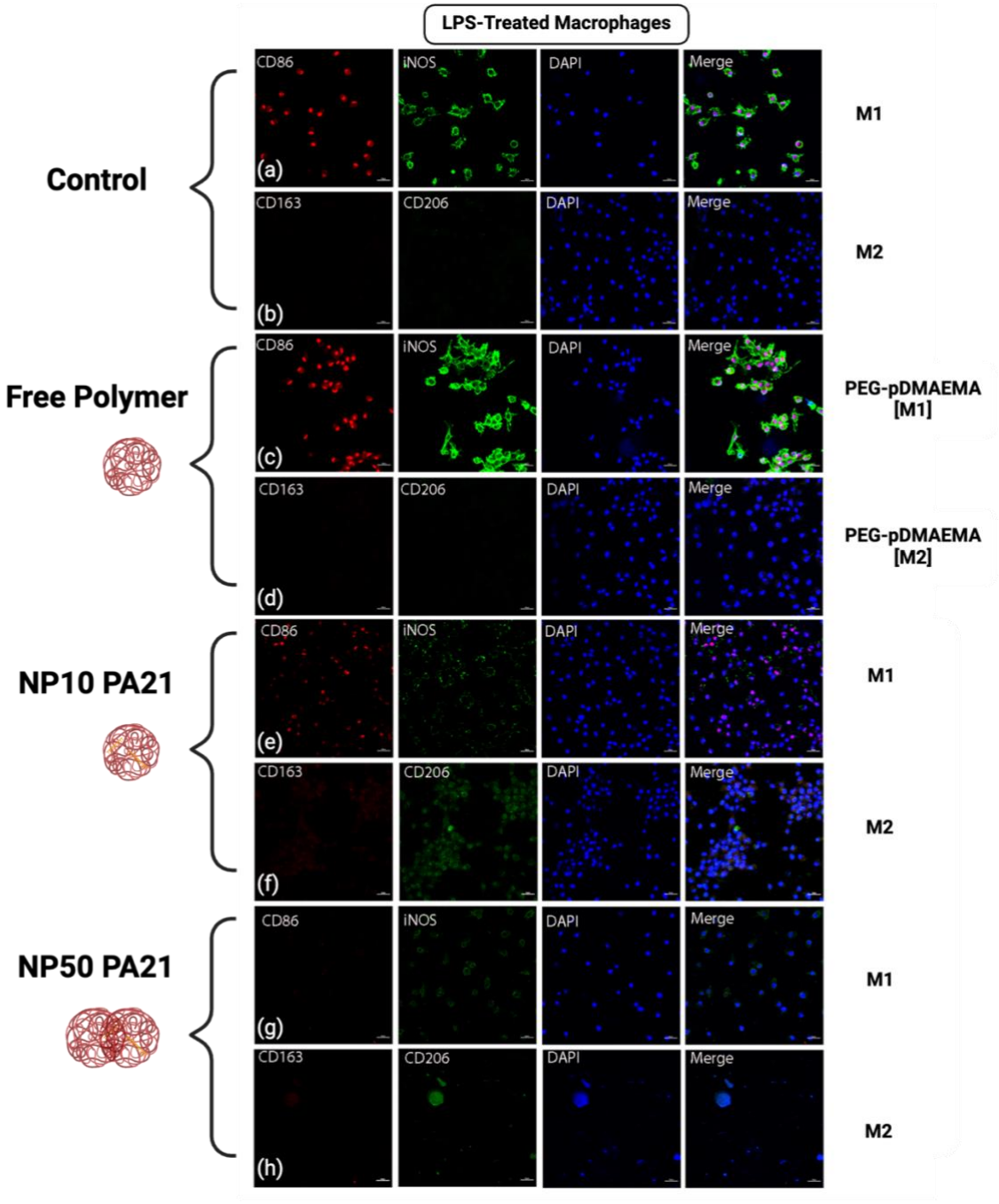

Figure 3. Phenotype polarisation of LPS-treated BMDM macrophages with free PEG-pDMAEMA; NP10PA21 and NP50PA21. No polarisation is noted with free polymer, while NP10PA21 shows the highest number of polarised M2 macrophages. Cytotoxicity was noted with NP50PA21.

3.3 Cell Internalization of GP155

NAs are notorious for their poor transfection efficiency. Employing a cationic polymer with an anionic NA greatly enhances the uptake of the polyplexes. This cellular uptake was investigated using a confocal laser microscope and quantified using fluorescence intensity (FI) in Fiji [40]. In Figure 4, we see GFAP-labelled astrocytes cultured with naked Amir-155 (a) and GP155 (b). After 24 hours of incubation time, there is a stark difference in the FI of the two samples. The Amir-155-treated astrocytes show a sporadic uptake of Amir-155 into the cells, marked by solitary arrowheads. However, the GP155 treated astrocytes show a much larger FI expressed by the Amir-155 in the polyplexes. The FI in the GP155-treated astrocytes is 2.3-fold higher than naked Amir-155-treated astrocytes. Moving on to the BIIIT-labelled neurons, we see the Amir-155-treated neurons in Figure 2(c) and GP155-treated neurons in Figure 2(d). As observed with astrocytes, the neuronal uptake of naked Amir-155 was lesser than GP155. The fluorescence from the uptaken GP155 in neurons is depicted with the arrowheads, and on calculating the FI with Fiji, we see that the use of polyplexes increased the uptake of Amir-155 by 12-fold, as compared to naked Amir-155. From these images, we also observed fluorescence in some unlabelled cells. We hypothesize that these cells could be either microglia or macrophages, as both are known to be present in similar inflammatory environments. To validate this, future studies should incorporate specific markers for microglia and macrophages to confirm their identity. Additionally, assessing the transfection efficiency of both naked Amir-155 and GP155 in these specific cell types would provide a clearer understanding of the delivery system's cellular targeting profile. Abundant resources have cited the increased transfection of genetic material with polymeric carriers [41–44]. Hachim *et al.* presented an enhanced polyplex transfection efficiency using a nanofilm method [42]. Godbey *et al* created a pDNA delivery system with polycation polyethylenimine for an efficient transfection in an inflammatory cell line [45]. Therefore, while our findings suggest that GP155 may facilitate effective delivery into target cells, the presence of fluorescence in unlabelled populations highlights the need for more targeted analysis. Characterizing the role and uptake behavior of non-target immune

cells like microglia and macrophages will be essential to refine this delivery platform and enhance its specificity and therapeutic potential.

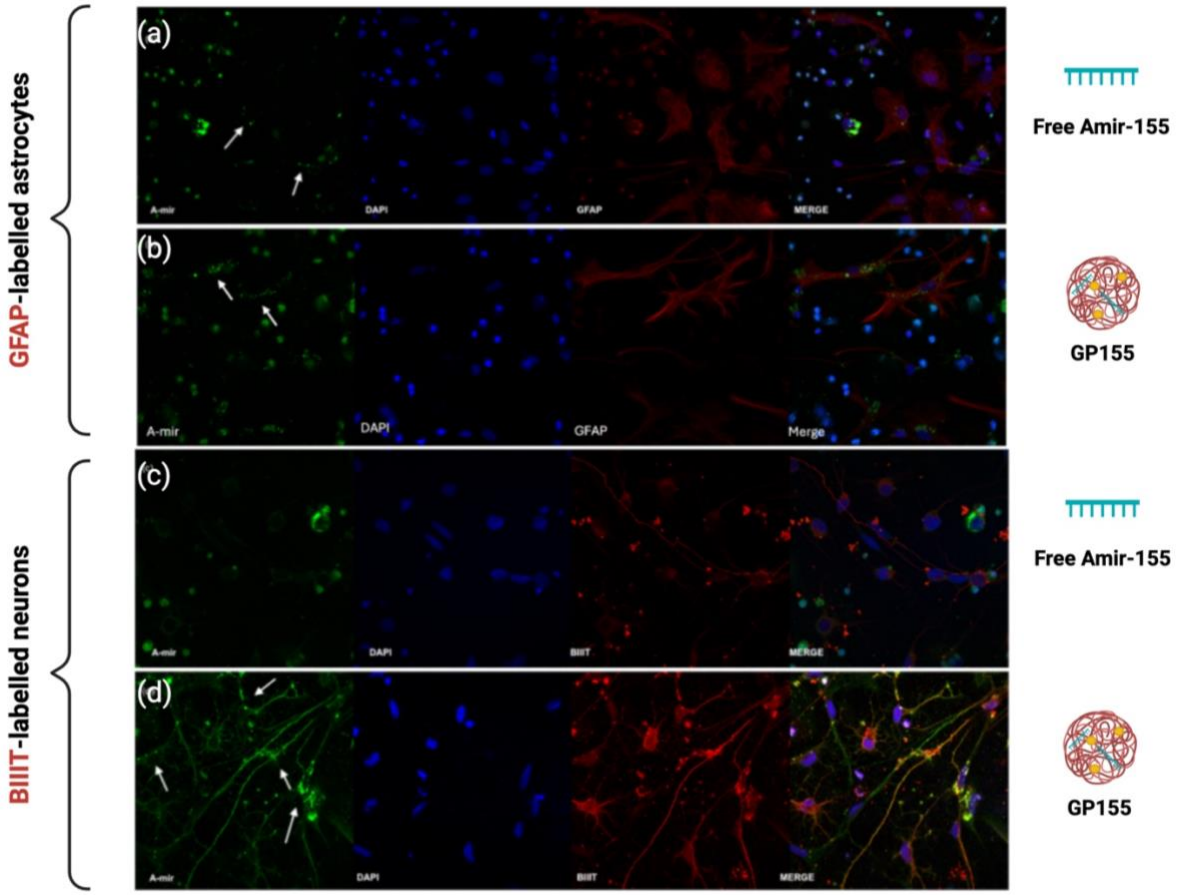

Figure 4. Confocal images of dorsal horn cells incubated with naked Amir-155 and GP155. (a) GFAP-labelled astrocytes incubated with naked Amir-155 show FI with slight uptake, (b) higher FI is noticed in GFAP-labelled astrocytes with GP155, (c) BIIIT-marked neurons incubated with naked Amir-155, (d) high FI in BIIIT-marked neurons with GP155.

3.4 Behavioural tests

To evaluate the therapeutic efficacy of GP155 in spinal cord injury (SCI), behavioural tests were conducted to assess both motor function and mechanical sensitivity. GP155 refers to the gold-polymer (GP) conjugate complexed with therapeutic antagomir-155 (Amir-155) at an optimal nanoparticle NP ratio of 10:1. This formulation was administered using a PNIPAM-based thermosensitive hydrogel, allowing for localized

and sustained release at the lesion site. The GP155 was injected immediately post-SCI and behavioural outcomes were monitored at different time points.

3.4.1 BBB Test Scores

Spinal cord injury (SCI) is a severe trauma that leads to rapid and marked impairment of hindlimb locomotion. By 3 days post-injury (dpi), animals in the CTRL group displayed minimal BBB locomotor scores, confirming significant motor deficits (Figure 5). In contrast, animals treated with GP155 (GP group) consistently scored slightly higher at all time points (3, 7, and 14 dpi) suggesting improved early motor recovery. This trend, although not statistically significant due to the limited sample size of this pilot study, is biologically meaningful. The BBB scoring system operates on a sensitive 21-point scale, where even a 1-point difference reflects a substantial change in functional limb movement. A score of 2–3, as observed in the GP group at 3 dpi, indicates consistent paw placement, whereas scores near 0 in CTRL and SCR groups reflect complete loss of hindlimb function, with animals dragging their lower bodies. The early improvement in the GP group may be attributed to the therapeutic action of GP155, the antagomir-155-loaded gold-polymer conjugate delivered via a PNIPAM-based hydrogel. The hydrogel allows for sustained release of the therapeutic at the lesion site, enabling miR-155 inhibition during the acute inflammatory phase of SCI. miR-155 is known to exacerbate neuroinflammation, and its suppression has been linked to enhanced neuronal survival. The GP group improved BBB scores suggest more rapid neuronal recovery, potentially due to early attenuation of inflammation. The inflammatory timeline post-SCI provides a compelling context: by 3 dpi, resident microglia and infiltrating macrophages mount a strong pro-inflammatory response [46]. In this “acute” SCI phase, neuroinflammation is most pronounced and noticing a difference in the scores of GP models, compared with SCR and CTRL, opens a slew of opportunities for investigations during this stage. Days 5-7 of SCI are characterised by another cycle of macrophage infiltration. In fact, macrophage expression in SCI peaks at 5-7 dpi [47]. Bisicchia *et al* has showed that by day 5 post SCI, activated microglia are the predominant cells inducing inflammation in the spinal cord [48]. During this second cycle of macrophage infiltration, more cases of axonal damage are reported. A secondary demyelination of surviving neurons in taken out and nerve damage is enhanced. This suggests that a second administration of GP155 around

5–7 dpi could potentially extend or amplify its neuroprotective effects. Future studies should investigate this hypothesis, incorporating repeat dosing and cellular profiling to evaluate changes in macrophage and microglial populations. Furthermore, all behavioural assessments were performed and recorded in a blinded manner, ensuring objective data collection. In summary, early improvements in BBB scores among GP-treated animals highlight the potential of miR-155 inhibition via hydrogel-mediated delivery to promote functional recovery after SCI, particularly when timed to coincide with key inflammatory milestones.

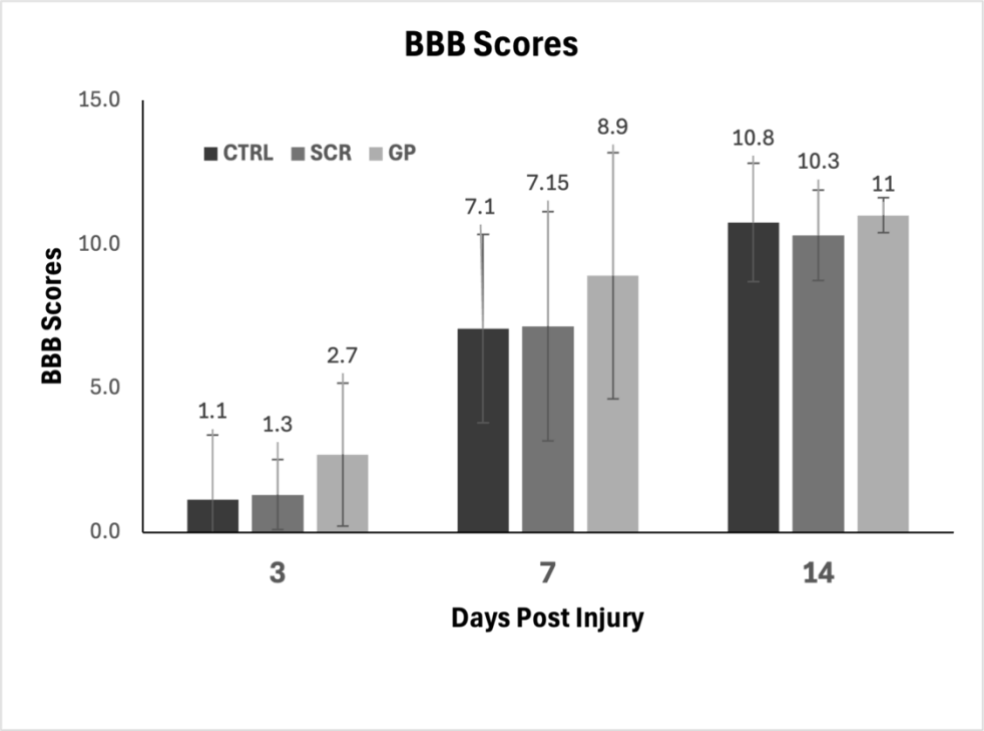

Figure 5. BBB locomotor scores at 3, 7, and 14 dpi. The GP group demonstrates superior hindlimb function at 3 dpi, indicating early recovery compared to SCR and CTRL. The difference narrows by 14 dpi as recovery plateaus across groups (n=6 per group).

3.4.2 RS Test Scores

The Randall-Selitto (RS) test, which assesses mechanical nociception and sensitivity to pressure, revealed ambiguous results across the three groups at 14 dpi (Figure 6). Interestingly, the SCR group recorded the highest tolerance to pressure on the paw, which may reflect a lack of sensory recovery or a potential desensitization effect. Conversely, the GP group exhibited lower pressure tolerance, which could be interpreted

as a partial return of sensory function and heightened responsiveness to noxious stimuli, potentially indicating a reversal of sensory deficits. However, without additional time points or supporting histological data, this interpretation remains speculative. The observed differences contrast with the clearer trends in the BBB locomotor test, where functional recovery differences were more distinct in the early post-injury phase, particularly up to 7 dpi. The RS results at 14 dpi do not offer a definitive picture of neuropathic pain or sensory recovery, and their variability may be due to the complex interplay between inflammation, neural regeneration, and individual pain thresholds. Given that the RS test is sensitive to both peripheral and central sensitization, it holds promise for evaluating neuropathic pain in SCI models. Yet, in this study, the small sample size and single time point limit the conclusions that can be drawn. Additional experimental groups, such as a sham-operated cohort, and extended follow-up periods would provide greater insight into the sensory effects of GP155 treatment. Moreover, repeated RS testing at earlier stages (e.g., 3 and 7 dpi) could help determine whether GP155 affects the trajectory of sensory recovery or pain development after SCI. Therefore, while the RS test aimed to reveal differences in sensory recovery and potential neuropathic pain among groups, the results at 14 dpi remain inconclusive. Future studies with larger sample sizes, longitudinal assessment, and complementary analyses will be essential to elucidate the impact of GP155 on sensory outcomes post-SCI.

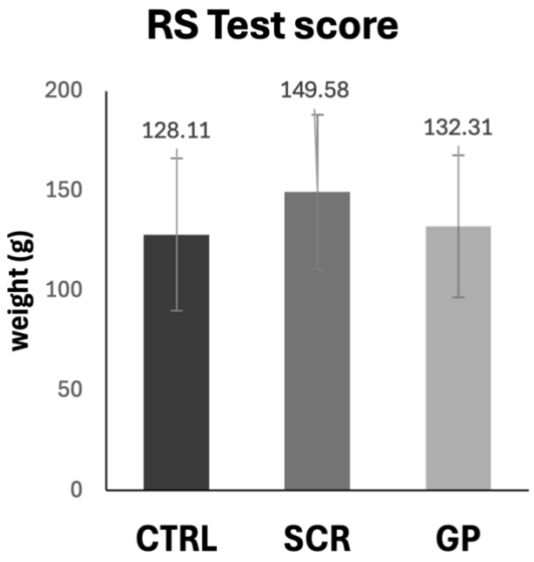

Figure 6. RS mechanical sensitivity scores at 14 dpi. The SCR group displays higher tolerance to applied pressure, possibly indicating hypoalgesia. GP and CTRL groups

show similar responses, potentially reflecting a return of sensory function in the GP group (n=6 per group).

4. Conclusion

In this study, polyplexes containing Amir-21 (PA21) and Amir-155 (PA155) were successfully synthesized for anti-inflammatory and antinociceptive applications. Gold nanoparticles were incorporated into PA155 to create GP155 nanoparticles, enhancing electrical conductivity and supporting axonal regeneration in neurons. The polyplexes exhibited an average size of 118 nm and a surface charge of 30 mV. In vitro experiments with PA21 polyplexes, when cultured with LPS-treated macrophages, resulted in a +30% increase in polarization toward the anti-inflammatory M2-m phenotype and a -20% decrease in M1-m expression, indicating the potential of Amir-21 in modulating inflammatory responses. Further research into cytokine expression changes with PA21 could provide a more comprehensive understanding of its anti-inflammatory effects. The uptake of Amir-155 was significantly enhanced when delivered with the polycationic carrier, with GP155 nanoparticles showing a 2.3-fold increase in astrocyte uptake and a remarkable 12-fold increase in neuronal uptake compared to naked Amir-155. When injected at the injury site in a pPNIPAM thermosensitive hydrogel, GP155 promoted slight locomotor improvement, although the small sample size made the results statistically insignificant. No mechanical hyperalgesia was observed in any of the experimental groups, leaving these results inconclusive. While traditional spinal cord injury (SCI) experiments are typically conducted over weeks or months to observe extensive cellular proliferation and behavior, this study primarily tested a novel non-viral gene delivery system within a thermosensitive hydrogel. Based on the findings, future studies should focus on a critical period between 5-7 days post-injury (dpi), as this is likely when Amir-155 exerted its most significant effects. Further optimization and extended studies are required to fully elucidate the therapeutic potential of this approach.

4. References

(1) Crowley, S. T.; Fukushima, Y.; Uchida, S.; Kataoka, K.; Itaka, K. Enhancement of Motor Function Recovery after Spinal Cord Injury in Mice by Delivery of Brain-Derived

Neurotrophic Factor MRNA. *Mol Ther Nucleic Acids* **2019**, *17*, 465–476. https://doi.org/10.1016/j.omtn.2019.06.016.

(2) Pajer, K.; Bellák, T.; Nógrádi, A. Nucleoside Modified MRNA-Lipid Nanoparticles as a New Delivery Platform for the Repair of the Injured Spinal Cord. *Neural Regen Res* **2024**. https://doi.org/10.4103/nrr.nrr-d-23-01231.

(3) Chakravarthy, M.; Chen, S.; Dodd, P. R.; Veedu, R. N. Nucleic Acid-Based Theranostics for Tackling Alzheimer's Disease. *Theranostics*. Ivyspring International Publisher 2017. https://doi.org/10.7150/thno.21529.

(4) Shao, X.; Cui, W.; Xie, X.; Ma, W.; Zhan, Y.; Lin, Y. Treatment of Alzheimer's Disease with Framework Nucleic Acids. *Cell Prolif* **2020**, *53*. https://doi.org/10.1111/cpr.12787.

(5) Li, J.; Wang, Y.; Zhu, Y.; Oupický, D. Recent Advances in Delivery of Drug-Nucleic Acid Combinations for Cancer Treatment. *Journal of Controlled Release*. 2013, pp 589–600. https://doi.org/10.1016/j.jconrel.2013.04.010.

(6) Jin, J. O.; Kim, G.; Hwang, J.; Han, K. H.; Kwak, M.; Lee, P. C. W. Nucleic Acid Nanotechnology for Cancer Treatment. *Biochimica et Biophysica Acta - Reviews on Cancer*. Elsevier B.V. August 2020. https://doi.org/10.1016/j.bbcan.2020.188377.

(7) Dorn, G.; Patel, S.; Wotherspoon, G.; Hemmings-Mieszczak, M.; Barclay, J.; Natt, F. J. C.; Martin, P.; Bevan, S.; Fox, A.; Ganju, P.; Wishart, W.; Hall, J. SiRNA Relieves Chronic Neuropathic Pain. *Nucleic Acids Res* **2004**, *32*. https://doi.org/10.1093/nar/gnh044.

(8) Goins, W. F.; Cohen, J. B.; Glorioso, J. C. Gene Therapy for the Treatment of Chronic Peripheral Nervous System Pain. *Neurobiology of Disease*. November 2012, pp 255–270. https://doi.org/10.1016/j.nbd.2012.05.005.

(9) Hall, A.; Lächelt, U.; Bartek, J.; Wagner, E.; Moghimi, S. M. Polyplex Evolution: Understanding Biology, Optimizing Performance. *Molecular Therapy*. American Society of Gene and Cell Therapy July 2017, pp 1476–1490. https://doi.org/10.1016/j.ymthe.2017.01.024.

(10) Casadidio, C.; Hartman, J. E. M.; Mesquita, B. S.; Haegebaert, R.; Remaut, K.; Neumann, M.; Hak, J.; Censi, R.; Di Martino, P.; Hennink, W. E.; Vermonden, T. Effect of Polyplex Size on Penetration into Tumor Spheroids. *Mol Pharm* **2023**, *20*, 5515–5531. https://doi.org/10.1021/acs.molpharmaceut.3c00397.

(11) Krützfeldt, J.; Kuwajima, S.; Braich, R.; Rajeev, K. G.; Pena, J.; Tuschl, T.; Manoharan, M.; Stoffel, M. Specificity, Duplex Degradation and Subcellular Localization of Antagomirs. *Nucleic Acids Res* **2007**, *35*, 2885–2892. https://doi.org/10.1093/nar/gkm024.

(12) Lu, T. X.; Hartner, J.; Lim, E.-J.; Fabry, V.; Mingler, M. K.; Cole, E. T.; Orkin, S. H.; Aronow, B. J.; Rothenberg, M. E. MicroRNA-21 Limits In Vivo Immune Response-Mediated Activation of the IL-12/IFN-γ Pathway, Th1 Polarization, and the Severity of Delayed-Type Hypersensitivity. *The Journal of Immunology* **2011**, *187*, 3362–3373. https://doi.org/10.4049/jimmunol.1101235.

(13) Ding, X.; Jing, N.; Shen, A.; Guo, F.; Song, Y.; Pan, M.; Ma, X.; Zhao, L.; Zhang, H.; Wu, L.; Qin, G.; Zhao, Y. MiR-21-5p in Macrophage-Derived Extracellular Vesicles Affects Podocyte Pyroptosis in Diabetic Nephropathy by Regulating A20. *J Endocrinol Invest* **2021**, *44*, 1175–1184. https://doi.org/10.1007/s40618-020-01401-7.

(14) Madhyastha, R.; Madhyastha, H.; Nurrahmah, Q. I.; Purbasari, B.; Maruyama, M.; Nakajima, Y. MicroRNA 21 Elicits a Pro-Inflammatory Response in Macrophages, with Exosomes Functioning as Delivery Vehicles. *Inflammation* **2021**, *44*, 1274–1287. https://doi.org/10.1007/s10753-021-01415-0.

(15) Zeboudj, L.; Sideris-Lampretsas, G.; Silva, R.; Al-Mudaris, S.; Picco, F.; Fox, S.; Chambers, D.; Malcangio, M. Silencing MiR-21-5p in Sensory Neurons Reverses Neuropathic Allodynia via Activation of TGF-β-Related Pathway in Macrophages. *Journal of Clinical Investigation* **2023**, *133*. https://doi.org/10.1172/JCI164472.

(16) Calame, K. MicroRNA-155 Function in B Cells. *Immunity*. December 2007, pp 825–827. https://doi.org/10.1016/j.immuni.2007.11.010.

(17) Costinean, S.; Zanesi, N.; Pekarsky, Y.; Tili, E.; Volinia, S.; Heerema, N.; Croce, C. M. Pre-B Cell Proliferation and Lymphoblastic Leukemia/High-Grade Lymphoma in Eμ-MiR155 Transgenic Mice. *Proc Natl Acad Sci U S A* **2006**, *103*, 7024–7029. https://doi.org/10.1073/pnas.0602266103.

(18) Landgraf, P.; Rusu, M.; Sheridan, R.; Sewer, A.; Iovino, N.; Aravin, A.; Pfeffer, S.; Rice, A.; Kamphorst, A. O.; Landthaler, M.; Lin, C.; Socci, N. D.; Hermida, L.; Fulci, V.; Chiaretti, S.; Foà, R.; Schliwka, J.; Fuchs, U.; Novosel, A.; Müller, R. U.; Schermer, B.; Bissels, U.; Inman, J.; Phan, Q.; Chien, M.; Weir, D. B.; Choksi, R.; De Vita, G.; Frezzetti, D.; Trompeter, H. I.; Hornung, V.; Teng, G.; Hartmann, G.; Palkovits, M.; Di Lauro, R.; Wernet, P.; Macino, G.; Rogler, C. E.; Nagle, J. W.; Ju, J.; Papavasiliou, F. N.; Benzing, T.; Lichter, P.; Tam, W.;

Brownstein, M. J.; Bosio, A.; Borkhardt, A.; Russo, J. J.; Sander, C.; Zavolan, M.; Tuschl, T. A Mammalian MicroRNA Expression Atlas Based on Small RNA Library Sequencing. *Cell* **2007**, *129*, 1401–1414. https://doi.org/10.1016/j.cell.2007.04.040.

(19) O'Connell, R. M.; Taganov, K. D.; Boldin, M. P.; Cheng, G.; Baltimore, D. MicroRNA-155 Is Induced during the Macrophage Inflammatory Response. *Proc Natl Acad Sci U S A* **2007**, *104*, 1604–1609. https://doi.org/10.1073/pnas.0610731104.

(20) Kurowska-Stolarska, M.; Hasoo, M. K.; Welsh, D. J.; Stewart, L.; McIntyre, D.; Morton, B. E.; Johnstone, S.; Miller, A. M.; Asquith, D. L.; Millar, N. L.; Millar, A. B.; Feghali-Bostwick, C. A.; Hirani, N.; Crick, P. J.; Wang, Y.; Griffiths, W. J.; McInnes, I. B.; McSharry, C. The Role of MicroRNA-155/Liver X Receptor Pathway in Experimental and Idiopathic Pulmonary Fibrosis. *Journal of Allergy and Clinical Immunology* **2017**, *139*, 1946–1956. https://doi.org/10.1016/j.jaci.2016.09.021.

(21) Liu, Z. Q.; Feng, J.; Shi, L. L.; Xu, J.; Zhang, B. J.; Chen, L. J. Influences of MIR-155/NF-KB Signaling Pathway on Inflammatory Factors in ARDS in Neonatal Pigs. *Eur Rev Med Pharmacol Sci* **2019**, *23*, 7042–7048. https://doi.org/10.26355/eurrev_201908_18746.

(22) Picco, F.; Zeboudj, L.; Oggero, S.; Prato, V.; Burgoyne, T.; Gamper, N.; Malcangio, M. Macrophage to Neuron Communication via Extracellular Vesicles in Neuropathic Pain Conditions. *Heliyon* **2025**, *11*, e41268. https://doi.org/10.1016/j.heliyon.2024.e41268.

(23) Paoletti, A.; Ly, B.; Cailleau, C.; Gao, F.; de Ponfilly-Sotier, M. P.; Pascaud, J.; Rivière, E.; Yang, L.; Nwosu, L.; Elmesmari, A.; Reynaud, F.; Hita, M.; Paterson, D.; Reboud, J.; Fay, F.; Nocturne, G.; Tsapis, N.; McInnes, I. B.; Kurowska-Stolarska, M.; Fattal, E.; Mariette, X. Liposomal AntagomiR-155-5p Restores Anti-Inflammatory Macrophages and Improves Arthritis in Preclinical Models of Rheumatoid Arthritis. *Arthritis and Rheumatology* **2024**, *76*, 18–31. https://doi.org/10.1002/art.42665.

(24) Zhang, T.; Ni, S.; Luo, Z.; Lang, Y.; Hu, J.; Lu, H. The Protective Effect of MicroRNA-21 in Neurons after Spinal Cord Injury. *Spinal Cord* **2019**, *57*, 141–149. https://doi.org/10.1038/s41393-018-0180-1.

(25) Hu, J. Z.; Huang, J. H.; Zeng, L.; Wang, G.; Cao, M.; Lu, H. Bin. Anti-Apoptotic Effect of MicroRNA-21 after Contusion Spinal Cord Injury in Rats. *J Neurotrauma* **2013**, *30*, 1349–1360. https://doi.org/10.1089/neu.2012.2748.

(26) Lv, X.; Liang, J.; Wang, Z. MiR-21-5p Reduces Apoptosis and Inflammation in Rats with Spinal Cord Injury through PI3K/AKT Pathway. *Panminerva Med* **2024**, *66*, 256–265. https://doi.org/10.23736/S0031-0808.20.03974-9.

(27) Adel, M.; Zahmatkeshan, M.; Johari, B.; Kharrazi, S.; Mehdizadeh, M.; Bolouri, B.; Rezayat, S. M. Investigating the Effects of Electrical Stimulation via Gold Nanoparticles on in Vitro Neurite Outgrowth: Perspective to Nerve Regeneration. *Microelectron Eng* **2017**, *173*, 1–5. https://doi.org/10.1016/j.mee.2017.03.006.

(28) Hai, A.; Dormann, A.; Shappir, J.; Yitzchaik, S.; Bartic, C.; Borghs, G.; Langedijk, J. P. M.; Spira, M. E. Spine-Shaped Gold Protrusions Improve the Adherence and Electrical Coupling of Neurons with the Surface of Micro-Electronic Devices. *J R Soc Interface* **2009**, *6*, 1153–1165. https://doi.org/10.1098/rsif.2009.0087.

(29) De Graaf, A. J.; Azevedo Próspero Dos Santos, I. I.; Pieters, E. H. E.; Rijkers, D. T. S.; Van Nostrum, C. F.; Vermonden, T.; Kok, R. J.; Hennink, W. E.; Mastrobattista, E. A Micelle-Shedding Thermosensitive Hydrogel as Sustained Release Formulation. *Journal of Controlled Release* **2012**, *162*, 582–590. https://doi.org/10.1016/j.jconrel.2012.08.010.

(30) Dinari, A.; Moghadam, T. T.; Abdollahi, M.; Sadeghizadeh, M. Synthesis and Characterization of a Nano-Polyplex System of GNRs-PDMAEA-PDNA: An Inert Self-Catalyzed Degradable Carrier for Facile Gene Delivery. *Scientific Reports 2018 8:1* **2018**, *8* (1), 1–12. https://doi.org/10.1038/s41598-018-26260-4.

(31) Cao, D.-L.; Jing, P.-B.; Jiang, B.-C.; Gao, Y.-J. Primary Culture of Mouse Neurons from the Spinal Cord Dorsal Horn. *Bio Protoc* **2017**, *7*. https://doi.org/10.21769/bioprotoc.2098.

(32) Basso, D. M.; Beattie, M. S.; Bresnahan, J. C. A Sensitive and Reliable Locomotor Rating Scale for Open Field Testing in Rats. *J Neurotrauma* **1995**, *12*, 1–21. https://doi.org/10.1089/neu.1995.12.1.

(33) Santos-Nogueira, E.; Redondo Castro, E.; Mancuso, R.; Navarro, X. Randall-Selitto Test: A New Approach for the Detection of Neuropathic Pain after Spinal Cord Injury. *J Neurotrauma* **2012**, *29*, 898–904. https://doi.org/10.1089/neu.2010.1700.

(34) Fliervoet, L. A. L.; Zhang, H.; van Groesen, E.; Fortuin, K.; Duin, N. J. C. B.; Remaut, K.; Schiffelers, R. M.; Hennink, W. E.; Vermonden, T. Local Release of SiRNA Using Polyplex-Loaded Thermosensitive Hydrogels. *Nanoscale* **2020**, *12* (18), 10347–10360. https://doi.org/10.1039/D0NR03147J.

(35) Van De Wetering, P.; Cherng, J. Y.; Talsma, H.; Hennink, W. E. Relation between Transfection Efficiency and Cytotoxicity of Poly(2-Dimethylamino)Ethyl Methacrylate)/Plasmid Complexes. *Journal of Controlled Release* **1997**, *49*, 59–69. https://doi.org/10.1016/S0168-3659(97)00059-X.

(36) Fliervoet, L. A. L.; van Nostrum, C. F.; Hennink, W. E.; Vermonden, T. Balancing Hydrophobic and Electrostatic Interactions in Thermosensitive Polyplexes for Nucleic Acid Delivery. *Multifunctional Materials* **2019**, *2*. https://doi.org/10.1088/2399-7532/ab12ee.

(37) Lee, H. Y.; Lee, H. Y.; Choi, J. Y.; Hur, J.; Kim, I. K.; Kim, Y. K.; Kang, J. Y.; Lee, S. Y. Inhibition of MicroRNA-21 by an Antagomir Ameliorates Allergic Inflammation in a Mouse Model of Asthma. *Exp Lung Res* **2017**, *43*, 109–119. https://doi.org/10.1080/01902148.2017.1304465.

(38) Mirna, M.; Paar, V.; Topf, A.; Kraus, T.; Sotlar, K.; Aigner, A.; Ewe, A.; Watzinger, S.; Podesser, B. K.; Hackl, M.; Pistulli, R.; Hoppe, U. C.; Kiss, A.; Lichtenauer, M. A New Player in the Game: Treatment with AntagomiR-21a-5p Significantly Attenuates Histological and Echocardiographic Effects of Experimental Autoimmune Myocarditis. *Cardiovasc Res* **2022**, *118*, 556–572. https://doi.org/10.1093/cvr/cvab015.

(39) Yu, S.; Chen, J.; Dong, R.; Su, Y.; Ji, B.; Zhou, Y.; Zhu, X.; Yan, D. Enhanced Gene Transfection Efficiency of PDMAEMA by Incorporating Hydrophobic Hyperbranched Polymer Cores: Effect of Degree of Branching. *Polym Chem* **2012**, *3*, 3324–3329. https://doi.org/10.1039/c2py20487h.

(40) Schindelin, J.; Arganda-Carreras, I.; Frise, E.; Kaynig, V.; Longair, M.; Pietzsch, T.; Preibisch, S.; Rueden, C.; Saalfeld, S.; Schmid, B.; Tinevez, J. Y.; White, D. J.; Hartenstein, V.; Eliceiri, K.; Tomancak, P.; Cardona, A. Fiji: An Open-Source Platform for Biological-Image Analysis. *Nature Methods*. July 2012, pp 676–682. https://doi.org/10.1038/nmeth.2019.

(41) Samal, S. K.; Dash, M.; Vlierberghe, S. Van; Kaplan, D. L.; Chiellini, E.; Blitterswijk, C. van; Moroni, L.; Dubruel, P. Cationic Polymers and Their Therapeutic Potential. *Chem Soc Rev* **2012**, *41*, 7147–7194. https://doi.org/10.1039/c2cs35094g.

(42) Hachim, D.; Zhao, J.; Bhankharia, J.; Nuñez-Toldra, R.; Brito, L.; Seong, H.; Becce, M.; Ouyang, L.; Grigsby, C. L.; Higgins, S. G.; Terracciano, C. M.; Stevens, M. M.

Polysaccharide-Polyplex Nanofilm Coatings Enhance Nanoneedle-Based Gene Delivery and Transfection Efficiency. *Small* **2022**, *18*. https://doi.org/10.1002/smll.202202303.

(43) Lungwitz, U.; Breunig, M.; Blunk, T.; Göpferich, A. Polyethylenimine-Based Non-Viral Gene Delivery Systems. In *European Journal of Pharmaceutics and Biopharmaceutics*; 2005; Vol. 60, pp 247–266. https://doi.org/10.1016/j.ejpb.2004.11.011.

(44) Zakeri, A.; Kouhbanani, M. A. J.; Beheshtkhoo, N.; Beigi, V.; Mousavi, S. M.; Hashemi, S. A. R.; Karimi Zade, A.; Amani, A. M.; Savardashtaki, A.; Mirzaei, E.; Jahandideh, S.; Movahedpour, A. Polyethylenimine-Based Nanocarriers in Co-Delivery of Drug and Gene: A Developing Horizon. *Nano Rev Exp* **2018**, *9*, 1488497. https://doi.org/10.1080/20022727.2018.1488497.

(45) Godbey, W. T.; Wu, K. K.; Mikos, A. G. Size Matters: Molecular Weight Affects the Efficiency of Poly(Ethylenimine) as a Gene Delivery Vehicle. *J Biomed Mater Res* **1999**, *45*, 268–275. https://doi.org/10.1002/(SICI)1097-4636(19990605)45:3<268::AID-JBM15>3.0.CO;2-Q.

(46) Bennett, J.; Das, J. M.; Emmady, P. D. *Spinal Cord Injuries*; 2025.

(47) Blight, A. R. Macrophages and Inflammatory Damage in Spinal Cord Injury. *Journal of Neurotrauma*. 1992.

(48) Bisicchia, E.; Latini, L.; Cavallucci, V.; Sasso, V.; Nicolin, V.; Molinari, M.; D'Amelio, M.; Viscomi, M. T. Autophagy Inhibition Favors Survival of Rubrospinal Neurons After Spinal Cord Hemisection. *Mol Neurobiol* **2017**, *54*, 4896–4907. https://doi.org/10.1007/s12035-016-0031-z.

Chapter 5

Hydrogel-Nanoparticle Patches for the Topical Delivery of Capsaicin for the Treatment of Neuropathic Pain

Abstract

Capsaicin is a potent molecule for treating neuropathic chronic pain. Use of creams and patches is a standard approach to deliver capsaicin topically. However, these medications often require frequent reapplication to provide long-lasting pain relief and can cause unpleasant burning and itching. To address these issues, we developed UV-crosslinked hydrogels from a biocompatible Poloxamer P188 with capsaicin-loaded poly(lactic-*co*-glycolic acid) nanoparticles. The chemical derivatization of Poloxamer P188 into acrylate derivatives by the use of aza- and thiol-Michael addition together with UV irradiation generated hydrogels with varying polymeric architectures and crosslinking density. This in turn allowed us to obtain low-swelling and mechanically robust hydrogels. The encapsulation of capsaicin into nanoparticles resulted in 194 nm size and 0.07 PDI. With a 99% encapsulation efficiency, the gradual release of capsaicin over a five-week period. Local release of nanoparticles from hydrogels was analysed with a Franz diffusion system, mimicking skin permeation. The studied hydrogel-nanoparticle patches can expand the spectrum of treatment options for neuropathic pain, offering long-term relief and improved patient compliance with reduced side effects.

1. Introduction

Neuropathic chronic pain is often a consequence of leading diseases in the modern society, such as cancer and diabetes.[1] Amongst the diabetic patients about 25% suffer from neuropathic pain[2]. The prevalence of neuropathic chronic pain worldwide is estimated to be around 7-10%[3]. Current treatment options focus on centrally acting drugs which often come with systemic side effects and limited therapeutic efficacy,[2,3] highlighting the need for more effective solutions with reduced adverse reactions.

To address these issues, localized drug delivery, in the form of patches, plasters, and creams, has been explored as an alternative treatment option for neuropathic pain. Such systems can be designed to act locally and limit systemic side effects, even promote transdermal permeation, since the action of the medicine will take place through passive diffusion, which negates the need for enhancers for enhanced transdermal delivery.[4] One drug of choice in these systems is capsaicin (Figure 1). Capsaicin is an agonist of one of the vanilloid receptors, namely transient receptor potential cation channel subfamily V member 1 (TRPV1).[5] These receptors are most prominent in the cell membranes of dorsal root ganglia (DRG) neurons. Prolonged exposure to capsaicin causes a paradoxical desensitization of TRPV1 resulting in an analgesic effect which explains the pain relief observed after topical application.[2,6]

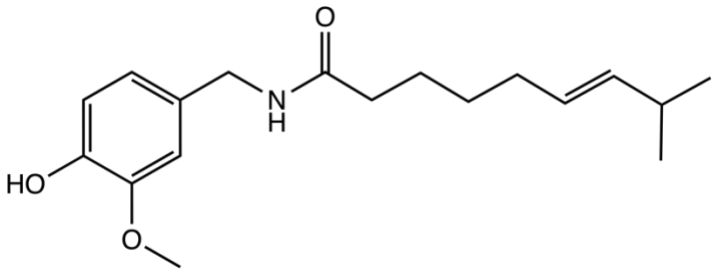

Figure 1. Structure of capsaicin.

Commercially capsaicin is available as low-dose creams (0.025-0.075% capsaicin) and high-dose patches (8% capsaicin). However, some reports point to pungency, erythema, and itching as a consequence of direct capsaicin application on the skin. Low dose

creams with capsaicin require frequent reapplication, which leads to repeated discomfort. On the other hand, the high dose capsaicin patch can only be applied by a physician and prior to application there is a need for local anesthesia to manage the discomfort. These disadvantages may affect the widespread use of capsaicin-based medications.[2,7]

Hydrogels are a reliable candidate for topical and transdermal drug delivery.[8] These materials combine robustness with flexibility supporting long time wear, while being non-toxic and biocompatible. Poloxamers, triblock copolymers of poly(ethylene glycol)-*b*-poly(propylene glycol)-*b*-poly(ethylene glycol) (PEG-PPG-PEG), are one of the primary representatives of biocompatible hydrogels.[9] The availability of a free hydroxyl group at the terminal enables easy chemical modification into photocrosslinkable hydrogels.[10] After crosslinking, the water-rich 3D matrix can become a reservoir for delivery of therapeutic cargo.[11] However, the direct loading of capsaicin into the hydrogel leads to the unpleasant effects, like burning and itching, as observed in commercial formulations.[2,7] Hence, capsaicin should be encapsulated into a more suitable carrier, like hydrophobic polymeric nanoparticles,[12,13] which then can be loaded into the hydrogel, generating a hydrogel-nanoparticle (HG-NP) drug delivery system.[14] One suitable carrier for capsaicin are poly(lactic-co-glycolic acid) nanoparticles (PLGA NPs). Capsaicin will then penetrate the skin while being embeded into PLGA NPs which minimzes the discomfort and side effects connected to topical capsaicin application. After penetrating the skin, the NPs will provide gradual release of capsaicin to the affected neurons, granting controlled and prolonged release.[13]

HG-NP composites have previously been studied, both as transdermal and injectable formulations. Bernal-Chávez et al.[12] reported the development of a Poloxamer based hydrogel with platelet lysate-loaded PLGA NPs for wound healing. Incorporating NPs into a hydrogel matrix prevented premature drug leakage and enabled localized drug delivery. Similarly, Mudhol's group developed a hydrogel patch with nanoformulated capsaicin for obesity treatment.[15] The use of NPs to deliver capsaicin resulted in improved bioavailability. Capsaicin-loaded PLGA NPs have been used topically, either directly

applied,[16] or in creams.[13] However, there are currently no mentions of hydrogel patches utilizing capsaicin-PLGA NPs to treat neuropathic pain.

In this work, we report the development of proof-of-concept hydrogel patches for topical delivery of nanoencapsulated capsaicin. The proposed system comprises a Poloxamer P188 (P188) UV-crosslinked hydrogel loaded with capsaicin-PLGA NPs. P188 was first converted into the corresponding diamine, dithiol, and diacrylate. Then, P188 diacrylate and P188 dithiol were subjected to a thiol-Michael addition, while P188 diamine and P188 diacrylate underwent an aza-Michael addition. This resulted in three P188 derivatives with free acrylate groups at the terminal ends, namely the initial P188 diacrylate and two Michael addition products. By using these three derivatives of varying molecular weight, UV-crosslinked hydrogels of varied polymeric architecture were prepared. The prepared patches possessed intrinsic adhesive properties, low swelling, as well as satisfactory stiffness under low stress.
Employing PLGA NPs for capsaicin delivery may help reduce unpleasant side effect associated with topical use of capsaicin. These HG-NP patches exhibit characterstics which could be suitable for long-acting pain relief combined with robustness tailored for the topical application.

2. Experimental Section

2.1. Materials

Poloxamer P188 (average MW = 8400 g/mol, Sigma-Aldrich) was used as a starting polymer. For the preparation of P188 derivatives reagents, such as triethylamine (TEA), mesyl chloride, acryloyl chloride, $Na_2S_2O_3$ were sourced from Sigma-Aldrich. Dichlormethane (DCM), methanol (MeOH), and ammonium hydroxide solution ($NH_{3(aq)}$) were purchased from VWR. Dithiothreitol (DTT) was received from *Iris Biotech*. Irgacure 2959 (2-Hydroxy-4'-(2-hydroxyethoxy)-2-methylpropiophenone, Sigma-Aldrich) was used as photoinitiator for UV-crosslinking.

For PLGA nanoparticles synthesis and characterization PLGA, acid terminated (average MW = 17000 g/mol, PURASORB PDLG 5002A, PURAC), Tween-80 (Sigma-Aldrich), cetyltrimethylammonium bromide (CTAB) (Sigma-Aldrich), and capsaicin (MW = 305.41 g/mol, Sigma-Aldrich) were used.

All chemicals were used as received without further purification.

2.2. Instrumentation

For preparation of PLGA NPs a T 25 digital ULTRA-TURRAX homogenizer was used. The resulting NPs were analyzed in terms of size and polydispersity index by dynamic light scattering (DLS) using Malvern Zetasizer Nano-S90. The measurements were performed at 25 °C.

The GC-MS analysis was performed using Agilent GC-MS 8890-5790B equipped with HP-5MS column (length 30 m, flow 1.2 mL/min) to obtain concentration of encapsulated and released capsaicin from capsaicin-PLGA NPs. The temperature program consisted of 1 min hold at 160 °C, ramp to 300 °C with a rate of 20 °C/min, followed by 1 min hold at 300 °C. The MS source was set at 280 °C and quadrupole at 150 °C. The ion of *m/z* = 305 was used to identify capsaicin.

The hydrogels were prepared under UV irradiation (365 nm, 36 W). The rheological measurements of hydrogels were performed using Anton Paar Modular Compact Rheometer MCR 92 equipped with a Peltier plate for temperature control. All measurements were done at 37 °C using a parallel plate (d = 50 mm) at a measuring gap of 0.2 mm with a frequency of 1 Hz. Raman spectroscopy was performed using Horiba iHR-320 spectrometer.

FTIR spectra of the polymers was obtained with PerkinElmer Frontier FTIR, operated in ATR mode at 25 °C. The ^{1}H NMR analysis was performed using Bruker Ascend™ 400 series operating at 400 MHz. The samples were analyzed in $CDCl_3$. The chemical shifts are listed in ppm relative to solvent residual peak at 7.29 ppm.

2.3. Preparation and characterization of PLGA NPs and capsaicin-PLGA NPs

Empty PLGA NPs and capsaicin-loaded PLGA NPs were prepared using the oil/water solvent evaporation method (as in Chapter 3). [17,18] Briefly, 100 mg of PLGA was dissolved in 3 mL of DCM. For capsaicin-loaded PLGA-NPs 10 mg of capsaicin was added into the dissolved PLGA. The DCM solution was then added dropwise to 18 mL of 0.5% (w/v) CTAB solution. The resulting emulsion was then homogenized using a homogenizer at 11000 rpm for 15 minutes while cooled in an ice bath. The homogenized solution was transferred into a beaker secured with perforated parafilm to ensure DCM evaporation. The solution was left overnight under constant stirring. The obtained solution was then centrifuged for 20 minutes at 5 °C at 8000 x g. The isolated PLGA NPs were resuspended in water, lyophilized and kept frozen until use.

The size and polydispersity index of PLGA NPs were determined by DLS. The measurements were performed at 25 °C. The results are reported as an average (n = 3) ± SD. The loading capacity (LC) and encapsulation efficiency (EE) of capsaicin-PLGA NPs was calculated from data obtained by GC-MS using the following formulas:

$$LC = \frac{CAP_{GC-MS}}{m_{PLGA} + m_{CAP}} \times 100\ [\%] \qquad (Equation\ 1)$$

$$EE = \frac{CAP_{GC-MS}}{m_{CAP}} \times 100\ [\%] \qquad (Equation\ 2)$$

$CAP_{GC\text{-}MS}$ – amount of capsaicin in the PLGA NPs as determined by GC-MS

m_{PLGA} – amount of PLGA used for PLGA NPs preparation

m_{CAP} – amount of capsaicin used for nanoparticle preparation

2.4. Preparation of P188 derivatives

2.4.1. General procedure for mesylation of P188-OH

P188-OH was dried by azeotropic distillation from toluene (2 mL/g of P188-OH) under vacuum. Neat P188-OH was then redissolved in DCM (10 mL/g of P188-OH) and mesyl chloride (2.5 molar equiv.) was added to the solution, followed by a dropwise addition of TEA (3.0 molar equiv.). The resulting reaction mixture was stirred overnight at 25 °C. The reaction mixture was then washed with H_3PO_4. (0.1 M, 3 mL/g of P188-OH) and DCM was removed under vacuum and the resulting product was dried under vacuum to give P188 dimesylate (P188-Ms) in 98 % gravimetrical yield.

2.4.2. General procedure for acrylation of P188-OH

P188-OH was dried by azeotropic distillation from toluene (2 mL/g of P188-OH) under vacuum. Neat P188-OH was then redissolved in DCM (10 mL/g of P188-OH) and acryloyl chloride (2.5 molar equiv.) was added to the solution, followed by a dropwise addition of TEA (3.0 molar equiv.). The resulting reaction mixture was stirred overnight at 25 °C. The reaction mixture was then washed with H_3PO_4 (0.1 M, 3 mL/g of P188-OH) and DCM was removed under vacuum and the resulting product was dried under vacuum to give P188 diacrylate (P188-DA) in 89 % gravimetrical yield.

2.4.3. General procedure for amination of P188-Ms

P188-Ms was dissolved in $NH_{3(aq)}$ (25 mL/g of P188-Ms) The resulting reaction mixture was stirred over two days at 25 °C. The reaction mixture was then extracted twice with DCM (10 mL/g of P188-OH). DCM was removed under vacuum and the resulting product was dried under vacuum to give P188 diamine (P188-NH_2) in 90 % gravimetrical yield.

2.4.4. General procedure for thiolation of P188-Ms

P188-Ms was dissolved in distilled water (75 mL/g of P188-OH) and methanol (25 mL/g of P188-Ms).

$Na_2S_2O_3$ (2.2 molar equiv.) was added to the solution. The resulting reaction mixture was stirred over two days at 60 °C. pH was then adjusted to pH = 9-10 with 1M NaOH, followed by the addition of DTT (2.5 molar equiv.). The reaction mixture was then extracted twice

with DCM (20 mL/g of P188-OH). DCM was removed under vacuum and the resulting product was dried under vacuum to give P188 dithiol (P188-SH) in 83 % gravimetrical yield.

^{1}H NMR (400 MHz, $CDCl_3$): **P188-OH** δ = 3.70-3.90 (br m, protons in repeating units of PEG (C**H**$_2$); protons in repeating units of PPG (C**H**)); 1.16 (br m, protons in the repeating methylene group of PPG C**H**$_3$). **P188-DA** δ = 6.42 (d, 2H, J = 17 Hz, -C**H** trans of the acrylate group), 6.13 (dd, 2H, J = 10 Hz and 27 Hz, -C**H** geminal protons of the acrylate group), 5.83 (d, 2H, J = 12 Hz, -C**H** cis protons of the acrylate group); 3.70-3.90 (br m, protons in repeating units of PEG (C**H**$_2$); protons in repeating units of PPG (C**H**)); 1.16 (br m, protons in the repeating methylene group of PPG C**H**$_3$). **P188-SH** δ = 3.70-3.90 (br m, protons in repeating units of PEG (C**H**$_2$); protons in repeating units of PPG (C**H**)); 2.69 (br s, methylene protons C**H**$_2$-SH), 1.57 (t, J = 8 Hz, 2H, thiol protons S**H**); 1.16 (br m, protons in the repeating methylene group of PPG C**H**$_3$). **P188-NH$_2$** δ = 3.70-3.90 (br m, protons in repeating units of PEG (C**H**$_2$); protons in repeating units of PPG (C**H**)); 2.90 (br s, 4H, methylene protons C**H**$_2$-NH_2), 1.71 (br s, 4H, amine protons N**H**$_2$); 1.16 (br m, protons in the repeating methylene group of PPG C**H**$_3$).

2.5. Preparation of P188 hydrogels

The obtained P188-DA was directly subjected to UV-crosslinking to generate a hydrogel. P188-SH and P188-NH_2 were both combined with excess of P188-DA (3 molar equiv. to P188-SH and 5 molar equiv. to P188-NH_2) to perform Michael addition and then subjected to UV-crosslinking. The polymers were dissolved in PBS buffer to yield 20% (w/v) solutions. The reactions were allowed to run for 48 h at 37 °C. The products of the Michael addition between P188-DA and P188-SH or P188-NH_2 was P188-DA-SH and P188-DA-NH_2, respectively. The samples were lyophilized and used for UV-crosslinking. To confirm successful formation of Michael addition products, FTIR and NMR analyses were performed.

^{1}H NMR (400 MHz, $CDCl_3$): **P188-DA-SH** δ = 6.47 (d, 2H, J = 15 Hz, -C**H** trans of the acrylate group), 6.18 (dd, 2H, J = 10 Hz and 27 Hz, -C**H** geminal protons of the acrylate

group), 5.85 (d, 2H, J = 12 Hz, -C**H** cis protons of the acrylate group); 3.70-3.90 (br m, protons in repeating units of PEG (C**H₂**); protons in repeating units of PPG (C**H**)); 2.69 (br s, methylene protons C**H₂**-SH), 1.57 (t, J = 8 Hz, 2H, thiol protons S**H**); 1.09 (br m, protons in the repeating methylene group of PPG C**H₃**). **P188-DA-NH₂** δ = 6.44 (d, 2H, J = 15 Hz, -C**H** trans of the acrylate group), 6.18 (dd, 2H, J = 10 Hz and 27 Hz, -C**H** geminal protons of the acrylate group), 5.85 (d, 2H, J = 12 Hz, -C**H** cis protons of the acrylate group); 3.70-3.90 (br m, protons in repeating units of PEG (C**H₂**); protons in repeating units of PPG (C**H**)); 3.11 (br s, 4H, methylene protons C**H₂**-NH_2), 1.84 (br s, 4H, amine protons N**H₂**); 1.16 (br m, protons in the repeating methylene group of PPG C**H₃**).

P188 hydrogels were prepared by dissolving the lyophilized powders of P188-DA, P188-DA-SH, and P188-DA-NH_2 in either PBS buffer or distilled water overnight at 5 °C to render 20% (w/v) solution. A photoinitiator solution (2.5% (w/v) in distilled water) was added to a final concentration of 0.5% (v/v) in the polymer solution. The hydrogels solutions with a photoinitiator were transferred to polystyrene molds and irradiated with a UV light until fully cured samples were obtained, giving HG-DA, HG-DA-SH, and HG-DA-NH_2.

2.6. Characterization of P188 hydrogels

The lyophilized UV-crosslinked hydrogels were collected for further characterization. The dried crosslinked hydrogels were studied by Raman spectroscopy. Raman: $\Delta\nu_{max}$ = 1719, 1634, 1477, 1282, 1141, 848, 536, 365 cm^{-1}

The *in vitro* swellability of the hydrogels was also determined. Briefly, 1 mL of hydrogels were crosslinked in 5 mL scintillation vials. The samples were dried in the incubator maintained at 37 °C for 72 h prior to testing. The starting weight of dried hydrogels was noted. Later, samples were submerged in 2 mL prewarmed PBS buffer. At defined time points, the PBS buffer was decanted, the surface of the samples was dried, and the weight was noted. The swelling was calculated using the following formula:

$$Q = \frac{m_{w(t)} - m_0}{m_0} \times 100\ [\%] \qquad (Equation\ 3)$$

Where, Q is the swelling degree, $m_{w(t)}$ is the weight of the hydrogel at a given time point, and m_0 is the weight of a dried hydrogel at t = 0. The values are reported as an average (n = 3) ± SD.

2.7. Rheological evaluation

The UV-crosslinked hydrogels were evaluated rheologically. The amplitude sweep was used to determine storage moduli (G') and loss moduli (G''). The time sweep oscillatory tests (viscosity curve, creep test) were used to evaluate the crosslinking of the hydrogel and resistance to deformation. The maximum phase angle values ($\tan\delta_{max}$) were calculated as the ratio between the maximum measured value of G'' and G' for each hydrogel.

2.8. *In vitro* release of capsaicin from capsaicin-PLGA NPs

The *in vitro* release of capsaicin from capsaicin-PLGA NPs was measured by direct suspension of capsaicin-PLGA NPs in PBS buffer. A water suspension (1 mL) of capsaicin-PLGA NPs was added into 100 mL of PBS buffer/Tween 80 with addition of 0.3% (w/v) Tween 80 to ensure sink conditions, i.e., enough excess of medium to ensure solubilization of capsaicin.[19] Aliquots of 500 µL were collected at defined time points and replaced with fresh portion of PBS buffer/Tween 80 solution. The collected samples were centrifuged for 10 minutes at 5 °C at 10000 rpm. The separated supernatant (100 µL) was diluted in acetone and analyzed using GC-MS to obtain concentration of released capsaicin.

2.9. *In vitro* release of capsaicin-PLGA NPs from hydrogels

Lyophilised samples of P188-DA, P188-DA-SH, and P188-DA-NH_2 were used to prepare 20 % (w/v) hydrogel solutions in 100 µL distilled water. The solutions were stirred and refigerated for 2 hours to ensure maximum dissolutions through cold method. Then, 1 mg capsaicin-PLGA NPs and 1% aqueous Irgacure solution were added to the gels before UV-

crossllinking (365 nm). On top of the hydrogels, 2 ml PBS (7.4 pH) was added and the samples were stored at 37˚ C until the end of the analysis. At different time points, 1 ml PBS was collected and same amount of fresh PBS was added back. The collected PBS was analysed with DLS to quantify capsaicin-PLGA NPs release from the hydrogels.

2.10. *In vitro* permeation analysis

Franz diffusion cells (9 mm jacketed, PermeGear, Inc., USA) were used for the *in vitro* permeation study of capsaicin-PLGA NPs from the P188-DA, P188-SH, and P188-NH_2 hydrogels. The capsaicin-PLGA NPs were loaded in the hydrogels as described in section 2.9. The Franz cells were set up in a circulating water bath at 37˚ C, and the receptor chamber was filled with 5 ml PBS (7.4 pH). The non-synthetic Strat-M Membrane (Transdermal Diffusion Test Model, 25mm, Merck Millipore, Italy) was used for transdermal diffusion. The donor chamber was clamped onto the membrane was filled with 100 µL of capsaicin-PLGA NPs loaded P188-DA/SH/NH_2 hydrogels. Every 15 minutes, the sampling port was used to withdraw 1 ml of the sample and same amount of fresh PBS was added back to the receptor chamber. The amount of capsaicin-PLGA NPs penetrating through the membrane was quantified by DLS.

The nanoparticle diffusion kinetics are presented as cumulative amount permeated (Q) per area (mg/cm^2) versus time (hour).[20,21]

$$Q = \frac{V(C1 + C2 + ..Ci)}{A} \qquad (Equation\ 4)$$

C1, C2 and Ci represent the nanoparticle concentration at 1, 2 and last time points respectively. V and A are the volume (mL) and area (cm^2) of the Franz diffusion cell.

Steady state flux (J; mg/cm^{2}h) is the rate at which the substance diffuses through a surface area with respect to time. It was calculated as:

$$J = dQ/dt/A \qquad (Equation\ 5)$$

The permeability coefficient (K; cm/h) was measured with the following equation:

$$K = \frac{Steady\ state\ flux}{Donor\ concentration} \qquad (Equation\ 6)$$

3. Results

3.1. Preparation of P188 derivatives

In order to obtain UV-crosslinkable hydrogels, P188 had to be derivatized into light-sensitive moieties. This was achieved in two steps. Firstly, the starting material **1** was derivatized into acrylate **3**, thiol **4**, and amine **5** derivatives (Scheme 1A). In the next step, Michael addition was performed (Scheme 1B) combining acrylate derivative with diamine or dithiol, generating new types of acrylated polymers **6** and **7**.

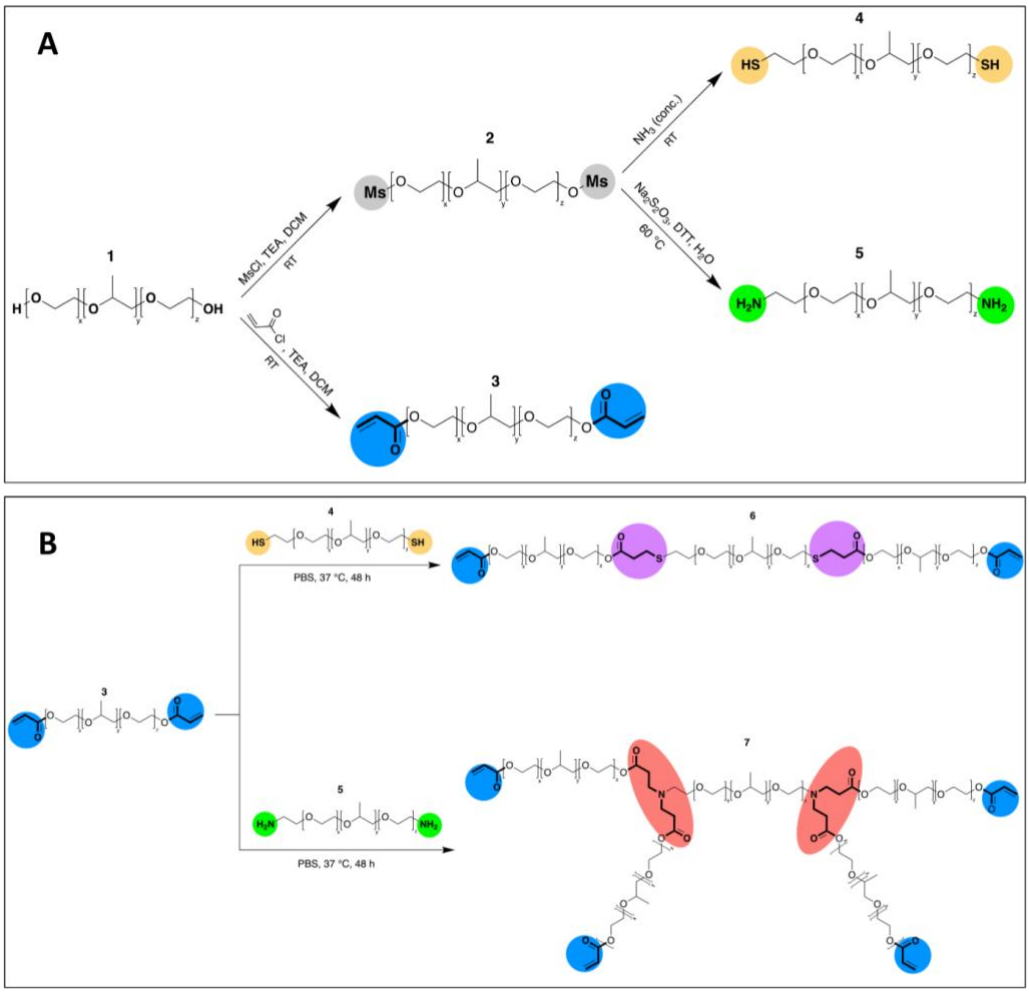

Scheme 1. A) P188-OH derivatization into acrylate-, thiol-, and amine-terminated P188; B) Michael addition between acrylate-, thiol-, and amine-terminated P188.

The successful derivatization was confirmed via FTIR (Figure 2A-C) and NMR (Figure 3). The FTIR spectra showed a typical fingerprint region of P188 between 800 and 1400 cm^{-1}.[22,23] The strongest peak at 1079 cm^{-1} correspond to symmetric stretching vibration of C-O-C.[22] Additionally, peaks at 941 cm^{-1} and 839 cm^{-1} are characteristic for CH_2-C-O rocking and stretching, respectively.[22] Outside of the fingerprint region, a broader peak at 2880 cm^{-1} was identified in all samples, corresponding to symmetric stretching of CH_2.[22,23]

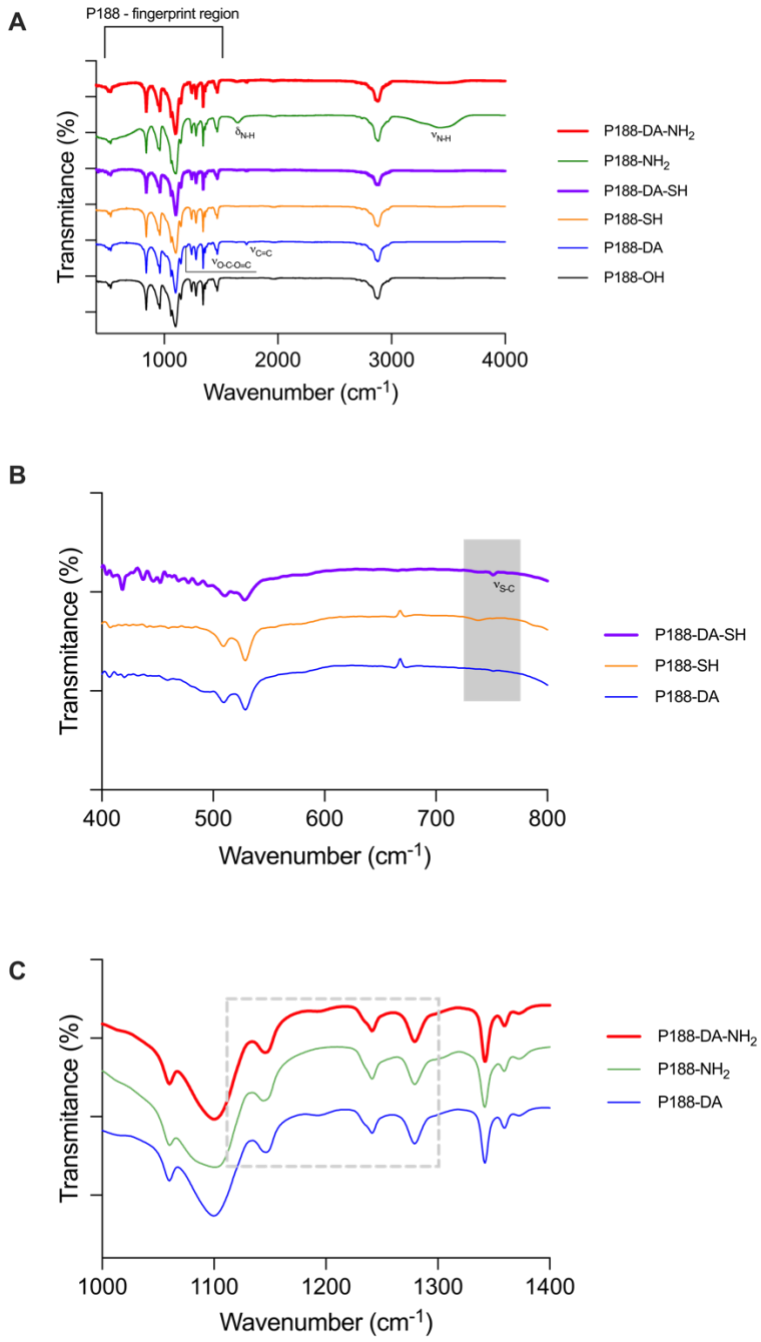

Figure 2. A) FTIR spectra of the prepared derivatives; B) Close-up of the spectra in the region of C-S bond stretching; C) and C-N bond stretching; D) NMR spectra of prepared P188 derivatives.

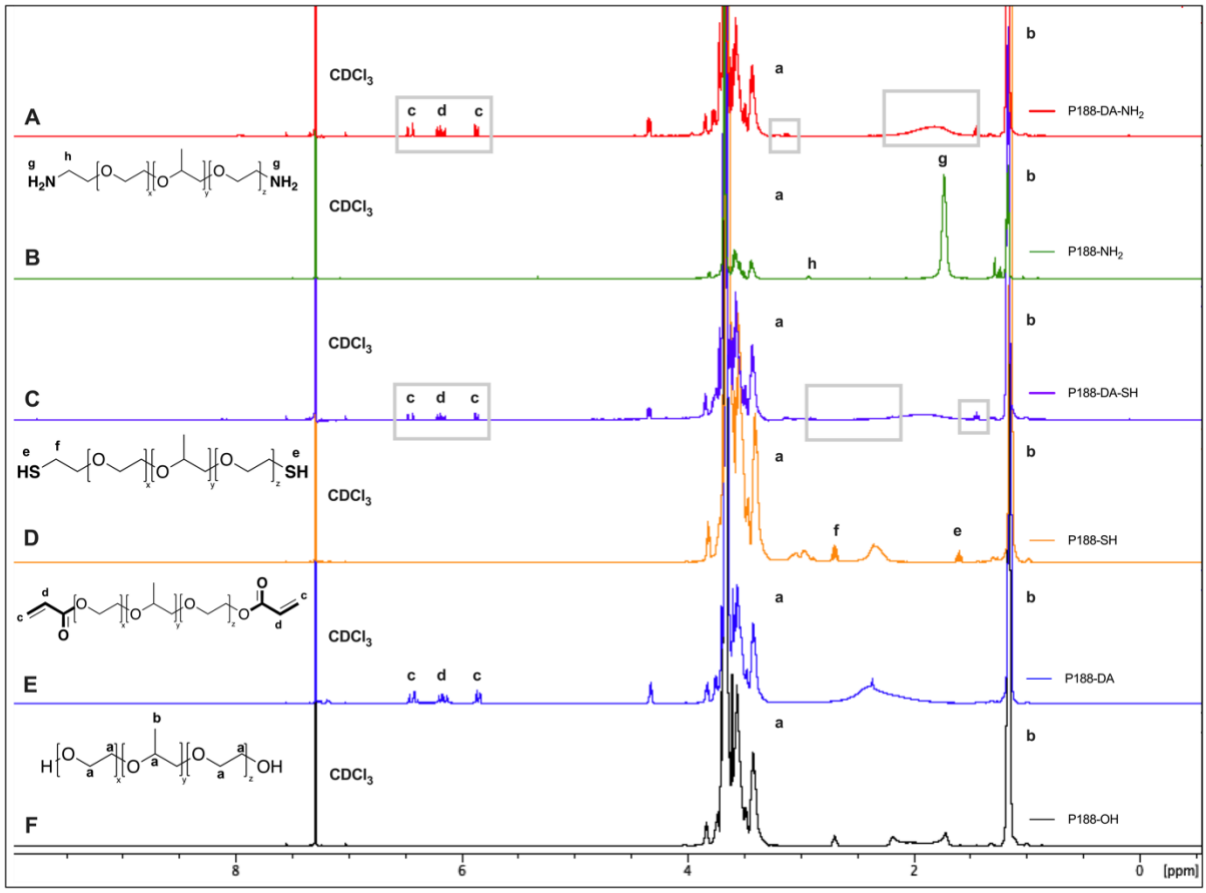

Figure 3. ^{1}H-NMR spectra of prepared P188 derivatives.

For the derivatized samples, specific signals for the introduced chemical groups were identified by means of FTIR. For P188-NH_2 **5**, two new wide peaks were identified (1602 and 3425 cm^{-1}), corresponding to stretching and bending of the amine group.[24] The presence of the thiol group was not clear in FTIR. However, it was later confirmed by ^{1}H NMR with the identified signal at 2.69 ppm, corresponding to signals from protons in C$\underline{H_2}$-SH. The free acrylate groups in P188-DA **3** were identified by two peaks at 1676 and 1158 cm^{-1} in the FTIR spectrum, corresponding to stretching of C=C and O-C-O=C.[25]

No strong evidence of C-N and C-S bond formation was found after Michael addition. A small peak at 750 cm^{-1} suggests the possible stretching of C-S (Figure 2B).[24] The peak for C-N stretching was not found in the expected region between 1100-1300 cm^{-1} (Figure 2C),[26,27] possibly due to overlap with the fingerprint region of P188. However, the characteristic amine peaks have been significantly reduced in P188-DA-NH_2. Furthermore, the presence of peaks characteristic for acrylate groups appeared in both

spectra of P188-DA-SH **6** and P188-DA-NH_2 **7**. This suggested successful formation of the acrylate-functionalized Michael addition products, namely P188-DA-SH **6**, and P188-DA-NH_2 **7**.

^{1}H NMR spectra again confirmed the successful derivatization with signals originating from the introduced groups. Typical signals for the P188 backbone were detected between 3.70-3.90 ppm corresponding to signals from C$\underline{H}_2$ and C$\underline{H}$ protons in both PEG and PPG (Figure 3, signal a),[28] as well as signals from C$\underline{H}_3$ protons of PPG (Figure 3, signal b) at 1.16 ppm.[29] Typical shifts between 5.83 and 6.47 ppm (Figure 2D signal c and d) confirmed acrylate presence.[28] The free thiol groups were confirmed by the shift at 1.57 (Figure 3, signal e) and 2.69 (Figure 3, signal f) ppm.[30] Finally, amine groups with signals at 1.71 (Figure 3, signal g) and 2.90 ppm (Figure 3, signal h).[30]

Similarly to FTIR results, for the product derived from the Michael addition significant reduction of signals characteristic for amine and thiol groups was observed with simultaneous appearance of shifts typical for acrylate groups. For the P188-DA-NH_2, the signals of amine groups (Figure 3, signal g and h) were reduced, however instead a widening of the peak appeared at 1.84 ppm, suggesting the presence of unreacted amine. For the P188-DA-SH, both signals (Figure 3, signal e and f) were diminished suggesting some product formation. On the other hand, weakened signals might be caused by the excess of diacrylate, leading to diminishing of the amine- and thiol-specific signals. Thus, further studies are required to surely confirm and quantitate product Michael addition products formation.

Reported yields of thiol-Michael and aza-Michael addition differ depending on reaction conditions, and vary from. Usually, thiol-Michael provides higher conversion under physiological conditions, nearly 100%, compared with 10-60% of aza-Michael.[31,32] Same can be observed here, where complete dissapearence of both signals characteristic signals (Figure 3, signal e and f) in NMR suggests some conversion in thiol-Michael addition, where signals for amine groups are only partially reduced in FTIR and NMR. In both instances, unreacted derivatives will be present in the obtained reaction mixture, which is later combined with a photoinitiator and subjected to UV irradiation. Hence, it is

expected that the linear chains of P188-SH and P188-NH_2 will be entangled between the acrylate-crosslinked network of P188-DA, impacting the properties of the hydrogel matrix.

3.2. Preparation and characterization of P188 hydrogels

The three P188 derivatives, namely P188 diacrylate **3** and two Michael addition products **6,7**, due to differences in molecular size and shape can generate different polymeric architectures once subjected to UV-crosslinking. Additionally, the incomplete conversion in Michael addition can lead to interupting the crosslinked P188-DA network in presence of linear P188-NH_2 and P188-SH. The UV-crosslinked hydrogels were prepared using a modified protocol by Parlato et al.[28] and Grubel et al.[33] Each of three acrylated polymers **3, 6, 7** was dissolved and combined with a photoinitiator. At this stage, PLGA NPs can be incorporated into the solution. In the final step, the solution is irradiated with UV, resulting in formation of solid-like chemical hydrogels, namely HG-DA, HG-DA-SH, and HG-DA-NH_2 (Figure 4).

Figure 4. Schematic representation of hydrogel preparation loaded with capsaicin-PLGA NPs.

Raman spectroscopy (Figure 5A) allowed confirmation of successful UV-crosslinking. The Raman spectrum of uncured P188-DA was compared with spectra of lyophilized hydrogels. For all three hydrogels, typical bands at 1600-1700 cm^{-1} for C=C stretching disappeared, indicating successful crosslinking.[25] The fingerprint spectra between 800-

1500 cm^{-1} of the Poloxamer chain itself was mostly retained.[34] However, some differences can be observed between hydrogels in the intensities of the characteristic peaks for P188. For instance, the peaks at 848 cm^{-1} and 1477 cm^{-1}, corresponding to rocking and scissoring of CH_2,[34] differed in intensity for all three hydrogels. Additionally, the maximum of these peaks in hydrogel samples were shifted towards lower Raman shift values compared to uncured P188-DA (see: vertical grey lines in Figure 5A). The more retained fingerprint region in HG-DA-SH and HG-DA-NH_2 might suggest lower degree of crosslinking, and thus higher mobility of the polymer architecture and higher exposition of the Poloxamer chain, leading to higher intensities.

The swellability studies were based on a protocol developed by Choi et al.[25] The adapted protocol implemented immersing dried hydrogels in a PBS buffer and periodically replacing the PBS buffer, followed by drying the hydrogel surface and weighing the hydrogel. The swelling ratio was calculated as the ratio between the weight of a swollen hydrogel at a given time point and the weight of the dried hydrogel at t = 0. The prepared hydrogels (Figure 4B) showed swelling of up to 15%. The fastest plateau was observed for HG-DA, reaching a stable swelling of around 6% after 2 days. The hydrogels based on Michael addition products, namely HG-DA-NH_2 and HG-DA-SH, reached a plateau much later, between 10-14 days, with a maximum swelling of around 11 and 16%, correspondingly. Higher swelling values are consistent with lower degree of crosslinking, as shown by Raman spectroscopy. No decrease in weight was noted, suggesting that limited erosion occurred in the 2-week period.

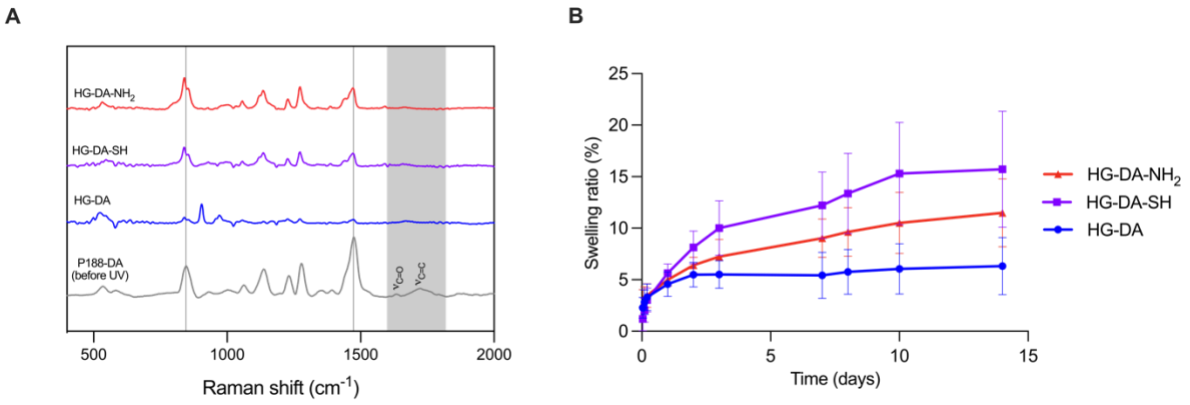

Figure 5. A) Raman spectra of UV-crosslinked hydrogels compared with P188-DA before UV exposure (grey lines mark maximum Raman intensity of the main peaks at 848 and 1477 cm^{-1} of uncured P188-DA ; B) *In vitro* swelling ratio of prepared hydrogels.

Conducting the rheological studies allowed to investigate the relationship between structure and mechanical properties of hydrogels. The strain sweeps (Figure 6A) are based on measuring storage (G') and loss moduli (G'') against increasing strain.[11] In all three hydrogels, a linear plateau of G' and no cross-over points between G' and G'' were observed, confirming their solid-like structure.[11,14,35] HG-DA-SH exhibited shorter plateau, i.e. 0.3% applied strain, compared with HG-DA and HG-DA-NH_2 which maintained the plateau up to 1% applied strain. Beyond the linear plateau, changes in the hydrogel structure tend to occur, namely development of microcracks and beginning of brittle fracture.[36] This early loss of linearity in HG-DA-SH pointed to lower stiffness.[35] While HG-DA and HG-DA-NH_2 remained solid without major structural changes. The phase angle values reflected the same behavior. The maximum values of tanδ for HG-DA ($tan\delta_{max}$ = 0.38) and HG-DA-NH_2 ($tan\delta_{max}$ = 0.37) were comparable and lower than for HG-DA-SH ($tan\delta_{max}$ = 0.53). The lower values for these hydrogels were caused by a higher number of intermolecular crosslinks in the polymeric network.[24]

Creep recovery tests (Figure 6B) were used to investigate the susceptibility of the material towards deformation.[11] Each test consisted of 300 s of applying constant load, followed by 100 s recovery. Similar trends were observed in stiffness of the hydrogels as in strain sweeps. HG-DA-SH showed the highest deformation in the loading step. This indicates the lowest stiffness out of all three hydrogels.[11] HG-DA and HG-DA-NH_2 exhibited significantly reduced deformation compared with HG-DA-SH, meaning these were more

resistant to applied stress. HG-DA-NH_2 compared with HG-DA showed lower stress strain, indicating higher resistance to deformation and stiffness.[36]

The flow curves (Figure 6C) further confirmed the viscoelastic character of the hydrogels based on decrease in viscosity with increasing shear rate.[11] The HG-DA-SH showed much lower initial viscosity compared to HG-DA and HG-DA-NH_2 further confirming softer gel formation and lower crosslinking degree.[36]

The rheological analysis provides useful information about potential mechanical performance when being applied on the skin surface. From the application standpoint, the strain sweeps of all three hydrogels with apparent plateau region of G' indicate that the patches will remain intact under low stress. The HG-DA-SH might be more flexible and pliable; however it might not be able to withstand high stress. In general, HG-DA and HG-DA-NH_2 showed very similar rheological and swelling properties. The chemical characterization revelead poor conversion into aza-Michael addition product. Consequently, a high excess of free diacrylates groups (5 molar. equiv of P188-DA used in respect to P188-NH_2) were available for UV-crosslinking, leading to a formation of a hydrogel very similar to HG-DA in terms of rheology and swelling. Based on FTIR and NMR, some thiol-Michael addition product was formed, leading to longer polymeric monomers subjected to UV-crosslinking in P188-DA-SH hydrogel, thus causing weaker hydrogels formation. Additionally, potential S-S bond formation under irradiation might have intensified softer gel formation in P188-DA-SH hydrogel.

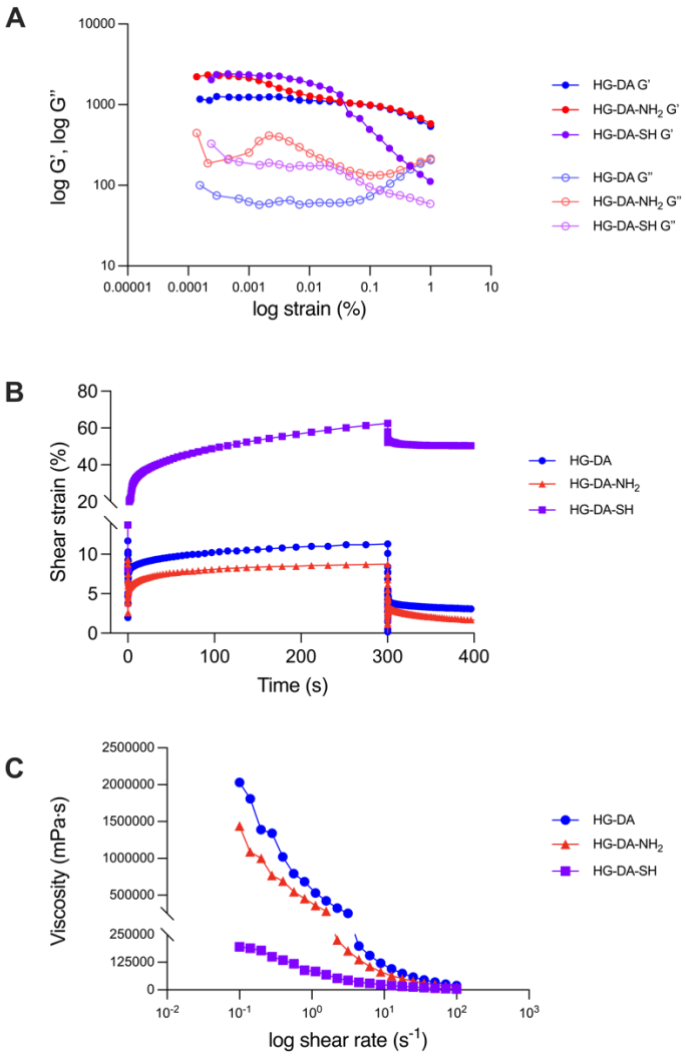

Figure 6. Rheological evaluation of hydrogels: A) strain sweep; B) creep test; and C) flow test.

3.3. Characterization and *in vitro* release of capsaicin from capsaicin PLGA NPs

Nanoparticles (NPs) (with and without capsaicin) were prepared using the oil/water solvent evaporation method from an adapted protocol by Cosco et al.[17] and Pradhan et al.[18] The particle size for NP without capsaicin (empty PLGA-NPs) was 179 nm and the NPs encapsulating capsaicin led only to a slight increase in size up to 195 nm (Table 1). The PDI was 0.0933 and 0.077 for empty and loaded PLGA NPs, respectively, thus both types of NPs approach monodispersity.

Table 1. Size and PDI of prepared PLGA NPs.

NP Type	Size (nm)	PDI (-)
Empty PLGA-NPs	178.90 ± 1.10	0.0933 ± 0.0047
Capsaicin-PLGA-NPs	194.50 ± 0.65	0.077 ± 0.033

Capsaicin-loaded PLGA NPs were characterized with encapsulation efficiency (EE) of 99.7% and loading capacity (LC) of 22.2%. The high EE is possibly due to the high hydrophobicity of capsaicin making it easy to be encapsulated within the hydrophobic PLGA NP core.[12] The protocol for determining the *in vitro* release of capsaicin was adapted from Peng et al.,[16] which involved directly suspending a portion of capsaicin-PLGA NPs in a 100x excess of PBS buffer with 0.3% of Tween 80 and incubating at 37 °C.

The Higuchi release kinetics were applied using the following equation:

$$F = k\sqrt{t} \qquad (Equation\ 7)$$

where, *F* is the fraction of drug released at time *t*; and *k* is the kinetic rate constant.

The samples of PBS/Tween 80 were periodically analyzed by GC-MS, revealing that the release of capsaicin from the NPs showed initial burst release of of ~30% in the first 3 h, which was subsequently followed by ~100% capsaicin release after 35 days (Figure 7). The initial drug release is attributed to the drug adsorbed close to or on the external surface of PLGA nanoparticles, which leads to the burst release phenomenon. In fact, 16% of the drug is observed to be immediately released in the first hour. This uncontrollable release behaviour continues for four more time points (until 3 hours), after which the rate of release is slowed down. The Higuchi model of kinetics was applied using Equation 7 to obtain the regression value (R^2) of 0.98 and rate constant (*k*) of 2.18. Higuchi model of release kinetics can be interpreted as capsaicin showing a diffusion release type. This is in line with literature where diffusion release behaviour of encapsulated capsaicin has been observed before.

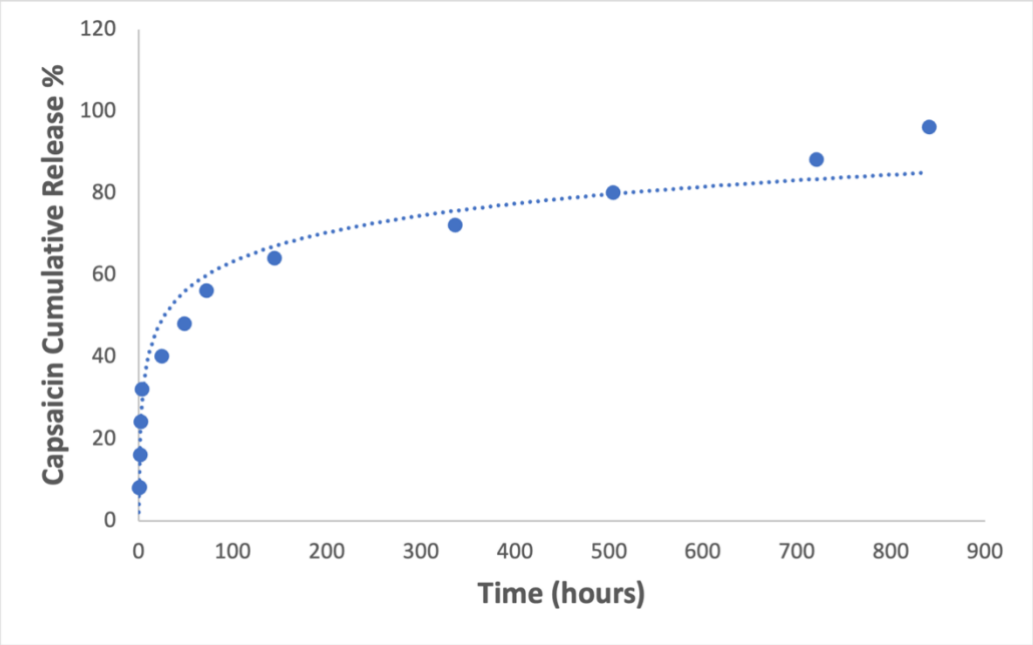

Figure 7. *In vitro* release of capsaicin from capsaicin-PLGA NPs analysed with GC-MS. A burst release of capsaicin was observed in the first 3 hours, leading to a sustained 100% release until 35 days. Data is presented as mean ± SD (n=3).

3.4. *In vitro* release of capsaicin-PLGA NPs from hydrogels

The release profile of capsaicin-PLGA NPs from HG-DA, HG-DA-SH, and HG-DA-NH_2 hydrogels is shown in Figure 8. All three hydrogels show a linear zero-order monophasic release profile. The NH2 hydrogels depicted the quickest release with 97% release in 1 hour. Longer than NH_2, was the release profile of DA with 95% release in 2 hours. The P188-SH hydrogels have the longest release time with 94% release in 3 hours.

The linear release profiles of the gels display a constant release of capsaicin-PLGA over an extended period of time. Considering that our system is designed to be used a transdermal hydrogel patch, the linear release profiles of hydrogels are beneficial for a steady delivery of therapeutic nanoparticles. The absence of burst release avoids the sudden increase in drug concentration in the skin, and the 2-3 hour long release is in line with bypassing the need for frequent administrations.

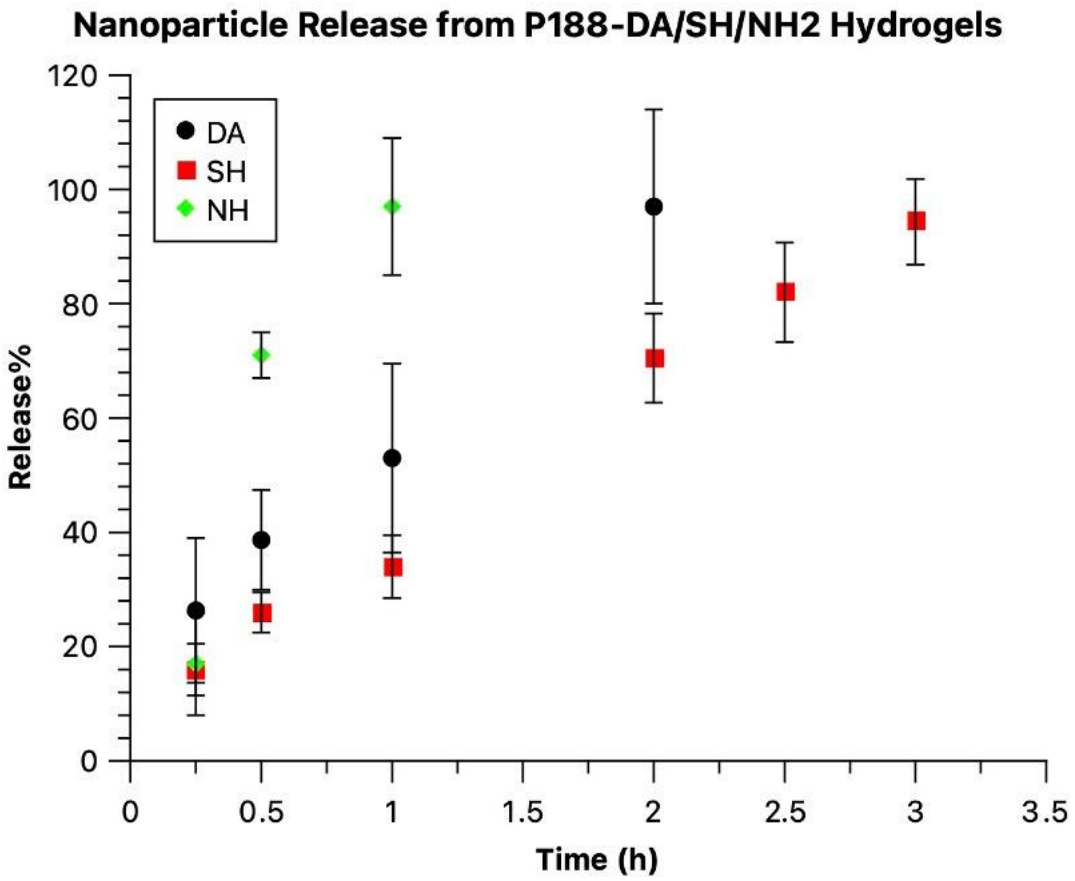

Figure 8. In vitro release of capsaicin-PLGA NPs from HG-DA, HG-DA-SH, and HG-DA-NH_2 hydrogels.

3.5. *In vitro* permeation analysis

The permeability of capsaicin-PLGA nanoparticles through Strat-M Membrane was studied with Franz diffusion cell technique. The cumulative nanoparticle concentration permeated is represented in Figure 5. The steady state flux (J) and permeability coefficient (K) of nanoparticle permeation from P188 DA/SH/NH_2 is shown in Table 2. The permeation graph of nanoparticles from P188-DA hydrogels displays an occlusive effect with a lag time of 0.33 hours, while 50% of nanoparticles were permeated in less than 1 hour, the rest of the graph showed a linear permeation past the point of occlusion with 100% permeation in less than 3 hours (Figure 9a). HG-DA-NH_2 also reported 100%

permeation in less than 3 hours (lag time 0.29 hours). However, the diffusion in P188-SH was accompanied by the longest lag time of 0.73 hours.

Despite the difference in the rate of diffusion, HG-DA and HG-NH_2 hydrogels reported intra-particle diffusion model.[37] The plot for this model is charactersied by different stages of diffusion with multiple points of equilibrium which can be seen in Figure 9a and 9c. Intra-particle diffusion model assumes Fick's second law, that film diffusion is negligible and particle diffusion is the only rate-controlling step. The first linear stage of HG-DA reaches upto 0.75 hours and 1.5 hours for HG-DA-NH_2 after which an equilibrium point is reached. The second stage stretches from 0.75 to 2 hours for HG-DA and 1.5 to 2.25 hours for HG-DA-NH_2, after which the final stage begins until 100% permeation.

Moreover, HG-DA-SH can be seen following the pseudo-first order diffusion model, which is characterised by "appearing" to be first order due to a large difference in reactant concentration.[38] The permeation started slower for HG-DA-SH, than DA and NH_2, at 0.75 hours, but a steady state is maintained completion. The halfway point of permeation (50%) is observed right after the 4-hour mark and complete permeation of capsaicin-PLGA nanoparticles was noted after 5.5 hours. HG-DA, HG-DA-SH, and HG-DA-NH_2 hydrogels reported a steady state flux (J) of 0.42, 0.27 and 0.41 respectively.

Table 2: Franz cell permeation analysis of capsaicin-PLGA nanoparticles from HG-DA, HG-DA-SH, and HG-DA-NH_2 hydrogels.

Sample	**J (mg/cm^{2}h)**	**Lag Time (h)**	**K (cm/h) x 10^{-2}**
HG-DA-SH	0.27	0.73	26.54
HG-DA	0.42	0.33	42.12
HG-DA-NH_2	0.41	0.29	40.87

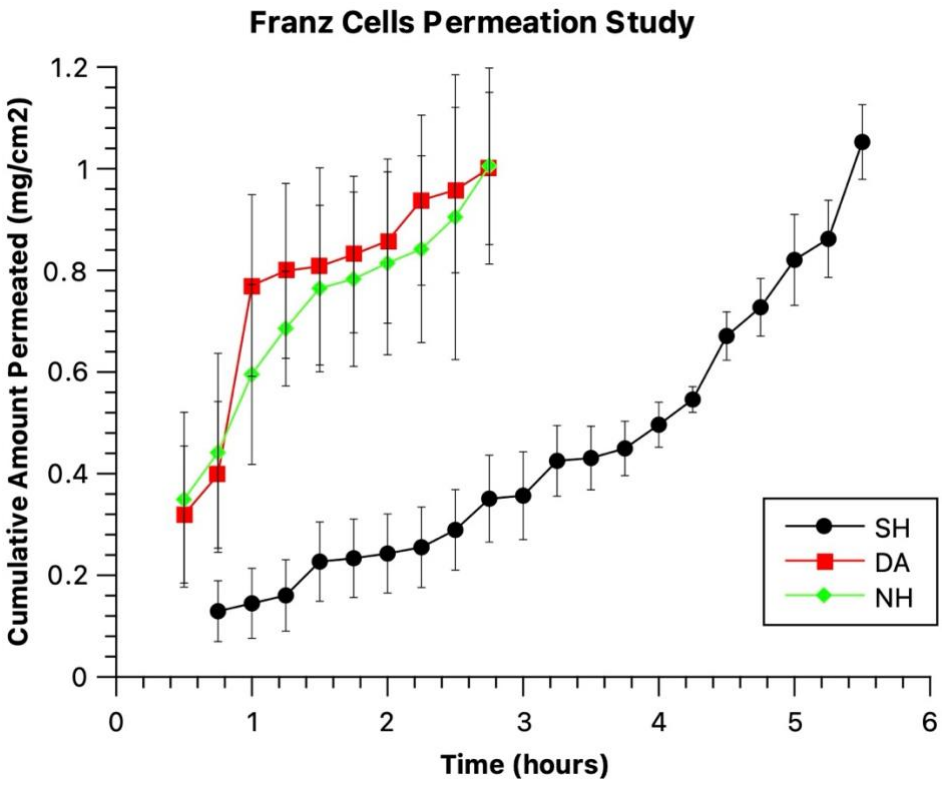

Figure 9. Cumulative amount of capsaicin-PLGA nanoparticles permeated through Strat-M membranes in Franz cells from HG-DA, HG-DA-SH, and HG-DA-NH_2 hydrogels.

4. Discussion

Commercial formulations for pain relief usually directly introduce capsaicin into the main excipient.[39] For instance, the commercial Qutenza patch, introduces capsaicin into the silicone adhesive layer.[40] Similarly, gels and creams contain directly incorporated capsaicin.[41,42] Consequently, capsaicin is rapidly released to the skin surface. With high doses of capsaicin, local anesthetic must be applied before application due to painful itching and burning sensation of the skin.[2,7] These side effects can be potentially overcome by employing polymeric NPs to encapsulate the analgesic.[13,43]

It has been shown that PLGA NPs can be used as a slow-release system for capsaicin[13] and other pain relief drugs, like opioids[44] and bupivacaine.[45] However, it is difficult to precisely apply and control the residence time of NPs suspension. When applied

transdermally, the mixture would tend to spread uncontrollably and leave the administration site.[12] Thus, nanoparticles should be embedded into a stable matrix.

A good candidate for controlled delivery of nanoparticles is a biocompatible hydrogel. Poloxamers, as an FDA-approved material,[46] are widely used in pharmaceutical formulations. These polymers can readily form a reversible physical hydrogel at physiological temperatures.[9] However, physical hydrogels suffer from low strength and are not suitable for long time wear on the skin. On the other hand, chemical hydrogels are permanently crosslinked to form a stable hydrogel with enhanced mechanical properties and stability. For obtaining chemical hydrogels from Poloxamers, derivatization can be employed by introducing acrylate[10] or maleimide moieties.[11]

In this work, we synthesized a library of P188 derivatives, which generated chemical hydrogels upon UV exposure. The hydrogels possessed varying rheological and swelling properties depending on the type of the polymeric network. In combination with capsaicin-PLGA NPs, a proof-of-concept composite system was prepared for prolonged *in vitro* release of the analgesic.

The prepared hydrogels can be classified as UV-crosslinked hydrogels, differing by type of starting 'monomers' subjected to UV irradiation (Figure 10). The HG-DA consisted only of one type of linear unit being crosslinked, namely P188-DA. In HG-DA-NH_2 and HG-DA-SH, different polymer chains were present. One component was unreacted linear chains of P188-NH_2 and P188-SH. Both types of Michael additions generated longer acrylate-terminated polymer chains. This presence of varying polymer starting polymers for UV-crosslinking lengths led to diverse final hydrogel architectures, influencing the physicochemical properties of the bulk material.

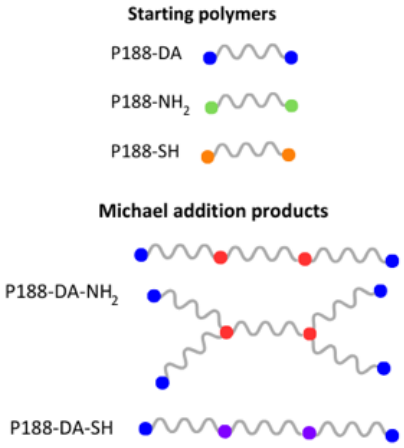

Figure 10. Cartoons of structures of starting polymers and Michael addition products. P188-DA, P188-DA-NH_2, and P188-DA-SH were subjected to UV-crosslinking giving hydrogels.

Limited swelling is a desired property for topical application since it guarantees long-term dimensional stability and good wet-adhesion performance.[47] Small differences in the swelling behavior between hydrogels could be observed. The highest swelling of HG-DA-SH could be explained by a higher number of longer polymeric units generated via the thiol-Michael addition, which are subjected to crosslinking. Similar relation has been shown for thiol-PEG hydrogels,[28] where increasing molecular weight of PEG between crosslinks increased equilibrium swelling. Despite small variations, the swellability of all three hydrogels was very low and these can be considered non-swelling hydrogels.[47]

The high viscosity of HG-DA and HG-DA-NH_2 at low shear rates demonstrates high deformation resistance, confirming possible long-time wear at low loading situation on skin surface. However, the HG-DA-SH suffered from reduced mechanical properties, which is in agreement with the highest swellability. Considering, almost 4-5 times higher shear strain in the creep compliance test, it suggests a lower degree of crosslinking and increased mesh size, compared with HG-DA and HG-DA-NH_2. This potential long-time wear is compatible with the gradual release of capsaicin from PLGA NPs of over 35 days.

Capsaicin is a potent molecule, where very small concentrations have shown significant pharmacological effect.[6] A single dose of 10 µg capsaicin (intraprantal injection, total

injection volume 25 µL, dissolved in 10% DMSO) was shown to provide 2 days analgesia in healthy mice and up to 30 days in mice with an inflammatory condition, i.e., thermal hyperalgesia.[48] In the literature, the amount of capsaicin loaded into NPs greatly varies, from 4 mg[49] up to 60 mg[13] per 100 mg polymer. These varying loading amounts, together with different preparation methods, result in different EE and cumulative *in vitro* release. Malewicz et al.[13] prepared capsaicin-PLGA NPs using 60 mg of capsaicin per 100 mg polymer, with EE = 16% and 34% release in the course of 8 h. While Peng et al.[16] reported mPEG-PCL NPs with 20 mg of capsaicin per 100 mg polymer, resulting in EE = 82% and 80% release over 60 h. We have prepared PLGA NPs with a moderate amount of capsaicin, yet with a higher EE of 99.7% and slower release of around 75% release achieved in 2 weeks. Additionally, incorporating the NPs into hydrogels with free Poloxamer chains provides some potential flanking and anti-aggregating effects of the NPs in the formulation.[50]

5. Conclusions

In this study, we have prepared and characterized proof-of-concept hydrogel patches for transdermal delivery of capsaicin. Capsaicin is an effective analgesic, yet current commercial formulations suffer from unpleasant side effects that may reduce patient compliance. Thanks to employing nanoencapsulation of capsaicin, the adverse reactions can be minimized.

To ensure successful transdermal delivery, the drug-loaded NPs need to be embedded in a skin-adhesive layer. We achieved this by preparing UV-crosslinkable hydrogels from a biocompatible Poloxamer P188. These hydrogels after curing provide a stable platform for retention and release of capsaicin-PLGA NPs. The low swelling properties of the hydrogel together with a 5-week long *in vitro* release of capsaicin from PLGA NPs offers a new potential treatment for neuropathic pain with single application and long-term pain relief effect.

References

(1) Colloca, L.; Ludman, T.; Bouhassira, D.; Baron, R.; Dickenson, A. H.; Yarnitsky, D.; Freeman, R.; Truini, A.; Attal, N.; Finnerup, N. B.; et al. Neuropathic pain. *Nat Rev Dis Primers* **2017**, *3*, 17002-17047. DOI: 10.1038/nrdp.2017.2.

(2) Abrams, R. M. C.; Pedowitz, E. J.; Simpson, D. M. A critical review of the capsaicin 8% patch for the treatment of neuropathic pain associated with diabetic peripheral neuropathy of the feet in adults. *Expert Rev Neurother* **2021**, *21*, 259-266. DOI: 10.1080/14737175.2021.1874920.

(3) Shinu, P.; Morsy, M. A.; Nair, A. B.; Mouslem, A. K. A.; Venugopala, K. N.; Goyal, M.; Bansal, M.; Jacob, S.; Deb, P. K. Novel Therapies for the Treatment of Neuropathic Pain: Potential and Pitfalls. *J Clin Med* **2022**, *11*, 3002-3028. DOI: 10.3390/jcm11113002.

(4) Knezevic, N. N.; Tverdohleb, T.; Nikibin, F.; Knezevic, I.; Candido, K. D. Management of chronic neuropathic pain with single and compounded topical analgesics. *Pain Manag* **2017**, *7*, 537-558. DOI: 10.2217/pmt-2017-0020.

(5) Yang, F.; Zheng, J. Understand spiciness: mechanism of TRPV1 channel activation by capsaicin. *Protein Cell* **2017**, *8*, 169-177. DOI: 10.1007/s13238-016-0353-7.

(6) Arora, V.; Campbell, J. N.; Chung, M. K. Fight fire with fire: Neurobiology of capsaicin-induced analgesia for chronic pain. *Pharmacol Ther* **2021**, *220*, 107743-107754. DOI: 10.1016/j.pharmthera.2020.107743.

(7) Bonezzi, C.; Costantini, A.; Cruccu, G.; Fornasari, D. M. M.; Guardamagna, V.; Palmieri, V.; Polati, E.; Zini, P.; Dickenson, A. H. Capsaicin 8% dermal patch in clinical practice: an expert opinion. *Expert Opin Pharmacother* **2020**, *21*, 1377-1387. DOI: 10.1080/14656566.2020.1759550.

(8) Ahsan, A.; Tian, W.-X.; Farooq, M. A.; Khan, D. H. An overview of hydrogels and their role in transdermal drug delivery. *Int J Polym Mater* **2020**, *70*, 574-584. DOI: 10.1080/00914037.2020.1740989.

(9) Bodratti, A. M.; Alexandridis, P. Formulation of Poloxamers for Drug Delivery. *J. Funct. Biomater.* **2018**, *9*, 11-35. DOI: 10.3390/jfb9010011.

(10) Law, T. K.; Whateley, T. L.; Florence, A. T. Some chemically modified poloxamer hydrogels: preparation, morphology and swelling properties. *International Journal of Pharmaceutics* **1984**, *21*, 277-287. DOI: 10.1016/0378-5173(84)90186-8.

(11) Stojkov, G.; Niyazov, Z.; Picchioni, F.; Bose, R. K. Relationship between Structure and Rheology of Hydrogels for Various Applications. *Gels* **2021**, *7*, 255-275. DOI: 10.3390/gels7040255.
(12) Bernal-Chavez, S. A.; Alcala-Alcala, S.; Cerecedo, D.; Ganem-Rondero, A. Platelet lysate-loaded PLGA nanoparticles in a thermo-responsive hydrogel intended for the treatment of wounds. *Eur J Pharm Sci* **2020**, *146*, 105231-105246. DOI: 10.1016/j.ejps.2020.105231.
(13) Malewicz, N. M.; Rattray, Z.; Oeck, S.; Jung, S.; Escamilla-Rivera, V.; Chen, Z.; Tang, X.; Zhou, J.; LaMotte, R. H. Topical Capsaicin in Poly(lactic-co-glycolic)acid (PLGA) Nanoparticles Decreases Acute Itch and Heat Pain. *Int J Mol Sci* **2022**, *23*, 5275-5294. DOI: 10.3390/ijms23095275.
(14) Rossi, F.; Ferrari, R.; Papa, S.; Moscatelli, D.; Casalini, T.; Forloni, G.; Perale, G.; Veglianese, P. Tunable hydrogel-nanoparticles release system for sustained combination therapies in the spinal cord. *Colloids Surf B Biointerfaces* **2013**, *108*, 169-177. DOI: 10.1016/j.colsurfb.2013.02.046.
(15) Mudhol, S.; Serva Peddha, M. Development of capsaicin loaded nanoparticles based microneedle patch for transdermal drug delivery. *J Drug Deliv Sci Technol* **2023**, *80*, 104120-104132. DOI: 10.1016/j.jddst.2022.104120.
(16) Peng, W.; Jiang, X. Y.; Zhu, Y.; Omari-Siaw, E.; Deng, W. W.; Yu, J. N.; Xu, X. M.; Zhang, W. M. Oral delivery of capsaicin using MPEG-PCL nanoparticles. *Acta Pharmacol Sin* **2015**, *36*, 139-148. DOI: 10.1038/aps.2014.113.
(17) Cosco, D.; Mare, R.; Paolino, D.; Salvatici, M. C.; Cilurzo, F.; Fresta, M. Sclareol-loaded hyaluronan-coated PLGA nanoparticles: Physico-chemical properties and in vitro anticancer features. *Int J Biol Macromol* **2019**, *132*, 550-557. DOI: 10.1016/j.ijbiomac.2019.03.241.
(18) Pradhan, R.; Ramasamy, T.; Choi, J. Y.; Kim, J. H.; Poudel, B. K.; Tak, J. W.; Nukolova, N.; Choi, H. G.; Yong, C. S.; Kim, J. O. Hyaluronic acid-decorated poly(lactic-co-glycolic acid) nanoparticles for combined delivery of docetaxel and tanespimycin. *Carbohydr Polym* **2015**, *123*, 313-323. DOI: 10.1016/j.carbpol.2015.01.064.
(19) Peng, W.; Jiang, X. Y.; Zhu, Y.; Omari-Siaw, E.; Deng, W. W.; Yu, J. N.; Xu, X. M.; Zhang, W. M. Oral delivery of capsaicin using MPEG-PCL nanoparticles. *Acta Pharmacol Sin* **2015**, *36* (1), 139-148. DOI: 10.1038/aps.2014.113.

(20) Wang, X. R.; Gao, S. Q.; Niu, X. Q.; Li, L. J.; Ying, X. Y.; Hu, Z. J.; Gao, J. Q. Capsaicin-loaded nanolipoidal carriers for topical application: design, characterization, and in vitro/in vivo evaluation. *Int J Nanomedicine* **2017**, *12*, 3881-3898. DOI: 10.2147/IJN.S131901.
(21) Anantaworasakul, P.; Chaiyana, W.; Michniak-Kohn, B. B.; Rungseevijitprapa, W.; Ampasavate, C. Enhanced Transdermal Delivery of Concentrated Capsaicin from Chili Extract-Loaded Lipid Nanoparticles with Reduced Skin Irritation. *Pharmaceutics* **2020**, *12* (5), 463-482. DOI: 10.3390/pharmaceutics12050463.
(22) Faglie, A.; Emerine, R.; Chou, S. F. Effects of Poloxamers as Excipients on the Physicomechanical Properties, Cellular Biocompatibility, and In Vitro Drug Release of Electrospun Polycaprolactone (PCL) Fibers. *Polymers (Basel)* **2023**, *15*, 2997-3016. DOI: 10.3390/polym15142997.
(23) Ponnusamy, C.; Sugumaran, A.; Krishnaswami, V.; Palanichamy, R.; Velayutham, R.; Natesan, S. Development and Evaluation of Polyvinylpyrrolidone K90 and Poloxamer 407 Self-Assembled Nanomicelles: Enhanced Topical Ocular Delivery of Artemisinin. *Polymers (Basel)* **2021**, *13*, 3038-3055. DOI: 10.3390/polym13183038.
(24) Guaresti, O.; Basasoro, S.; González, K.; Eceiza, A.; Gabilondo, N. In situ cross–linked chitosan hydrogels via Michael addition reaction based on water–soluble thiol–maleimide precursors. *Eur Polym J* **2019**, *119*, 376-384. DOI: 10.1016/j.eurpolymj.2019.08.009.
(25) Choi, D.; Lee, W.; Park, J.; Koh, W. Preparation of poly(ethylene glycol) hydrogels with different network structures for the application of enzyme immobilization. *Biomed Mater Eng* **2008**, *18*, 345-356. DOI: 10.3233/BME-2008-0551.
(26) Das, P.; Devi, N.; Puzari, A. One-pot solvent-free microwave-assisted aza-Michael addition reaction of acrylonitrile. *J Indian Chem Soc* **2022**, *99*, 100411-100421. DOI: 10.1016/j.jics.2022.100411.
(27) Jancirani, A.; Kohila, V.; Meenarathi, B.; Anbarasan, R. Effect of substituents on the adsorption behaviour of aza-Michael addition polymers: a comparative study. *Polym Bull* **2021**, *79*, 6193-6209. DOI: 10.1007/s00289-021-03801-y.
(28) Parlato, M.; Reichert, S.; Barney, N.; L., M. W. Poly(ethylene glycol) hydrogels with adaptable mechanical and degradation properties for use in biomedical applications. *Macromol Biosci* **2014**, *14*, 687-698. DOI: 10.1002/mabi.201300418.

(29) Stenstrom, P.; Fan, Y.; Zhang, Y.; Hutchinson, D.; Garcia-Gallego, S.; Malkoch, M. UV-Cured Antibacterial Hydrogels Based on PEG and Monodisperse Heterofunctional Bis-MPA Dendrimers. *Molecules* **2021**, *26*, 2364-2379. DOI: 10.3390/molecules26082364.
(30) Mahou, R.; Wandrey, C. Versatile Route to Synthesize Heterobifunctional Poly(ethylene glycol) of Variable Functionality for Subsequent Pegylation. *Polymers (Basel)* **2012**, *4*, 561-589. DOI: 10.3390/polym4010561.
(31) Konuray, A. O.; Fernández-Francos, X.; Serra, À.; Ramis, X. Sequential curing of amine-acrylate-methacrylate mixtures based on selective aza-Michael addition followed by radical photopolymerization. *Eur Polym J* **2016**, *84*, 256-267. DOI: 10.1016/j.eurpolymj.2016.09.025.
(32) Kharkar, P. M.; Rehmann, M. S.; Skeens, K. M.; Maverakis, E.; Kloxin, A. M. Thiol-ene click hydrogels for therapeutic delivery. *ACS Biomater Sci Eng* **2016**, *2*, 165-179. DOI: 10.1021/acsbiomaterials.5b00420.
(33) Grubel, J.; Albernaz, V. L.; Tsianaka, A.; Jauch, C. O.; Quirin, S.; Kerger, C.; Kohl, C. G.; Burger-Kentischer, A.; Tovar, G. E. M.; Southan, A. Preparation of multifunctional hydrogels with accessible isothiouronium groups via radical cross-linking copolymerization. *Sci Rep* **2023**, *13*, 10361-10375. DOI: 10.1038/s41598-023-36956-x.
(34) La Verde, G.; Sasso, A.; Rusciano, G.; Capaccio, A.; Fusco, S.; Mayol, L.; Biondi, M.; Silvestri, T.; Netti, P. A.; La Commara, M.; et al. Characterization of Hyaluronic Acid-Coated PLGA Nanoparticles by Surface-Enhanced Raman Spectroscopy. *Int J Mol Sci* **2022**, *24*, 601-615. DOI: 10.3390/ijms24010601.
(35) Tee, H. T.; Zipp, R.; Koynov, K.; Tremel, W.; Wurm, F. R. Poly(methyl ethylene phosphate) hydrogels: Degradable and cell-repellent alternatives to PEG-hydrogels. *Eur Polym J* **2020**, *141*, 110075-110084. DOI: 10.1016/j.eurpolymj.2020.110075.
(36) Grillet, A. M.; Wyatt, N. B.; Gloe, L. M. Polymer Gel Rheology and Adhesion. In *Rheology*; De Vicente, J., Ed.; InTech Rijeka, 2012; pp 60-80. DOI: 10.5772/36975.
(37) Kumar, A. K.; Mohan, S. V.; Sarma, P. N. Sorptive removal of endocrine-disruptive compound (estriol, E3) from aqueous phase by batch and column studies: kinetic and mechanistic evaluation. *J Hazard Mater* **2009**, *164* (2-3), 820-828. DOI: 10.1016/j.jhazmat.2008.08.075.

(38) Revellame, E. D.; Fortela, D. L.; Sharp, W.; Hernandez, R.; Zappi, M. E. Adsorption kinetic modeling using pseudo-first order and pseudo-second order rate laws: A review. *Clean Eng Technol* **2020**, *1*. DOI: 10.1016/j.clet.2020.100032.
(39) Thouaye, M.; Yalcin, I. Neuropathic pain: From actual pharmacological treatments to new therapeutic horizons. *Pharmacol. Ther.* **2023**, *251*, 108546-108564. DOI: 10.1016/j.pharmthera.2023.108546.
(40) *Qutenza (capsaicin) 8% topical system. Prescribing Information.* Averitas Pharma, Inc., https://www.qutenza.com/pdfs/qutenza_prescribing_information.pdf (accessed 12-08-2024).
(41) Maloney, J.; Pew, S.; Wie, C.; Gupta, R.; Freeman, J.; Strand, N. Comprehensive Review of Topical Analgesics for Chronic Pain. *Curr Pain Headache Rep.* **2021**, *25*, 7-15. DOI: 10.1007/s11916-020-00923-2.
(42) *Zacin 0.025% w/w Cream. Package Leaflet.* Pharmaserve, https://www.hpra.ie/img/uploaded/swedocuments/892d026b-6a27-4462-8924-f04681789ddc.pdf (accessed 12-08-2024).
(43) Martínez-Benavidez, E.; Higuera-Ciapara, I.; Herrera-Rodríguez, S. E.; Lugo-Melchor, O. Y.; Goycoolea, F. M.; Jazo, F. J. G. Capsaicin Nanoparticles as Therapeutic Agents against Gliomas. *Nano Biomed Eng* **2021**, *13*, 433-445. DOI: 10.5101/nbe.v13i4.p433-445.
(44) Kovaliov, M.; Li, S.; Korkmaz, E.; Cohen-Karni, D.; Tomycz, N.; Ozdoganlar, O. B.; Averick, S. Extended-release of opioids using fentanyl-based polymeric nanoparticles for enhanced pain management. *RSC Advances* **2017**, *7*, 47904-47912, 10.1039/C7RA08450A. DOI: 10.1039/C7RA08450A.
(45) Wang, T.; Hurwitz, O.; Shimada, S. G.; Tian, D.; Dai, F.; Zhou, J.; Ma, C.; LaMotte, R. H. Anti-nociceptive effects of bupivacaine-encapsulated PLGA nanoparticles applied to the compressed dorsal root ganglion in mice. *Neurosci Lett* **2018**, *668*, 154-158. DOI: 10.1016/j.neulet.2018.01.031.
(46) *Inactive Ingredient Search for Approved Drug Products. U.S. Food & Drug Administration (FDA).* https://www.accessdata.fda.gov/ (accessed 2024-07-24).
(47) Feng, W.; Wang, Z. Tailoring the Swelling-Shrinkable Behavior of Hydrogels for Biomedical Applications. *Adv Sci* **2023**, *10*, 2303326-2303367. DOI: 10.1002/advs.202303326.

(48) Menéndez, L.; Lastra, A.; Hidalgo, A. n.; Baamonde, A. The analgesic effect induced by capsaicin is enhanced in inflammatory states. *Life Sci* **2004**, *74*, 3235-3244. DOI: 10.1016/j.lfs.2003.11.019.
(49) Azin Rashidy, A.; Atefeh, S.; Saeed, S.-S.; Somaye, A.; Hadi, G.; Bogumil, E. B. Capsaicin-loaded alginate nanoparticles embedded polycaprolactone-chitosan nanofibers as a controlled drug delivery nanoplatform for anticancer activity. *J Colloid Interface Sci* **2023**, *638*, 616-628. DOI: 10.1016/j.jcis.2023.01.139.
(50) Miyazawa, T.; Itaya, M.; Burdeos, G. C.; Nakagawa, K.; Miyazawa, T. A Critical Review of the Use of Surfactant-Coated Nanoparticles in Nanomedicine and Food Nanotechnology. *Int J Nanomedicine* **2021**, *16*, 3937-3999. DOI: 10.2147/IJN.S298606.

Chapter 6

Conclusion and Perspectives

Conclusion

Spinal cord injury (SCI) represents a devastating neurological event that extends far beyond the immediate physical trauma. It encompasses a complex interplay of secondary conditions, chief among which are chronic pain and inflammation, debilitating consequences that profoundly diminish the quality of life for individuals with SCI, leading to long-term disability and diminished overall well-being. SCI can have catastrophic outcomes on physical movement, bladder function, and various other voluntary and involuntary functions [1–3], highlighting the pressing need for innovative therapeutic strategies. This thesis has explored such avenues through the targeted application of polymeric drug delivery systems (DDSs) encapsulating potent hydrophobic drugs and nucleic acids. This concluding chapter will synthesize the key findings, delve into their implications, and outline future directions for research in this crucial field.

In **Chapter 1**, we introduced chronic pain that arises from SCI. This typically manifests in two primary forms: neuropathic and nociceptive pain, each characterized by distinct underlying mechanisms and clinical presentations[4]. Neuropathic pain arises from damage or dysfunction within the nervous system, affecting both peripheral and central pathways. According to Masri *et al.* [5], this type of pain typically emerges months or even years after the initial SCI, and is often localized below the level of injury, though above-level pain is not uncommon. This increased discomfort caused by chronic pain can prevail for approximately 20% of a person's lifespan. The presence of allodynia and hyperalgesia further complicates the experience of neuropathic pain, intensifying discomfort and limiting functional abilities. Nociceptive pain, conversely, stems from the activation of nociceptors due to tissue damage or inflammation. In the context of SCI, nociceptive pain may result from musculoskeletal issues, visceral complications, or other secondary conditions that cause tissue injury. As highlighted by Yezierski *et al.* [6], both neuropathic and nociceptive pain can coexist in individuals with SCI, creating a complex pain syndrome that necessitates comprehensive management strategies. This leads to lower reported quality of life metrics and creates a significant healthcare burden, especially when the pain becomes treatment-resistant. The development and maintenance of chronic pain following SCI have been attributed to the hyperexcitability

of dorsal root ganglion (DRG) neurons. DRG neurons play a crucial role in transmitting sensory information from the periphery to the central nervous system, and their sensitization can lead to amplified pain signals and chronic pain states. Berta *et al.* [7] have demonstrated that this sensitization is influenced by a multitude of factors, including inflammatory cytokines, neuronal plasticity, and alterations in ion channel transmission. Macrophages exhibit remarkable plasticity, adapting their function in response to local environmental cues such as cytokines and tissue signals. Consequently, they can be categorized into inflammatory macrophages (M1-m) and anti-inflammatory macrophages (M2-m). At the site of injury, M1-m trigger an inflammatory response by releasing inflammatory cytokines. M2 macrophages contribute to tissue repair and the resolution of inflammation by releasing anti-inflammatory cytokines and growth factors. Inflammatory cytokines, such as TNF-α, IL-1β, and IL-6, can directly sensitize DRG neurons, enhancing their excitability and responsiveness to various stimuli [8,9]. The manipulation of inflammatory cytokines, neuronal and macrophage plasticity, and ion channel transmissions through targeted drug delivery systems can be an effective method of therapy. Polymeric nanoparticles were introduced as a versatile drug delivery platform which can also be modified with target-specific moeties. We also introduced polymers, like polylactic-co-glycolic acid (PLGA), and poly(2-(dimethylamino)ethyl methacrylate) (pDMAEMA), as an alternative to viruses for genetic delivery. Polymers present lower cytotoxicity than their viral counterparts, and also don't run the risk of genetic side effects.

In **Chapter 2** we focus on one endogenous polysaccharide, hyaluronic acid (HA), which is specific ligand for the CD44 receptor on macrophages. The use of HA, in literature, for targeting pain and inflammation was discussed, with a special attention to nanosystems. It was also discussed if manipulating the molecular weight of HA would have different effects on inflammation. However, considering different studies concluded differently, this theory still needs concrete research[10–12]. The benefits of employing HA, biocompatibility, hydrophilicity, CD44 binding ability, make it a great candidate for an anti-inflammatory study. This conclusion was carried on into **Chapter 3** where inflammatory M1-m were targeted with PLGA nanoparticles that were coated with HA, and the organic compound carvacrol was encapsulated inside to form CHP. The

nanoparticles were optimised with small size, to effectively trigger endocytosis. Characterisation techniques like dynamic light scattering (DLS) and scanning electron microscopy (SEM) were used to analyse the size and morphology of the nanoparticles. Additionally, the drug release studies of CHP showed an initial burst phase due to drug adsorption close to the nanoparticle surface and subsequent slow zero-order release which is linked to polymer erosion. Carvacrol has untapped potential in inflammatory studies and its effect was seen when the expression of M1-m was sigificantly decreased (~80%) in LPS-treated macrophages, whereas the expression of M2-m was increased (~300%). As expected, the inclusion of HA also increased the uptake of nanoparticles into macrophages as compared to nanoparticles that were not coated with HA. In fact, further studies also showed that the effect of CHP was also significant in the production of cytokines. Inflammatory cytokines like interleukin-1α/β and TNF-α saw a significant decrease in expression when macrophages were treated with CHP, whereas anti-inflammatory cytokines like interleukin-1ra/4/10 saw a boost in their expressions with CHP. These findings also revealed that carvacrol alone could not achieve these results. In fact, PLGA-HA nanoparticles without carvacrol also did not show any significant results. It should be highlighted that the effects of carvacrol are only enhanced when it is encapsulated in nanoparticles which have the enhanced ability to be uptaken by macrophages. There is a lot of potential in PLGA nanoparticles and their ability to be excellent drug carriers.

Genetic technology, especially nucleic acids (NA), has also seen a boost in their usage in recent years [13–15]. Targeting microRNAs (miRs) with antagomirs (Amirs) has proven to be an effective method of gene therapy. However, NAs have a high degradability and need to be partnered with carriers like, cationic polymers, for successful administrations[16–18]. In **Chapter 4** we designed and synthesised polymer-Amir conjugations, also known as polyplexes. Polyplexes are designed with cationic polymers which aim to condense the anionic NA in their core to form nanosized systems. This condensation avoids rapid degradation and clearance of the NA and enhances cellular uptake. We aimed to target miR-21, which is heavily expressed in peripheral inflammatory conditions, and miR-155, which enhances neuronal degradation in spinal cord injuries (SCI). The polyplexes were synthesised with different NP ratios, which refer to the number of nitrogen (N) in the

pDMAEMA polymer backbone and phosphorous (P) in the NA. Polyplexes with Amir-21 (PA21) were synthesised in NP ratios of 10 and 50 (NP10PA21 and NP50PA21, respectively) and the *in vitro* studies were conducted on bone marrow derived macrophages (BMDMs). The results showed that the NP10PA21 were successfully able to polarise the M1-m to M2-m in an LPS-treated culture, however, NP50PA21 were significantly toxic. This cytotoxicity can be attributed to higher amount of cationic polymer in the polyplexes. To enhance the axonal regeneration of neurons, PA155 were also conjugated with gold nanoparticles (Au nps), to form GP155. A cell culture of neurons and glial cells was used to study the uptake of naked Amir-155 and GP155. As expected, the encapsulation of Amir-155 in GP155 enhanced the internalizations. A pilot *in vivo* study with 18 animals in three groups – control, scramble, GP155 – was also conducted on contusion SCI rat models. for ease of administration, GP155 were loaded in a thermosensitive hydrogel of poly(N-isopropylacrylamide) (PNIPAM). The behavioural analyses showed difference in the paw movement of the rats at 3 days post injury (dpi) and 7 dpi, which GP155 showing enhanced movements. However, this study was still in its pilot stages and significant differences between the three groups could not be recorded. But it is important to note that GP155 managed to show improved locomotion after only 3 days.

Moving on, the ability of polymers to effectively carry and deliver organic loads was tested again in **Chapter 5** where we employed PLGA nanoparticles to encapsulate capsaicin (PCap). Capsaicin is a potent compound that desensitises ion channels as a method of effective antinociception[19,20]. This ability, if converted into skin patches, would be a beneficial therapy for a lot of cases. Therefore, to effectively deliver PCap transdermally, we created three diacrylate hydrogel systems – diacrylate (DA), thiolated-diacrylate (DA-SH), and amine-modified diacrylate (DA-NH_2). Successful modifications were verified with Raman, FTIR and NMR spectra. The three hydrogel systems were rheologically tested for their mechanical stability with creep, strain, flow and amplitude tests. PCap were encapsulated in the hydrogel and Franz cells were used to mimic transdermal penetration of the nanoparticles. The DA and DA-NH_2 gels showed rapid penetration in 2 hours, whereas DA-SH showed a sustained penetration with 100% in <6 hours. Moreover, release of capsaicin from PLGA nanoparticles also showed an initial burst and

subsequent sustained delivery which lasted for 5 weeks. This work highlights the potential of topical DDSs to deliver pain-relieving agents directly to the site of injury, reducing the need for systemic administration and minimizing side effects.

Perspectives

1. **Potential for *in vivo* inflammatory and nociceptive studies**

Deeper insights into the underlying mechanisms of chronic pain and inflammation in SCI are crucial for developing more targeted and effective DDSs. This includes elucidating the roles of specific immune cells, cytokines, and signaling pathways in the pathogenesis of these conditions. Advanced proteomic and genomic analyses can provide a comprehensive understanding of the molecular changes that occur following SCI, leading to the identification of novel therapeutic targets. Polymeric nanosystems not only act as effective drug carriers, but the delayed and sustained drug release ability they provide can effectively lower the frequency of drug administrations, without losing the drug efficacy. In **Chapter 3** we see that efficacy of carvacrol in macrophages is enhanced when it is encapsulated in CHP. It is also demonstrated that CHP modulates the amount of inflammatory and anti-inflammatory cytokines. Macrophages are an important target in inflammatory conditions, and having a nanosystem that properly modulates them makes for an interesting study that should be further analysed in *in vivo* conditions. The *in vitro* studies provide a good picture of how good a DDS can be but it is only in *in vivo* where it is tested for its full potential. While in **Chapter 4** we employed a thermosensitive hydrogel for the delivery of the polyplexes, using that same administration route for delivering CHP in an inflammatory model can provide more insights into the mechanism of efficient and sustained delivery of carvacrol. The *in vivo* studies in antibacterial models with carvacrol have been conducted before with promising results, but the inflammatory studies are still lacking.

Regarding *in vivo* studies with Amirs, a full-fledged study with a bigger samples size would be better in painting the picture of the effect of GP155, as seen in **Chapter 4**. Since, it was a novel territory, it was not expected to see results just 3 days after the surgery. However, now that we observe a difference in the rate of recovery of the animals between control and GP155 groups, another study which stops at day 3 and day 7, would bring more clarity.

2. **Integration of Gene Therapy and Immunomodulation**

Combining gene therapy with immunomodulatory drugs could offer synergistic therapeutic effects. For example, delivering antagomirs to silence pro-inflammatory genes while simultaneously delivering drugs that promote M2 macrophage polarization could create a microenvironment conducive to tissue repair and pain reduction. One route for a powerful cocktail of anti-inflammatory drugs would be co-delivering Amir-21 with carvacrol in a nano-DDS. The co-delivery method of different compounds to combine therapy and diagnostics has been employed in multiple studies, and even carvacrol has been co-delivered with other organic compound with the same root or origin (like thymol). But it is worth analysing if including technology, like gene delivery, that is slowly overtaking therapeutic studies, with a tried and tested anti-inflammatory compound, like carvacrol, would show enhanced targeting of inflammatory and nociceptive pathways.

While the co-delivery of genetic material with organic compounds has been published before, but it is evident that designing the delivery system for this method is a crucial step[21–23]. Considering the different mechanisms of encapsulation of both compounds, creativity would have to be incorporated in synthesising a delivery system that encapsulated hydrophobic organic compounds and condenses anionic NAs.

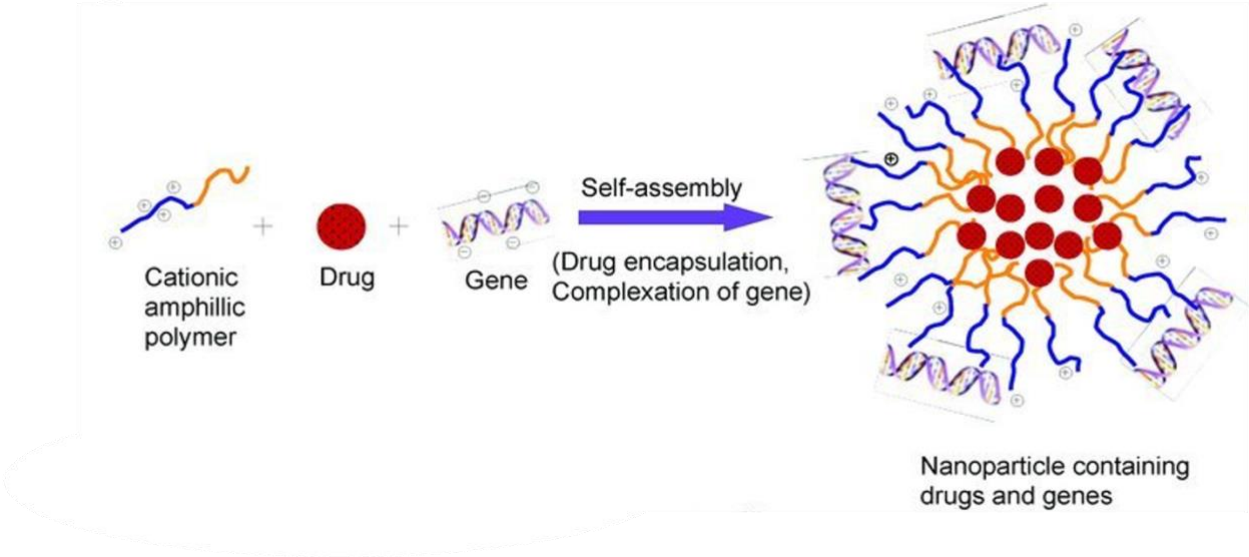

Figure 1: Schematic diagram of co-delivery of drug and gene using a polymeric cationic micellar nanoparticle. Adapted with permission[24]

3. Long-Term Safety and Efficacy Studies

A critical aspect of future research is the rigorous evaluation of the long-term safety and efficacy of DDSs in pre-clinical and clinical studies. This involves assessing potential toxicities, immune responses, and off-target effects. Despite the biocompatibility of polymers used in this research, another study related to the biodegradability of PLGA (as in **Chapters 3** and **5**), pDMAEMA and PNIPAM (**Chapter 4**) should be conducted. Biodegradability and effective clearance from the body are also features of a successful DDS. Panagi *et al.* studied the pharmacokinetics and the circulatory half-life of PLGA in the blood [25] and its modified version with polyethylene glycol. However, it is to be studied whether coating HA on the surface of these nanoparticles makes any difference to its clearance. HA is an endogenous compound and can be easily degraded with hyaluronidases.

Verbaan *et al.* and Fang *et al.* have reported the pharmacokinetics and rapid clearance of pDMAEMA after intravenous administration through the endothelial cells [26,27]. They have also reported that polymers can be easily filtered renally when their molecular weights (MWs) are lower than the renal thresholds (50 kDa). Despite using PLGA and pDMAEMA which have lower MWs than the renal thresholds, a study which observes the biodistribution of these DDSs should be conducted for verifying their renal clearance.

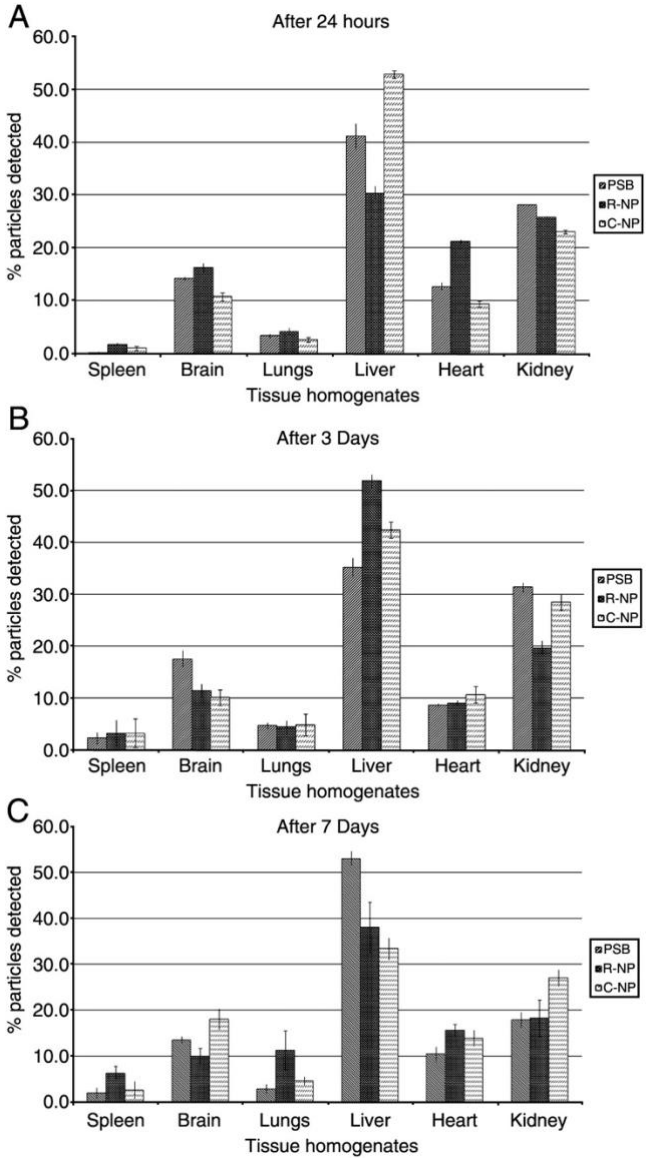

Figure 2: Tissue distribution graphically represented as a measure of percentage of particles detected of the total particles. The data represent three repeats of n = 6; error bars indicate SEM. (A) 24 hours; (B) 3 days; (C) 7 days. PSB, polystyrene beads; R-NP, rhodamine nanoparticles; C-NP, coumarin nanoparticles. Adapted with permission[28]

Conclusion

The research presented in this thesis underscores the cathartic potential of polymeric drug delivery systems in overcoming the limitations of conventional anti-inflammatory and antinociceptive therapies. Through employing the characteristics of biocompatible compounds in the form of nanoparticles, polyplexes and hydrogels, the work authorises

foundations in targeted, controlled, and effective pain management. The work not only overcomes the current limitations in pain management but also presents advanced therapeutic endeavours involving organic compounds and genetic material.

References

(1) Blight, A. R. Macrophages and Inflammatory Damage in Spinal Cord Injury. *Journal of Neurotrauma*. 1992.

(2) Bennett, J.; Das, J. M.; Emmady, P. D. *Spinal Cord Injuries*; 2025.

(3) Oyinbo, C. A. Secondary Injury Mechanisms in Traumatic Spinal Cord Injury: A Nugget of This Multiply Cascade. *Acta Neurobiologiae Experimentalis*. 2011, pp 281–299. https://doi.org/10.55782/ane-2011-1848.

(4) Armstrong, S. A.; Herr, M. J. *Physiology, Nociception*; 2019.

(5) Masri, R.; Keller, A. Chronic Pain Following Spinal Cord Injury. *Adv Exp Med Biol* **2012**, *760*, 74–88. https://doi.org/10.1007/978-1-4614-4090-1_5.

(6) Yezierski, R. P. Pain Following Spinal Cord Injury: Pathophysiology and Central Mechanisms. *Prog Brain Res* **2000**, *129*, 429–449. https://doi.org/10.1016/S0079-6123(00)29033-X.

(7) Berta, T.; Qadri, Y.; Tan, P. H.; Ji, R. R. Targeting Dorsal Root Ganglia and Primary Sensory Neurons for the Treatment of Chronic Pain. *Expert Opin Ther Targets* **2017**, *21* (7), 695–703. https://doi.org/10.1080/14728222.2017.1328057.

(8) Guisasola, M. C.; Alonso, B.; Bravo, B.; Vaquero, J.; Chana, F. An Overview of Cytokines and Heat Shock Response in Polytraumatized Patients. *Cell Stress and Chaperones 2017 23:4* **2017**, *23* (4), 483–489. https://doi.org/10.1007/S12192-017-0859-9.

(9) Mateen, S.; Zafar, A.; Moin, S.; Khan, A. Q.; Zubair, S. Understanding the Role of Cytokines in the Pathogenesis of Rheumatoid Arthritis. *Clinica Chimica Acta* **2016**, *455*, 161–171. https://doi.org/10.1016/J.CCA.2016.02.010.

(10) Rayahin, J. E.; Buhrman, J. S.; Zhang, Y.; Koh, T. J.; Gemeinhart, R. A. High and Low Molecular Weight Hyaluronic Acid Differentially Influence Macrophage Activation. *ACS Biomater Sci Eng* **2015**, *1* (7). https://doi.org/10.1021/acsbiomaterials.5b00181.

(11) Lee, B. M.; Park, S. J.; Noh, I.; Kim, C.-H. The Effects of the Molecular Weights of Hyaluronic Acid on the Immune Responses. *Biomater Res* **2021**, *25* (1), 27. https://doi.org/10.1186/s40824-021-00228-4.

(12) Sharath, S. S.; Ramu, J.; Nair, S. V.; Iyer, S.; Mony, U.; Rangasamy, J. Human Adipose Tissue Derivatives as a Potent Native Biomaterial for Tissue Regenerative Therapies. *Tissue Engineering and Regenerative Medicine*. 2020. https://doi.org/10.1007/s13770-019-00230-x.

(13) Mirna, M.; Paar, V.; Topf, A.; Kraus, T.; Sotlar, K.; Aigner, A.; Ewe, A.; Watzinger, S.; Podesser, B. K.; Hackl, M.; Pistulli, R.; Hoppe, U. C.; Kiss, A.; Lichtenauer, M. A New Player in the Game: Treatment with AntagomiR-21a-5p Significantly Attenuates

Histological and Echocardiographic Effects of Experimental Autoimmune Myocarditis. *Cardiovasc Res* **2022**, *118*, 556–572. https://doi.org/10.1093/cvr/cvab015.

(14) Preethi, K. A.; Lakshmanan, G.; Sekar, D. Antagomir Technology in the Treatment of Different Types of Cancer. *Epigenomics*. 2021. https://doi.org/10.2217/epi-2020-0439.

(15) Lee, H. Y.; Lee, H. Y.; Choi, J. Y.; Hur, J.; Kim, I. K.; Kim, Y. K.; Kang, J. Y.; Lee, S. Y. Inhibition of MicroRNA-21 by an Antagomir Ameliorates Allergic Inflammation in a Mouse Model of Asthma. *Exp Lung Res* **2017**, *43*, 109–119. https://doi.org/10.1080/01902148.2017.1304465.

(16) Wang, C.; Pan, C.; Yong, H.; Wang, F.; Bo, T.; Zhao, Y.; Ma, B.; He, W.; Li, M. Emerging Non-Viral Vectors for Gene Delivery. *Journal of Nanobiotechnology*. BioMed Central Ltd December 2023. https://doi.org/10.1186/s12951-023-02044-5.

(17) Lungwitz, U.; Breunig, M.; Blunk, T.; Göpferich, A. Polyethylenimine-Based Non-Viral Gene Delivery Systems. In *European Journal of Pharmaceutics and Biopharmaceutics*; 2005; Vol. 60, pp 247–266. https://doi.org/10.1016/j.ejpb.2004.11.011.

(18) Zhang, N.; Chin, J. S.; Chew, S. Y. Localised Non-Viral Delivery of Nucleic Acids for Nerve Regeneration in Injured Nervous Systems. *Exp Neurol* **2019**, *319*. https://doi.org/10.1016/J.EXPNEUROL.2018.09.003.

(19) Mason, L.; Moore, R. A.; Derry, S.; Edwards, J. E.; McQuay, H. J. Systematic Review of Topical Capsaicin for the Treatment of Chronic Pain. *British Medical Journal*. BMJ Publishing Group April 2004, pp 991–994. https://doi.org/10.1136/bmj.38042.506748.ee.

(20) O'Neill, J.; Brock, C.; Olesen, A. E.; Andresen, T.; Nilsson, M.; Dickenson, A. H. Unravelling the Mystery of Capsaicin: A Tool to Understand and Treat Pain. *Pharmacological Reviews*. October 2012, pp 939–971. https://doi.org/10.1124/pr.112.006163.

(21) Li, Y.; Thambi, T.; Lee, D. S. Co-Delivery of Drugs and Genes Using Polymeric Nanoparticles for Synergistic Cancer Therapeutic Effects. *Adv Healthc Mater* **2018**, *7*. https://doi.org/10.1002/adhm.201700886.

(22) Wang, H.; Zhao, P.; Su, W.; Wang, S.; Liao, Z.; Niu, R.; Chang, J. PLGA/Polymeric Liposome for Targeted Drug and Gene Co-Delivery. *Biomaterials* **2010**, *31*, 8741–8748. https://doi.org/10.1016/j.biomaterials.2010.07.082.

(23) Yang, Z.; Gao, D.; Cao, Z.; Zhang, C.; Cheng, D.; Liu, J.; Shuai, X. Drug and Gene Co-Delivery Systems for Cancer Treatment. *Biomater Sci* **2015**, *3*, 1035–1049. https://doi.org/10.1039/c4bm00369a.

(24) Khan, M.; Ong, Z. Y.; Wiradharma, N.; Attia, A. B. E.; Yang, Y. Y. Advanced Materials for Co-Delivery of Drugs and Genes in Cancer Therapy. *Adv Healthc Mater* **2012**, *1*, 373–392. https://doi.org/10.1002/adhm.201200109.

(25) Panagi, Z.; Beletsi, A.; Evangelatos, G.; Livaniou, E.; Ithakissios, D. S.; Avgoustakis, K. Effect of Dose on the Biodistribution and Pharmacokinetics of PLGA and PLGA-MPEG Nanoparticles. *Int J Pharm* **2001**, *221*, 143–152. https://doi.org/10.1016/S0378-5173(01)00676-7.

(26) Verbaan, F.; Van Dam, I.; Takakura, Y.; Hashida, M.; Hennink, W.; Storm, G.; Oussoren, C. Intravenous Fate of Poly(2-(Dimethylamino)Ethyl Methacrylate)-Based Polyplexes. *European Journal of Pharmaceutical Sciences* **2003**, *20*, 419–427. https://doi.org/10.1016/j.ejps.2003.09.005.

(27) Fang, J.; Sawa, T.; Akaike, T.; Maeda, H. Tumor-Targeted Delivery of Polyethylene Glycol-Conjugated d-Amino Acid Oxidase for Antitumor Therapy via Enzymatic Generation of Hydrogen Peroxide. *Cancer Res* **2002**, *62* (11), 3138–3143.

(28) Semete, B.; Booysen, L.; Lemmer, Y.; Kalombo, L.; Katata, L.; Verschoor, J.; Swai, H. S. In Vivo Evaluation of the Biodistribution and Safety of PLGA Nanoparticles as Drug Delivery Systems. *Nanomedicine* **2010**, *6*, 662–671. https://doi.org/10.1016/j.nano.2010.02.002.

Acknowledgements

This work has received funding from the European Union's Horizon 2020 research and innovation programme H2020-MSCA-ITN-2020-PIANO under the Marie Sklodowska-Curie grant agreement No 956477.